ANALYSING MODELLED NEARSHORE WAVE CLIMATE VARIABILITY AND CHANGE AS RELEVANT TO THE TRADITIONAL HANDLINE FISHERY OF THE SOUTH AFRICAN SOUTH COAST

Mini-thesis submitted in part of the fulfilment of a

Master's degree in the

Department of Environmental and Geographical Science of the

University of Cape Town (UCT)

2018

Casey Tara Lyttle

SUPERVISORS: Prof. Astrid Jarre; Dr Björn Backeberg; Dr Christo Rautenbach

Declaration:

This work has not been previously submitted in whole, or in part, for the award of any degree. It is my own work. Each significant contribution to, and quotation in, this dissertation from the work, or works, of other people has been attributed, and has been cited and referenced.

Signed: _____

UCT Master's Candidate

Date: _____

Submitted to UCT in partial fulfilment of the requirements for the Degree of Masters in *Climate Change and Sustainable Development* through the Environmental and Geographical Science Department and the African Climate and Development Initiative (ACDI).

Acknowledgements:

This dissertation would not have been possible without the guidance and support of the following people. Firstly, I would like to collectively thank all my supervisors for the passion they have in their respective disciplines, for sharing their knowledge with me and for guiding me towards the best possible version of my mini-thesis. Additionally, I would like to thank them for taking the time to read through and comment on my work. I particularly would like to thank Astrid Jarre for teaching me about South African fisheries and the Master's level thesis writing process. I would also like to thank Astrid for her constant understanding and care for my wellbeing throughout this process. I would like to thank Björn Backeberg for helping me with the result analysis and wave theory. I would like to thank Christo Rautenbach for helping me understand the Simulating WAves Nearshore model and how to use the data. I would like to thank Catherine Ward for helping me with the Sequential Regime Shift Detection analyses, Emma Lockerbie for helping me with R and linear regression analysis, and Florian Weller for proof reading. Additionally, I would like to thank them and the other members of the South African Research Chair in Marine Ecology and Fisheries (SARChI ME&F) team (Lynne Shannon, Louise Gammage, Sven Ragaller and Samantha Grusd) for their constant support and advice throughout this process. I would also like to thank Marieke Norton for putting me in contact with Astrid, and for not only being an enthusiastic course convenor, but also for constructively helping me improve my Master's dissertation writing. I would like to thank my friends, Tanya Marshall and Jess Burger, who were always there at UCT to listen to my woes and to give advice. I would like to thank Gavin for putting up with all my stress, and for helping me with my thought process and writing. Thank you to my mom for the constant support and care you have provided me with throughout this process while you were also going through stressful times. And thank you to my dad for showing a big passion and love for my passion and love for the ocean. To the Craggs, who have done so much for me and my family – I cannot thank you all enough for caring for me as you would for any other family member, and for providing me with a happy and safe place whenever I needed it. Thank you to my close friends who are always there to take my mind off things. And to the rest of my family, my aunt, grandparents and cousin, thank you for supporting so much over the last few years. Last but not least, this thesis would not have been possible without the support and funding I have received for the last year and a half from the SARChI ME&F and UCT.

Abstract:

The South Coast traditional handline fishing communities of South Africa are integrated into a complex ecosystem where human and natural components interact and overlap on many different spatial and temporal scales. The South Coast marine ecosystem, on which the fishers depend, already suffers from depleted fish stocks. The South Coast handline fishery is therefore vulnerable to added stresses such as those induced by climate change. While fishers have noted that deteriorating sea state and a declining number of sea days caused by shifts in wind patterns are affecting their livelihood, applicable scientific research and data on scales relevant to the fishers is insufficient. Insight into the complexities involved in climate change and local-scale responses of these highly integrated social-ecological system therefore remains sparse. While South Coast nearshore winds have been the subject of recent research, the wave climate aspect of the nearshore sea state has not.

In a recent project conducted by the Department of Environmental Affairs and the Council for Scientific and Industrial Research, Simulating WAves Nearshore model outputs spanning 17 years (from 1997 to 2014) were produced for the South African coastline, including the South Coast. Wind (speed and direction) and swell (significant wave height, peak wave direction and period) outputs from the WaveWatch III model (provided by National Centre of Environmental Prediction, US) were used as boundary conditions. The present study uses these wave model outputs to conduct an investigation into the nearshore local-scale wave climate of four traditional handline fishing towns of the South Coast: Witsand, Still Bay, Gouritz and Mossel Bay.

Results suggest that the shape and bathymetry of the coastal sites influence average significant wave height, peak wave directions, and seasonal variability of the approaching swell waves. This is due to the nearshore processes of refraction, bottom friction and sheltering by headlands from the approaching swell, driven by the offshore swell. Additionally, the presence of low peak period waves depended on the focussing of waves that were generated by easterly winds during summer (i.e., wind-waves, which are shorter period waves compared to swell) driven by the synoptic-scale winds.

While summer afternoon waves remained higher than morning waves from 1997 to 2014, the significant wave height difference did not change over time; however, variability increased post-2006, particularly for sites more exposed to approaching swell. A regime shift in mean significant wave height was detected for 2006 across the South Coast, from lower to higher waves. The more exposed study sites showed a strong seasonality (higher waves during winter than summer), where the duration of summer conditions lengthened post-2006 during the period of higher significant wave heights. Significant wave height increased significantly from 1997 to 2014 across the South Coast. Since swell dominates across the South Coast, the observed regime shift (including interannual variability) and trend is likely to be attributed to offshore swell.

The recent increase in wave height variability is in line with fishers observations where increase in climate variability has been observed. The increase in wave height is also in line with fishers' observations which state that the sea state has deteriorated, and sea days have decreased. Additionally, the lengthening duration of summer conditions in waves was also observed by fishers in terms of winds. This analysis of South Coast wave climate contributes to bridging the gap between the first hand observations of fishers and conclusions drawn from coarse resolution scientific data.

Contents

List of Figures and Tables:

List of Acronyms

UCT	University of Cape Town
ACDI	African Climate and Development Initiative
SARChI ME&F	South African Research Chair in Marine Ecology and Fisheries
SCIFR	Southern Cape Interdisciplinary Fisheries Research
EAF	Ecosystem Approach to Fisheries
ERA	Ecological Risk Assessment
CPUE	Catch Per Unit Effort
SRSD	Sequential Regime Shift Detection
RSSI	Residual Sum of Squares Index
RSI	Regime Shift Index
TCU	Total Cumulative Upwelling
NCEP-DOE	The National Centre of Environmental Prediction and the Department of Energy
NCEP	National Centre of Environmental Prediction
CFSR	Climate Forecast System Reanalysis
DEA-CSIR	The Department of Environmental Affairs and the Council for Scientific and Industrial Research
EMD	Empirical Mode Decomposition
IMF	Intrinsic Mode Function
SWAN	Simulating WAves Nearshore
SBMA	Still Bay Modelled Area
MBMA	Mossel Bay Modelled Area
PDF	Probability Density Function
BCLME	Benguela Current Large Marine Ecosystem
SAH	South Atlantic high-pressure system
ITCZ	Inter-tropical Convergence Zone
TAE	Total Allowable Effort
FRAP	Fisheries Rights Allocation Process
SSFP	Small-Scale Fisheries Policy
SST	Sea Surface Temperature
ENSO	El Niño Southern Oscillation
SAM	Southern Annual Mode
JONSWAP	JOint North Sea WAve Project
WAM	WAve Model
WAMDI	WAve Model Development and Implementation
NOAA	National Oceanic and Atmospheric Administration
IPOSS	Integrated Port Operation Support System
SANHO	South African Navy Hydrographic office
CSIR	Council for Scientific and Industrial Research
FFT	Fast Fourier Transform
DFT	Discrete Fourier Transform
EEMD	Ensemble Empirical Mode Decomposition
STARS	Sequential T-test Algorithm for Analysing Regime Shifts
MPK	Mariott-Pope and Kendall
IP4	Inverse Proportionality with 4 corrections
AR1	First order Autoregressive model

CHAPTER 1: Introduction

1.1. Problem statement and motivation:

The Benguela Current Large Marine Ecosystem (BCLME) is one of the four large eastern boundary current upwelling systems (Jarre et al., 2015), which collectively cover less than 1% of the ocean's surface but contribute about 20% to global fish catches (Pauly & Christensen, 1995). The BCLME is characterised by intense upwelling and high variability (Blamey et al., 2015). It consists of northern and southern components, the latter including the West Coast and Agulhas Bank (**Fig. 1.1**) which display biological and physical differences from each other (Hutchings et al., 2009; Watermeyer et al., 2016). The southern Benguela supports several of South Africa's important subsistence and commercial fisheries, including the small-scale traditional handline fishery on the southern Cape along the central region of the Agulhas Bank (Blamey et al., 2015; Raemaekers & Sowman, 2015).

This fishery is part of a highly complex social-ecological marine system subject to many external natural and anthropogenic forces. Since most of the involved fishers are operating under economic pressure, they are vulnerable to changes within the system (Gammage, Jarre & Mather, 2017a). Against a background of already heavily exploited linefish resources, fishers along the South Coast have indicated that their productive days at sea have decreased and the sea state has deteriorated (Laing et al., 1998; Duggan, 2012; Gammage, Jarre & Mather, 2017a). They have attributed this to changes in intra-seasonal wind patterns such as summer winds arriving late and blowing for longer periods. Furthermore, many of the local fishers associate diminishing catches and changes in Silver Kob (*Argyrosomus inodorus*) behaviour with increasing climate variability (Duggan, 2012; Gammage, Jarre & Mather, 2017a).

Despite the importance of the Agulhas Bank (adjacent to the South Coast) for the productivity of South African fisheries, past high resolution social-ecological marine systems research in South Africa has been biased towards the West Coast and offshore large-scale fisheries (Blamey et al., 2012, 2015). There is therefore a lack of high resolution nearshore datasets of sufficient lengths for the South Coast (Blamey et al., 2012, 2015; Lamont et al., 2018). Consequently, scientific studies of the inshore environment have had to use varying sets of data that are often not suited for the nearshore and thus these studies have shown conflicting results (Rouault, Pohl & Penven, 2010; Blamey et al., 2015). Additionally, while fishers have a wealth of knowledge about their fishing grounds, their observations on climate variability are sometimes difficult to match with scientific observations (Ward, 2018). Such

climate observations along the South Coast vary amongst fishers in spatial and temporal scales and in degree of importance of different climate variables. Additionally, their climate observations focus on the fishing grounds adjacent to the coast, the period during which fishing mostly takes place (morning to late afternoons during summer) and the last few decades (Duggan, Green & Jarre, 2014; Gammage, Jarre & Mather, 2017a). These spatial and temporal scale mismatches and lack of understanding of the fishers' perspectives makes it challenging to try to corroborate local fishers' knowledge with scientific data, which until recently have mostly been available at the shelf scale. Lastly, to discern changes in sea days and sea state entails understanding many different components and forces, such as winds and waves, all interacting on varying scales of time and space.

To address the lack of high resolution environmental data and climate research, as well as incorporating more local knowledge, the Southern Cape Interdisciplinary Fisheries Research (SCIFR) project recently began investigating wind variability along the South Coast (Ward, 2018; Duggan, 2012; Duggan, Green & Jarre, 2014; Gammage, Jarre & Mather, 2017a,b). While some consistency has already been demonstrated between fishers' environmental observations and scientific research in terms of offshore synoptic-scale winds and upwelling variability (Ward, 2018.; Blamey et al., 2012), the South Coast sea state has yet to be scientifically examined. To this end, the current study uses existing wave data from the Simulating WAves Nearshore (SWAN) model (significant wave height (H_{m0}), peak

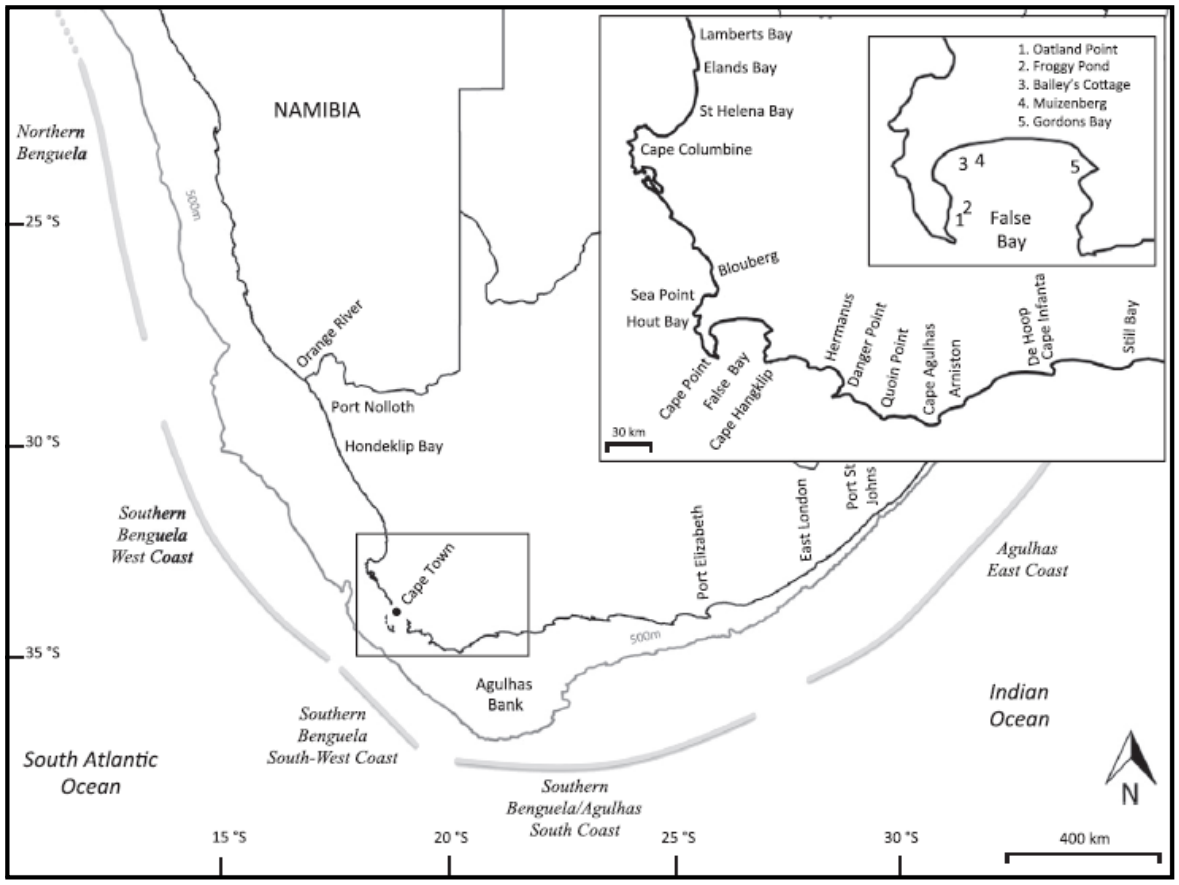

Fig. 1.1: *Coastal zonation of South Africa's oceanographic systems (from Blamey et al., 2015).*

wave direction and period) to investigate wave climate along the South Coast, focussing on four fishing towns along the South Coast (Witsand, Still Bay, Gouritz, and Mossel Bay) during the period of 1997 to 2014. While these wave data have already been analysed in terms of wave run-up and coastal vulnerability along the entire South African coast (Theron et al., 2014), analyses of change and variability in the nearshore local-scale wave climate along the South Coast have not yet been performed.

This study also qualitatively compares scientific results (wave model data) to fishers' observations (Duggan, 2012; Gammage, Jarre & Mather, 2017a). The intention is to better understand the uncertainties in high resolution scientific data by contrasting them with fishers' first-hand experience of this complex highly integrated marine system. However, it is understood that fishers' observations are mostly not formally recorded, and their memory and scale may be obscured. One possible outcome of the present study is to help protect the South Coast social-ecological system (social, biological, and environmental) against future vulnerabilities by understanding it more.

1.2. Aim and research questions:

This study aims to investigate the variability and change in sea state (wave climate) and how this might influence on the amount of sea days, as defined by South Coast traditional handline fishers' ability to launch their boats. In this case, the appearance of the surface ocean waves (height, period and direction) determines the state (from calm to rough seas) of the sea (i.e., 'sea state'). 'Sea days' are the days when the fishers can go out and fish (towards the 'calm' end of the sea state range). In this context, the term 'fishers' refers to anyone who is involved in the small-scale traditional handline fishery, including the skippers, crew, rights holders, fish processors, spouses and family. The term 'launch' refers to the ability of fishers to leave the nearshore coastal waters to the offshore fishing grounds and being able to remain there and fish; it is thus not restricted to getting the boat off the slipway and into the water.

Using wave data simulated by the SWAN model, this study attempts to answer the following questions:

1. What is the general modelled nearshore wave climate of four South Coast fishing towns – Witsand, Still Bay, Gouritz and Mossel Bay – for the period 1997 to 2014?
    - How and to what degree do the wave climates (in terms of significant wave height (H_{m0}), peak wave period and peak wave direction) differ (or not) between the towns for this period?
    - How and to what degree do the average nearshore local-scale wave climates of each town compare to the average offshore synoptic-scale wave climate for this period?
    - What is the average synoptic-scale wind conditions over the region for this period?
    - How do the wave climates of each town compare to the southern hemisphere three-month summer season (December to February) for this period, which is important for the fishery?

- What are the sub-daily and seasonal H_{m0} cycles for each town and how do they differ (or not) between the towns over this period?

2. How has the average nearshore H_{m0} changed on various timescales at each fishing town for the period 1997 to 2014?
   - Focussing on the southern hemisphere three-month summer season, has the sub-daily H_{m0} changed (or remained the same) in terms of variability and trends for each town for the period? How do the towns differ (or not)?
   - How and to what degree has the interannual H_{m0} changed (or remained the same) in terms of variability and trends for each town for the period? How do the towns differ (or not)?
3. How do the SWAN model results for the period 1997 to 2014 in this study compare to local fishers' observations outlined in recent studies?

1.3. Thesis outline:

Chapter 2 provides a review of literature relevant to this study, focussing primarily on the physical and biological components of the study area, the background of the small-scale traditional handline fishery, climate change and variability of the marine system of interest, and approaches to studying coastal waves, including background on various methods used to study wave time series. Chapter 3 provides background on the data and methods used. Chapter 4 presents the results of the study. Chapter 5 provides a discussion of the results in the context of the research questions, offers recommendations for future work, and concludes the study.

CHAPTER 2: Literature Review

2.1. The Agulhas Bank ecosystem:

The Benguela Current Large Marine Ecosystem (BCLME) is one of the four largest eastern boundary current upwelling systems that exists along the West and South Coasts of South Africa, and is characterised by intense upwelling and high variability (Jarre et al., 2015). The BCLME consists of northern and southern components (Blamey et al., 2015). The southern component is biologically and physically split into the West Coast and the Agulhas Bank at Cape Agulhas (**Fig. 1.1**; Hutchings et al., 2009; Watermeyer et al., 2016). The Agulhas Bank is a large triangular continental shelf region, more than 200 m deep, that extends from Cape Point to Port Alfred (18–26ºE) and about 250 km southward from Cape Infanta (Griffiths, 2000; Blanke et al., 2009). The South Coast is located in the southern Cape along the central region of the Agulhas Bank (Jarre et al., 2015).

2.1.1. Physical components:

While wind-driven upwelling is dominant along the West Coast of South Africa, the Agulhas Bank's hydrology is driven by both upwelling and temperate shelf dynamics (Watermeyer et al., 2016) that are induced by the western boundary Agulhas Current and atmospheric features. As the Agulhas Current flows southward along the eastern shelf break, it diverges from the coast and meanders along the shelf-edge, then retroflects back towards the Indian Ocean south of South Africa (Hutchings et al., 2002; Lutjeharms, 2006). The divergence of the current from the coast upwells deep water onto the shelf, which in turn feeds the subsurface waters that upwell to the surface at coastal upwelling centres such as the persistent upwelling centre near Port Alfred (about 26ºE) on the Eastern Agulhas Bank. This upwelling centre feeds the Central Agulhas Bank cool subsurface water ridge (Hutchings et al., 2002). The meandering Agulhas Current can move warm water from the current onto the Agulhas Bank, and can induce intense shear-edge anti-cyclonic (downwelling) or cyclonic (upwelling) water eddies which may move onto the bank (Lutjeharms, 2006).

Latitudinal displacement of the anti-clockwise rotating South Atlantic high-pressure system (SAH) and the westerly wind belt drives the large-scale seasonality of the surface winds of South Africa and the surrounding ocean (Kruger et al., 2010), and hence those of the Agulhas Bank. The main driver of the latitudinal displacement of the SAH is the Inter-tropical Convergence Zone (ITCZ) which migrates south during the austral summer and north during the austral winter (Ahrens & Henson, 2016).

Consequently, the southern hemisphere's subtropical high-pressure belt (including the SAH) around 30°S and the mid-latitude low-pressure belt (including the westerly wind belt) around 30–40°S are similarly more south during austral summer compared to austral winter. While the winds are mostly from a westerly direction in the westerly wind belts, the clockwise-rotating low-pressure systems (often associated with cold fronts) move from west to east within the wind belt. Therefore, southern Africa is less exposed to low-pressure systems within the westerly wind belt during summer (**Fig. 2.1 (a)**) compared to winter (**Fig. 2.1 (b)**; Rossouw, 1989; Kruger et al., 2010). Additionally, the SAH occasionally (mostly during austral summer) ridges south of South Africa and drives strong upwelling favourable winds, south-easterly and easterly along the West and South Coasts respectively (Schumann, 1999; Kruger et al., 2010; Rouault, Pohl & Penven, 2010).

In summary, westerly winds are dominant over the Agulhas Bank throughout the year with strongest winds during austral winter; but strong and temporary easterly wind periods are also

(a)

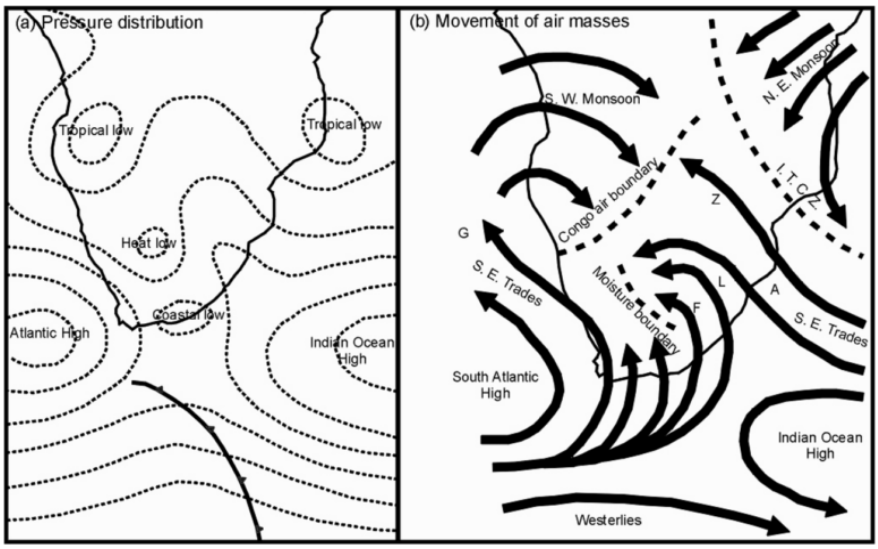

(b)

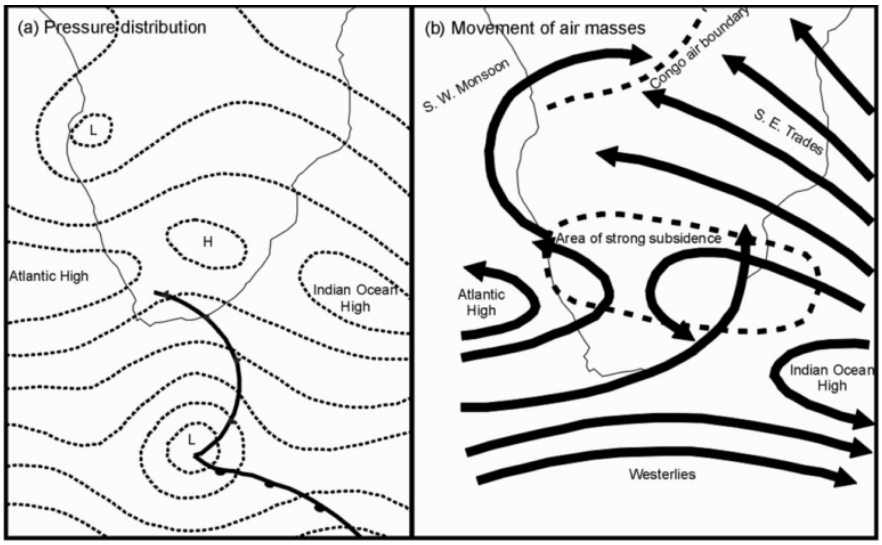

Fig. 2.1: *Pressure distributions and movement of air masses during (a) summer and (b) winter over southern Africa and the surrounding oceans (adapted from Kruger et al., 2010).*

experienced throughout the year and are strongest during the austral summer (Schumann, in press; Blanke et al., 2009). Therefore, the Agulhas Bank water column experiences mixing during austral winter through upwelling driven by strong westerly winds (Lutjeharms, Cooper & Roberts, 2000; Lutjeharms, 2006), but is strongly stratified during austral summer except during the intermittent easterly winds periods which induce coastal upwelling at headlands along the Agulhas Bank coasts, including the South Coast (Schumann, 1999; Lutjeharms, Cooper & Roberts, 2000).

The same seasonality of winds is replicated for waves along the Agulhas Bank coasts (Rossouw, 1989). The South African coastal wave climate is predominantly influenced by swell (Cooper, 2001; Rossouw, Terblanche & Moes, 2013). These are mainly produced by the low-pressure synoptic-scale storms produced within the large-scale westerly wind belt, from which they propagate in a north-eastward direction towards the South African coast. The West and South Coast are therefore exposed to the eastward moving storms, and thus strongly influenced by the south-westerly swell. Since the westerly wind belt is located closer to southern Africa in winter and with higher wind speeds, more severe wave conditions occur along the South Coast during austral winter compared to austral summer (Rossouw, 1989; Theron et al., 2010; Rossouw, Terblanche & Moes, 2013).

On a smaller scale, shorter period waves compared to swell known as wind-waves (also referred to as 'chop') at the coast can be driven by surface pressure differences between high-pressure at sea and low-pressure on land (Remya & Kumar, 2013; Jarre et al., 2015). Locally produced wind-waves can thus be superimposed on the remotely produced swell (Laing et al., 1998). On a daily scale, this pressure difference builds up during the day as the land heats up faster than the ocean, resulting in a surface thermal low above land and a surface thermal high above the adjacent ocean. As a result, a sea breeze blowing from the sea towards the land develops with winds ranging from 5–10 m/s. This is typically strongest in the afternoon and coincides with higher wave heights, while in the morning and evening the opposite phenomenon occurs, known as land breeze, which dampens the wave heights (Sonu et al., 1973; Remya & Kumar, 2013). Land-sea breezes are typically on a spatial scale of about 20-100 km or more (Preston-Whyte, 1969; Schumann, Illenberger & Goschen, 1991; Miller et al., 2003; Ahrens & Henson, 2016). On a seasonal scale, sea breeze systems are strongest during summer while land breeze systems are strongest during winter (Ahrens & Henson, 2016). Sea-land breezes have been the subject of previous studies along the South African coast, particularly on the East Coast (Preston-Whyte, 1969; Tyson & Preston-Whyte, 1972; Schumann, Illenberger & Goschen, 1991).

2.1.2. Biological components:

Compared to the West Coast of the southern Benguela, the Agulhas Bank has a relatively moderate primary and pelagic fish productivity (Hutchings et al., 2009). West Coast surface waters are nutrient-rich due to coastal upwelling and thus this region is a primary nursery ground for many marine species, including important marine living resources (Hutchings et al., 2002, 2009; Blanke et al., 2009).

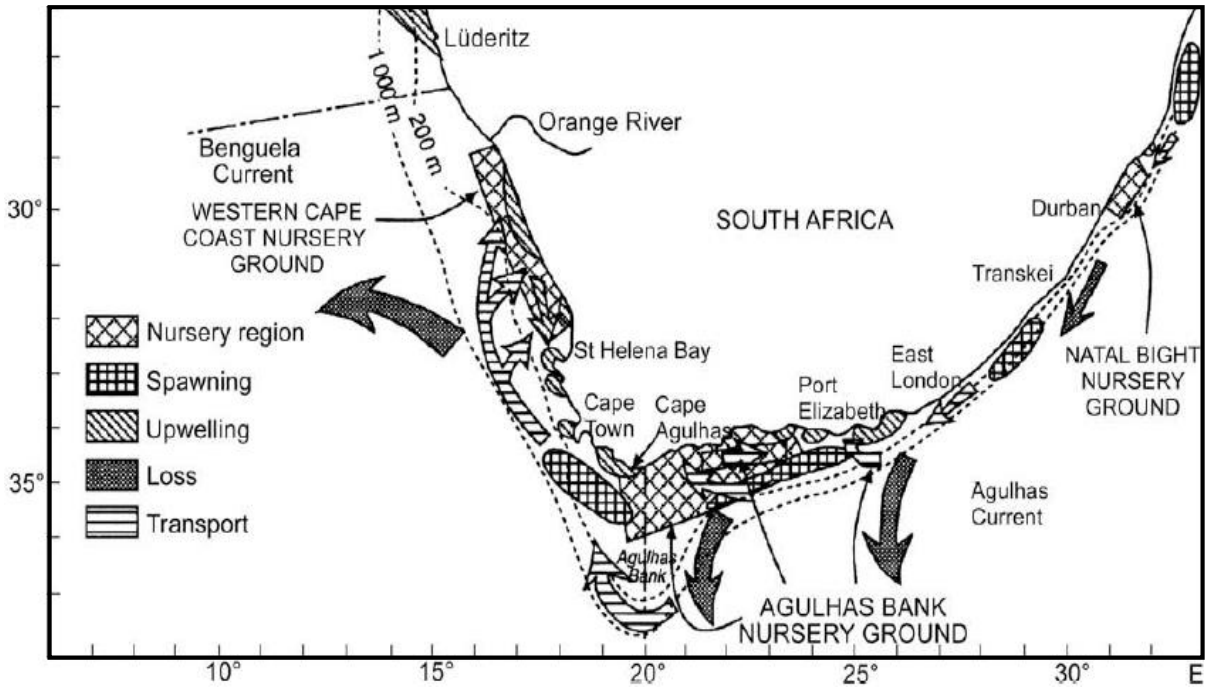

Fig. 2.2: *Coastal distribution of nursery and spawning grounds, as well as upwelling, loss and transport regions for southern Africa pelagic fish (from Hutchings et al., 2009).*

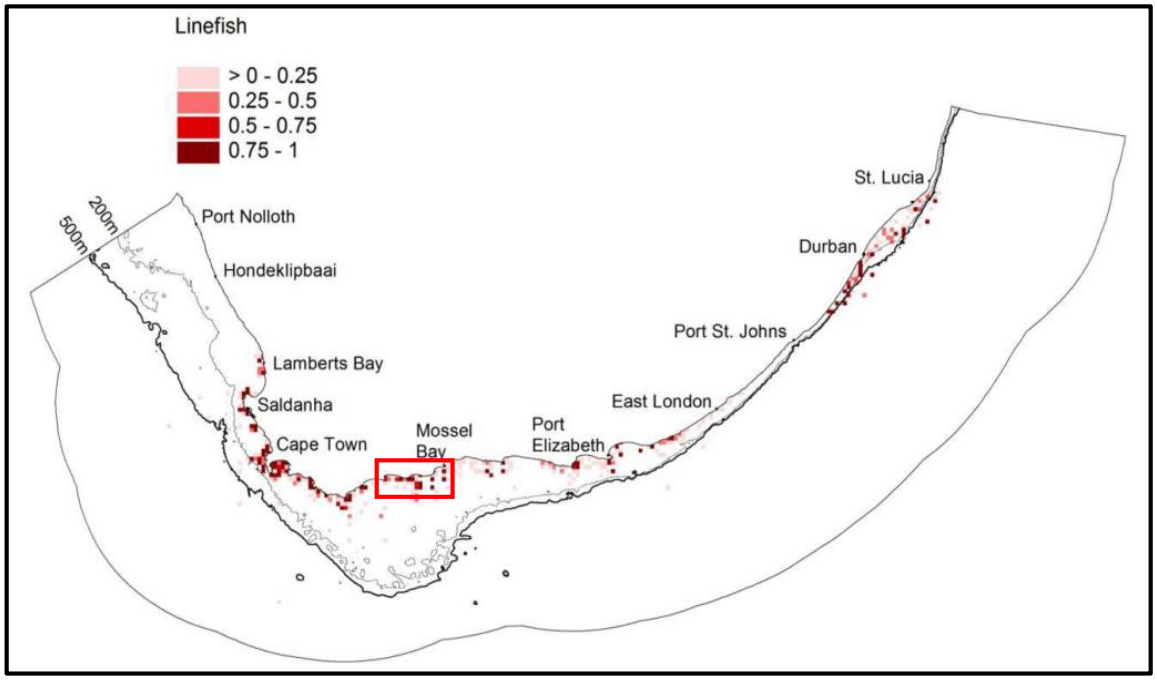

Fig. 2.3: *Distribution of the relative fishing effort of the South African commercial linefish fishery, indicated by scaled red colours. The red box outlines the Southern Cape Interdisciplinary Fisheries Research (SCIFR) study area (Witsand to Mossel Bay) (adapted from Sink et al., 2012).*

Nevertheless, the Agulhas Bank is an important spawning and nursery area for many commercially fished species of South Africa (**Fig. 2.2**). Pelagic fish eggs and larvae spawned onto the stratified Central and Western Agulhas Bank following summer upwelling and during maximum light levels, are transported by an alongshore current jet to the nutrient-rich nursery grounds along the West Coast, where they mature (Hutchings et al., 2002, 2009; Blanke et al., 2009). Eggs and larvae spawned onto the Central and Eastern Agulhas Bank usually mature in the Agulhas Bank nursery grounds (Hutchings et al., 2002).

The Agulhas Bank also plays an important role in the South African inshore linefishery, which consists of commercial, recreational and small-scale (previously subsistence) sectors (Sink et al., 2012; Blamey et al., 2015). Unlike the commercial sector, the small-scale sector is more labour intensive, uses simple technology and low capital inputs (Sowman, 2006). While this linefishery is one of the oldest fisheries in South Africa, dating back as far as the 1500s, it has only been regulated since 1985 (Griffiths, 2000; Petersen et al., 2010). The fishing grounds extend along the entire coastline but are heavily concentrated along the southern Benguela coastal regions, including the Agulhas Bank, where fishing occurs about 3–60 km offshore in 20–60 m deep waters (**Fig. 2.3**; Duggan, Green & Jarre, 2014; Blamey et al., 2015). Many different shelf species (>200), mostly with low population sizes, are targeted and caught using dingies, deck boats or ski boats, and handline or rod-and-reel methods. Similar to other South African inshore fisheries (Abalone and West Coast Rock Lobster), the inshore handline fishery is based on catching relatively small amounts of fish with a higher per-unit value (Griffiths, 2000; Petersen et al., 2010; Blamey et al., 2015).

2.2. The small-scale traditional handline fishery:

Failing to consider South African fisheries as highly integrated social-ecological marine systems has in the past led to continuous resource depletion in the linefishery (Sink et al., 2012; Winker, Kerwath & Attwood, 2016). The small-scale linefishery sector has in particular struggled because, unlike the linefishery commercial sector, the participants not only depend on the linefishery resources for income but also for food (Petersen et al., 2010; Blamey et al., 2015; Gammage, Jarre & Mather, 2017b). The subsistence sector was first recognized as a legal user group in the 1998 Marine Living Resource Act (MLRA). However, legal rights for the new small-scale fisheries sector, including both subsistence and small commercial user groups, is yet to be fully implemented under the Small-Scale Fisheries Policy (SSFP; Winker, Kerwath & Attwood, 2016; Gammage, Jarre & Mather, 2017a). This study focusses on the South Coast small-scale traditional handline linefishery which has been defined as extending from about Witsand to just east of Plettenberg Bay (21-24^{o}E). This definition is based on the extent of the various commercial linefish catches, as illustrated in **Fig. 2.4** (from Blamey et al., 2015).

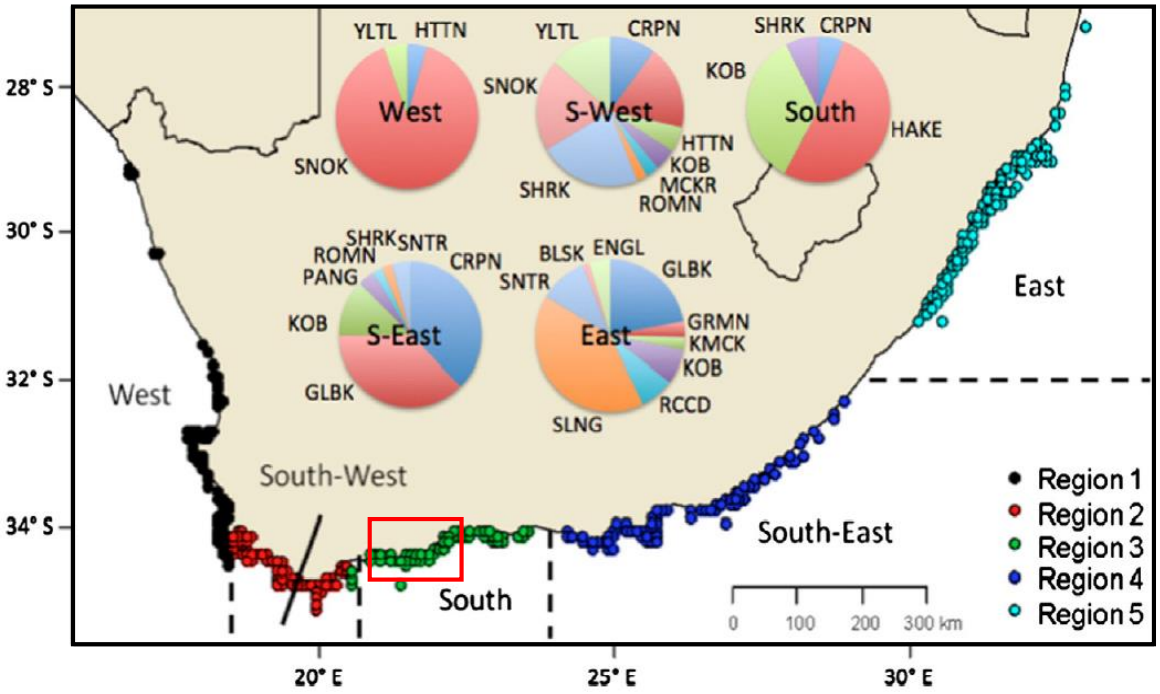

Fig. 2.4: *Coastal Management Zonation based on commercial linefish catch composition, and the Southern Cape Interdisciplinary Fisheries Research (SCIFR) study area (Witsand to Mossel Bay) outlined in red (adapted from Blamey et al., 2015).*

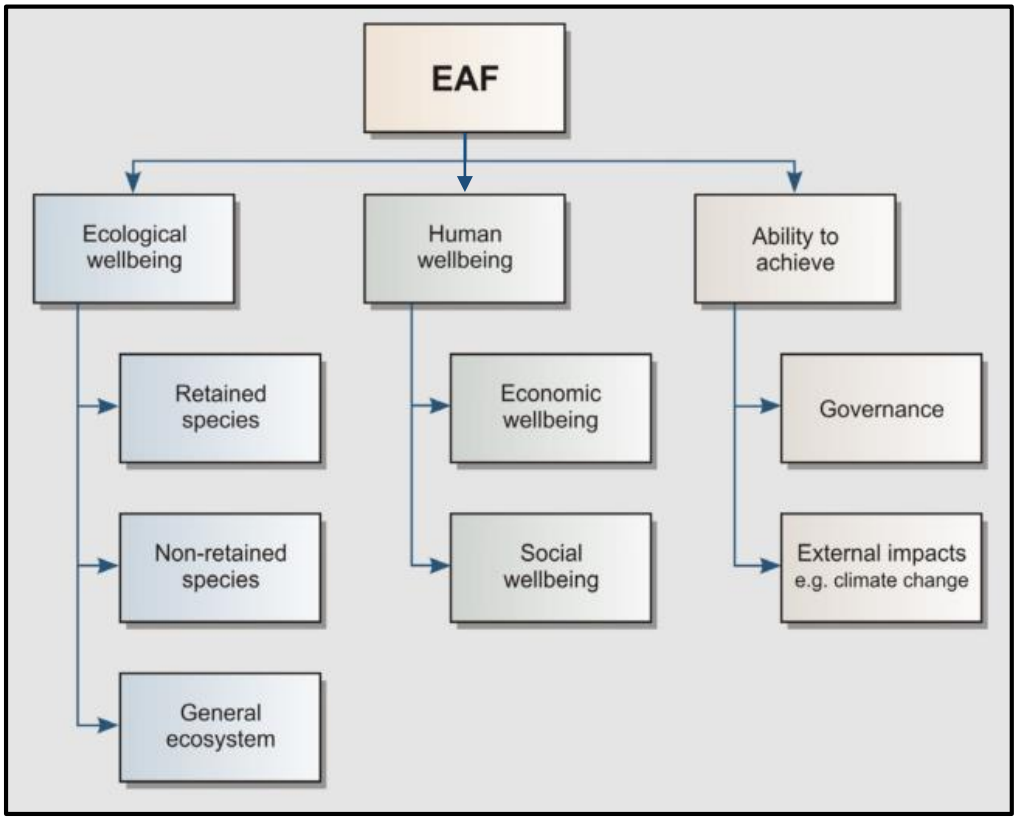

Fig. 2.5: *Diagram of the Ecosystem Approach to Fisheries (EAF) used in the Ecological Risk Assessment (ERA), showing the three main components and their subcomponents (from Petersen et al., 2010).*

An Ecosystem Approach to Fisheries (EAF; **Fig. 2.5**) has recently become the basis for integrated research and the preferred adaptive management approach for human activity within the BCLME in an attempt to address past management failures, including those of the linefishery. This management approach considers the ecological and social aspects, as well as the relationships between these two aspects, while trying to meet the needs and values of all stakeholders involved. Part of the EAF is to use Ecological Risk Assessments (ERAs) and ERA reviews to identify issues and prioritize them. In 2009, 113 issues were identified for the linefishery and categorised into three groups: ecological wellbeing, human wellbeing and ability to achieve. Of these, 38% were considered of extreme urgency to address, which is not an unexpected outcome based on the state of this fishery (Petersen et al., 2010).

2.2.1. Ecological well-being:

The South Coast small-scale traditional handline fishery targets about 50 commercially important species, of which Silver Kob (*Argyrosomus inodorus*; hereafter 'Kob') is the primary target (Gammage, Jarre & Mather, 2017a,b). About 600 tonnes of Kob were collectively landed annually by the commercial (including all small-scale commercial) and recreational linefishery and the inshore trawl between 1987 and 2011 along the South and East Coasts according to Winker, Kerwath & Attwood (2016). Kob is the primary target because they are considered the most valuable species in the fishery, and handline fishers have indicated that Cape Hake (*Merluccius capensis*) has been difficult to catch in the recent past (Winker, Kerwath & Attwood, 2016; Gammage, Jarre & Mather, 2017a,b). Kob are a widely distributed demersal species associated with warm temperate waters. They retreat offshore during austral winter and return inshore during austral summer to spawn. The inshore season is expected to occur from austral spring, the start of the fishing season, until austral autumn. Silvers, also known as Carpenters (*Argyrozona argyrozona*), and reef fish such as Red Roman (*Chrysobleplus laticeps*) and sharks, are usually targeted in the absence of Kob (Griffiths, 2000; Gammage, Jarre & Mather, 2017a,b).

Overfishing is known to be a major problem and one of the main drivers of observed changes in a fishery's ecosystem state, increasing the system's vulnerability to changes by lowering overall resilience (Petersen et al., 2010; Blamey et al., 2015). Overfishing of linefish is a result of easy access from the shore and excessive illegal fishing, together with added pressure from inshore trawl fisheries who catch certain species of linefish as bycatch (WWF, 2011). Stock assessments of linefish have been difficult to complete in the past because of the lack of appropriate stock assessment methods available to account for catches from multispecies fisheries, such as the linefishery. As a result, poor levels of fisheries management and high fishing pressures have persisted, and most linefish stocks remain in an unknown or collapse state (Petersen et al., 2010; Winker, Kerwath & Attwood, 2013). However, novel methods developed by Winker, Kerwath & Attwood (2013) allowed for recent stock assessments of four linefish species by Winker, Kerwath & Attwood (2016).

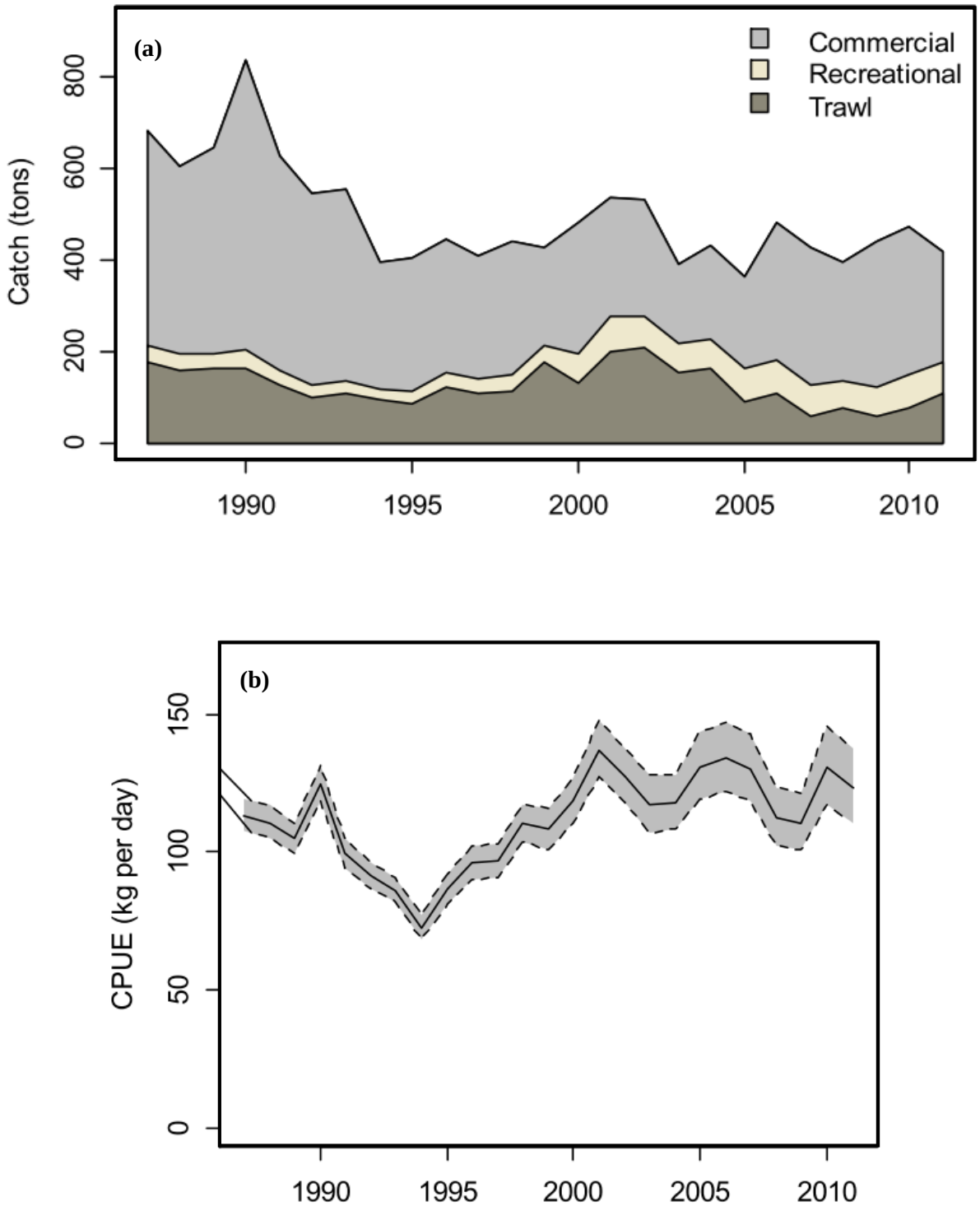

Fig. 2.6: *(a) Silver Kob (Argyrosomus inodorus) catch by commercial and recreational linefishery and demersal trawl fishery along the South Coast. (b) Standardized Catch Per Unit Effort (CPUE) time series, based on catch and effort data of the commercial linefishery, for Silver Kob along the South Coast (adopted from Winker, Kerwath & Attwood 2016).*

Kob and many other linefish species were heavily depleted along the South Coast during the 1990s, as indicated by a decrease in catches and catch per unit effort (CPUE) together until 1994 (**Fig. 2.6 (a)**). Since this was the case generally on the South African coasts, a state of emergency was declared in 2000 for the handline fishery (Winker, Kerwath & Attwood, 2016). Total Allowable Effort (TAE) was mandatorily reduced considerably in an attempt to create conditions conducive to the recovery of linefish stocks. As a result, CPUE levelled off after 2000 at a higher CPUE than the late 1980s (**Fig. 2.6 (b)**). Despite the 2000 TAE decrease, Kob catches for commercial, recreational and trawl fisheries along the South Coast increased slightly (still lower than pre-1990s) until 2003. With the recent increasing effort from the recreational and trawl sectors, the Kob biomass along the South Coast has not yet fully recovered and remains over-exploited because effort remains high while biomass is low (Winker, Kerwath & Attwood, 2016). In the absence of Kob in the traditional handline fishery, pressure on the lower economic valued Silvers and reef fish species has increased. While this may be economically unsustainable in the long term, some fishers remain in this fishery. The many reasons for the continued existence of this fishery have been outlined in Gammage, Jarre & Mather (2017b). The number of active boats have declined recently, partly due to low Kob abundance, increased fuel prices or adverse sea state conditions (Norton, 2014; Gammage, 2015; Gammage, Jarre & Mather, 2017b). Consequently, research into local-scale sea-state becomes important to disentangle the possible causes.

2.2.2. Human well-being:

In addition to low Kob biomass (and other stressors, see Gammage et al., 2017a), the sustainability of the South Coast handline fishers' livelihoods are aggravated by the lack of control they have of the sale price of Kob (Petersen et al., 2010). While the price of Kob remained the same from 2009-2013, living costs and fishing operational costs (fuel and bait, etc.) increased (Petersen et al., 2010; Gammage, Jarre & Mather, 2017a). Even though alternative species may have been available in the fishery, such as Silvers, the profit margin for the fishers has decreased due to lower prices for alternative species and higher input costs to harvest these species compared to Kob. Consequently, in the recent past when Kob biomass has been low, income has been low within the handline fishery, and many fishers have indicated that they do not have the financial means to repair or maintain their boats and have therefore often neglected this (Gammage, Jarre & Mather, 2017a). This makes them vulnerable to sea-state variability and change (Gammage, Jarre & Mather, 2017a).

2.2.3. Ability to achieve:

Governance, policy and regulations were considered to be key stressors for the fishers of the small-scale traditional handline fishery (Gammage, Jarre & Mather, 2017a). This fishery currently consists of two policy and regulatory components: the fully commercial component with individual

rights; and the community-based rights geared towards poverty alleviation. Individual commercial rights based on TAE were allocated for an eight-year period, starting at the beginning of 2003 (under the MLRA of 1998), to fishers who are currently considered part of the fishery (Gammage, Jarre & Mather, 2017a). The number of allocated rights was limited and thus some fishers were excluded. However, those excluded and with no other source of income were given interim relief rights which allowed them access to the fisheries resources until the implementation of formal small-scale fishery polices (Petersen et al., 2010; Visser, 2015). After 2013 and the expiration of individual rights, fishers had to reapply for rights through the Fisheries Rights Allocation Process (FRAP) of 2013, by justifying their involvement in the fishery over the past eight years (Gammage, Jarre & Mather, 2017a). The FRAP stimulated considerable fraud and is currently still in the process of revision.

In an attempt to address shortcomings of the first rights allocation in the early 2000s, an additional sector (the small-scale sector) has been recognised in the SSFP (gazetted in 2012) which is currently under implementation (Gammage, Jarre & Mather, 2017a). Interim relief rights of traditional handline fishers have been absorbed into the people-centred SSFP. It is hoped that the policy will address the inequalities of the past with respect to fishing rights and segregation, as well as the high poverty and low economic development in the coastal fishing communities. The policy will allow for co-operative fishing rights of baskets of species, which means a single right for multiple species instead of many individual species rights. These small-scale community-based rights have to be included into the linefishery's TAE and will run in parallel with the commercial sector rights (Department of Agriculture Forestry and Fisheries, 2012; Winker, Kerwath & Attwood, 2016).

The detrimental effects of ineffective fisheries management as well as poor compliance and enforcement have in the past resulted in overexploitation of many species (Petersen et al., 2010; WWF, 2011; Sink et al., 2012). For example, the inshore demersal trawl hake fishery mainly targets shallow-water Cape Hake and Sole but has bycatches of Kob. While the Kob handline fishery has for some while been subjected to restrictions such as minimum size, no restrictions on bycatch landings from the trawl fishery have existed until very recently (Sink *et al.*, 2012; Blamey *et al.*, 2015; Gammage, Jarre & Mather, 2017a). Competition from the inshore trawl fishery is thought to be one of the causes of the recent Kob catch declines, in addition to changes in climate. This and similar circumstances demonstrate why inadequate fisheries management has been established as one of the main stressors for handline fishers in the southern Cape (Gammage, Jarre & Mather, 2017a,b).

2.3. Climate change and variability:

Human-induced global warming is expected to exacerbate the impacts of fishing pressure on marine ecosystems across the globe (IPCC, 2014). While sea surface temperatures (SSTs) have been observed to increase on a global scale, smaller-scale SST trends in coastal upwelling ecosystems are

more varied in rates and sometimes opposite in trends (Rouault, Pohl & Penven, 2010; Blamey et al., 2015). Attributing climate change drivers to changes observed on ecosystem scales is very challenging when multiple drivers are acting together at varying scales (Blamey et al., 2015). Attribution is further complicated because it is difficult to determine whether a driver is a climate trend or just variability. This is especially a problem for the BCLME region where interannaual and decadal variability are common (Hutchings et al., 2009). Furthermore, because the BCLME region is highly variable, the attributions are further confused by variability in the relative influence of drivers (Blamey et al., 2015). Comprehension of environmental drivers and changes is, however, crucial for an understanding of the regime shifts that they can cause in upwelling ecosystems, which can impact a fishery's production (Howard et al., 2007; Blamey et al., 2012; Conversi et al., 2014). Understanding these forces is a prerequisite for a better incorporation of climate change and variability into fisheries management with the aim of making fisheries more resilient to change (Petersen et al., 2010).

2.3.1. Observed environmental changes (by fishers):

South Coast small-scale traditional handline fishers have observed environmental and climate changes that they believe to influence the marine ecosystem in which their fishery exists, as documented by Duggan (2012) and Gammage, Jarre & Mather (2017a). Gammage, Jarre & Mather (2017a) found that one of the main stressors identified by the fishers was climate variability. Specifically, 'normal' climate patterns have become increasingly variable and less predictable for the fishers, which they attribute mostly to changes in prevailing winds. For example, the south-easterlies have been observed to start blowing later in the year (end of September rather than August) and for longer periods at a time, from about 2006 to 2011. Fishers also highlighted that these changes in wind regimes are deteriorating the sea state, decreasing the amount of sea days and contribute to reducing Kob availability on the Agulhas Bank (Duggan, 2012; Gammage, Jarre & Mather, 2017a).

Corroborating observed environmental changes by fishers with scientific observations is, however, difficult. Firstly, fishers' observations are usually not formally recorded but instead recalled from memory. However, fishers' memory may be obscured by their memory span, the period between launching and returning (about 06h00 to 15h00) during the summer fishing season), as well as the spatial limitation to adjacent, nearshore fishing grounds (Gammage, Jarre & Mather, 2017a). Furthermore, it is not merely a single variable which determines the amount of sea days in the lives of fishers, but rather a set of variables with different weights in the evaluation whether proceeding to sea is likely to be productive (Duggan, 2012; Duggan, Green & Jarre, 2014; Gammage, 2015; Gammage, Jarre & Mather, 2017a). **Fig. 2.7** shows the most common factors influencing the decision to go sea as highlighted by the fishers in Duggan (2012), Gammage (2015) and Gammage, Jarre & Mather (2017a); this selection is by no means exhaustive.

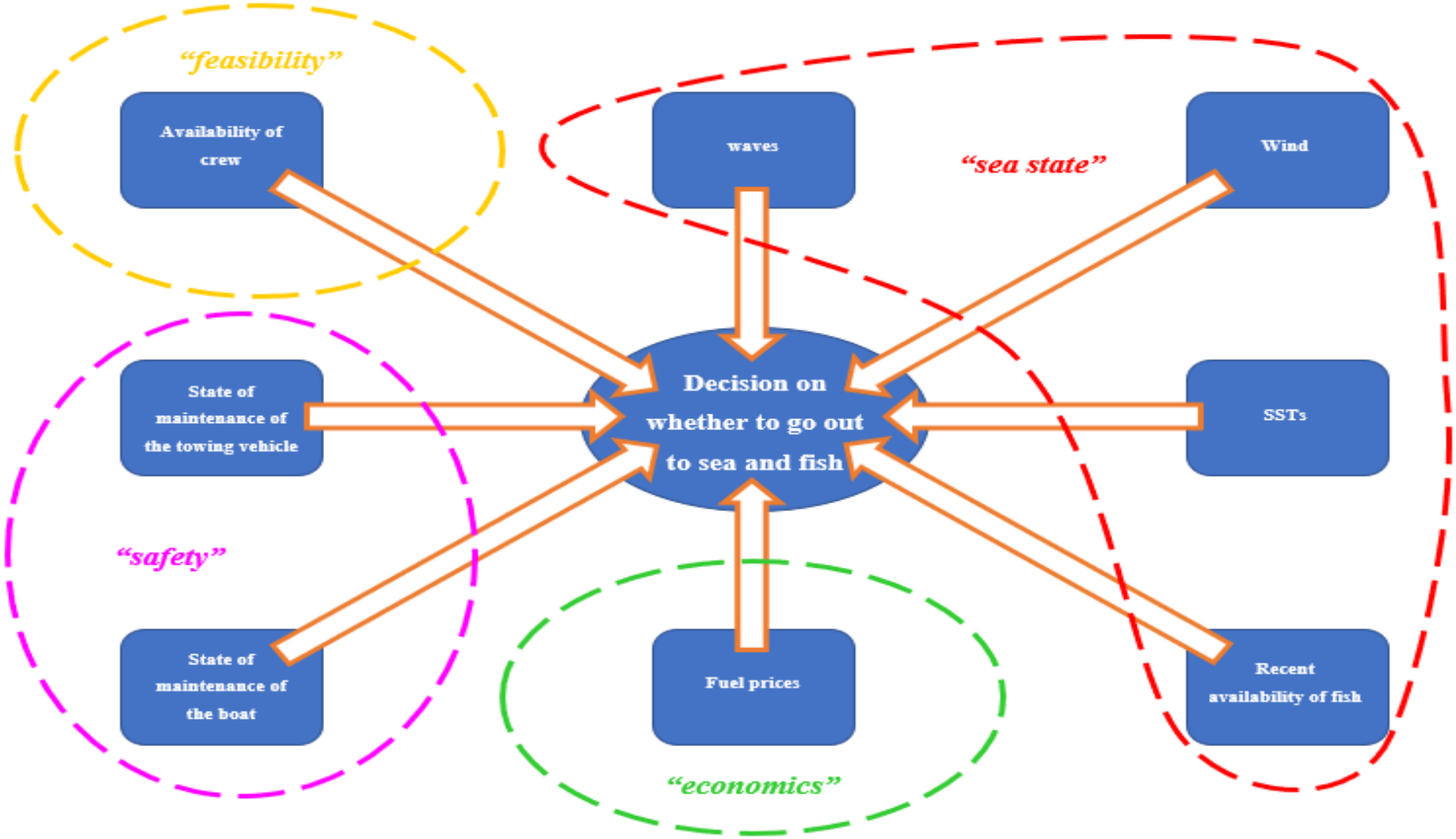

Fig. 2.7: *Different variables contributing to the decision on whether to go out to sea and fish based on fishers from Duggan (2012) and Gammage (2015).*

Short-term weather is usually the primary aspect of determining whether or not one should go out to sea; websites providing global wind and wave forecasts, like Windguru, are used to source wind and swell forecasts for the current day and the next few days. Of course, the weather in the immediate past also has considerable influence; for example, adverse launching conditions could imply adverse return conditions. Skippers also need to find good crew and will consider the amount of recent fishing activity, in terms of catches, biting, and available species. Often, the fishers correlate species availability to warmer or cooler temperatures – for example, highly valuable Kob is linked with warmer SSTs. Since most fishers are under economic pressure, considering all the possible factors that influence their ability to maximize their daily catch is important to make sure that they economically benefit from going out to sea. The current study focusses on waves as descriptors of sea state as one important aspect in these considerations.

2.3.2. Scientifically researched environmental changes:

While many changes in the southern Benguela ecosystem are strongly linked to overexploitation, some have also been attributed to environmental forces (Blamey et al., 2012). These can act both gradually and suddenly, and the affected ecosystem may respond by shifting abruptly to a different but long-lasting state that can substantially impact its biological components. This shift is usually referred to as a 'regime shift' (Blamey et al., 2012; Conversi et al., 2014). The late 1990s southward and eastward shift of Anchovy (*Engraulis encrasicolus*) and Sardine (*Sardinops sagax*) on the shelf have been linked with the increased productivity in the Agulhas Bank subsystem (including the South Coast) after 1996 (Blamey et al., 2012, 2015; Watermeyer et al., 2016). This eastward shift has also been observed for other inshore marine species like Rock Lobster (*Jasus lalandii*) and Kelp (*Ecklonia maxima*), although these shifts were prior to the mid-1990s (Rock Lobster) and post mid-2000s (Kelp). However, Kelp is thought to have been increasing Eastward for the past few decades (Blamey et al., 2012, 2015). One of the drivers of this eastward shift is the post-1996 cooling of the inshore shelf waters along the South Coast on the Agulhas Bank, east of Cape Agulhas (Roy et al., 2007; Blamey et al., 2012; Jarre et al., 2015). However, determination of this cooling trend is dependent on which data are used, as shown by Blamey et al. (2015). Such inconsistencies in findings have made assigning distinct causes to the observed environmental regime shifts in the southern Benguela system difficult.

Based on increased upwelling, some researchers have attributed the mid-1990s inshore cooling to an increase in upwelling-favourable winds (Roy et al., 2007; Blamey et al., 2012; Lamont et al., 2018). These are southerly and south-easterly along the South-West Coast and more easterly along the South Coast (Roy et al., 2007; Blamey et al., 2012). Roy et al. (2007) found a strong correlation between lower SSTs along the Central and Eastern Agulhas Bank coastal regions and more easterly winds. Blamey et al. (2012) detected shifts in mean austral summer (October-March) upwelling on the

Agulhas Bank, calculated from geostrophic winds from the period 1981–2010 (**Fig. 2.8**). They distinguished environmental regime shifts at Cape Agulhas in the late 1980s (1989) of increasing mean austral summer upwelling, and in the early 2000s (2002) of decreasing mean austral summer upwelling, however with a net increase over time (**Fig. 2.8 (a)**). Monthly upwelling variability was also shown to increase during the late 1980s (1989) and to a smaller degree again in the mid- to late-2000s (2007) (**Fig. 2.8 (b)**; Blamey et al., 2012). Working with the US National Centre of Environmental Prediction and the Department of Energy (NCEP-DOE) Reanalysis 2 wind product, Lamont et al. (2018) found an overall increasing trend of Total Cumulative Upwelling (TCU) on the Central Agulhas Bank from 1979–2015, with periods of high upwelling occurring from the early- to mid-1980s, mid-1990s to early 2000s, and 2007–2014 (**Fig. 2.9 (a)**).

Some regime shifts in easterly winds along the South Coast (east of Cape Agulhas, along the Agulhas Bank) detected by Ward (2018) occurred at similar times to the upwelling shifts and trends detected by Blamey et al. (2012) and Lamont et al. (2018). Data were sourced from the 32563 National Centre of Environmental Prediction (NCEP) point off the South Coast (22.5ºE, 35ºS) for the period 1979–2015 (Ward, 2018). Increasing mean easterly wind shifts were detected for the austral summer (October to March) during 1992/1993 and 2006/2007 (Ward, 2018). Additionally, a shift towards increasing variability in annual westerly-easterly winds was detected during 2006/2007 (Ward, 2018).

The southerly shift of the SAH has been considered one of the drivers of the cooler inshore SSTs observed along the South Coast during this time period (Jarre et al., 2015; Lamont et al., 2018). When the SAH shifts southwards, upwelling-favourable winds of south-easterly direction in the southern Benguela and easterly direction along the Agulhas Bank coasts strengthen, which increases coastal upwelling and decreases coastal SSTs. The opposite occurs when the SAH shifts northward (Blamey et al., 2015; Lamont et al., 2018). Jarre et al. (2015) found that the mean summer SAH latitudinal position shifted about 1.5º south in the late 1980s and remained there throughout the 1990s but started retreating northward again in the mid-2000s. Lamont et al. (2018) also found that the annual SAH centre location shifted towards the south in the 1980s and remained there until 2015, indicating a long-term southward shift (**Fig. 2.9 (b)**). This southward shift is significantly correlated with increasing TCU along the Central Agulhas Bank coastal region, because of the increase in upwelling favourable winds here when the SAH is located farther south (Lamont et al., 2018). This is also in accordance with the increase of the number of extreme wind days (>10 m/s) observed offshore of the South Coast for the period 1979–2015 during austral summer (October-March) by Ward (2018).

The southern Benguela is subject to various modes of variability. The dominant large-scale modes of climate variability over the southern hemisphere are the El Niño Southern Oscillation (ENSO) and the Southern Annual Mode (SAM) (Reason, Landman & Tennant, 2006; Rouault, Pohl & Penven, 2010). During a positive (negative) ENSO phase, also known as El Niño (La Niña) event, the SAH and subsequently the westerly wind belt shift northwards (southwards). Upwelling-favourable winds along

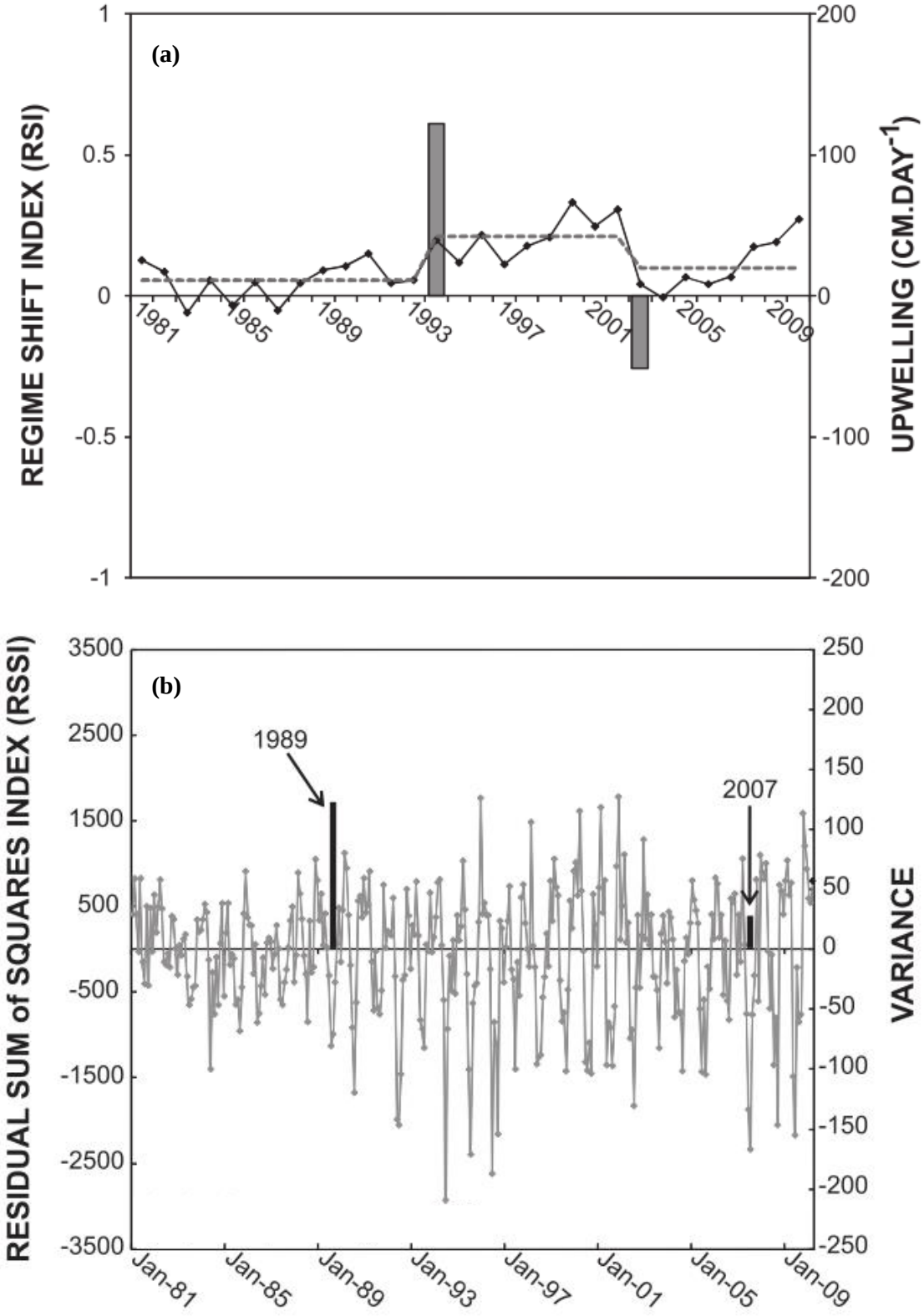

Fig. 2.8: *Sequential Regime Shift Detection (SRSD) analyses for Cape Agulhas 1981–2010, based on (a) mean annual summer (October-March) upwelling calculated using geostrophic wind data derived from monthly sea level pressure (black solid line with black dots = time series; grey dashed line = weighted mean; grey bars = regime shifts as determined by the Regime Shift Index (RSI)); and (b) variation in upwelling cycles (grey line = variability time series; black bars = regime shifts as determined from the SRSD method in variance index, known as the Residual Sum of Squares Index (RSSI) (adapted from Blamey et al., 2012).*

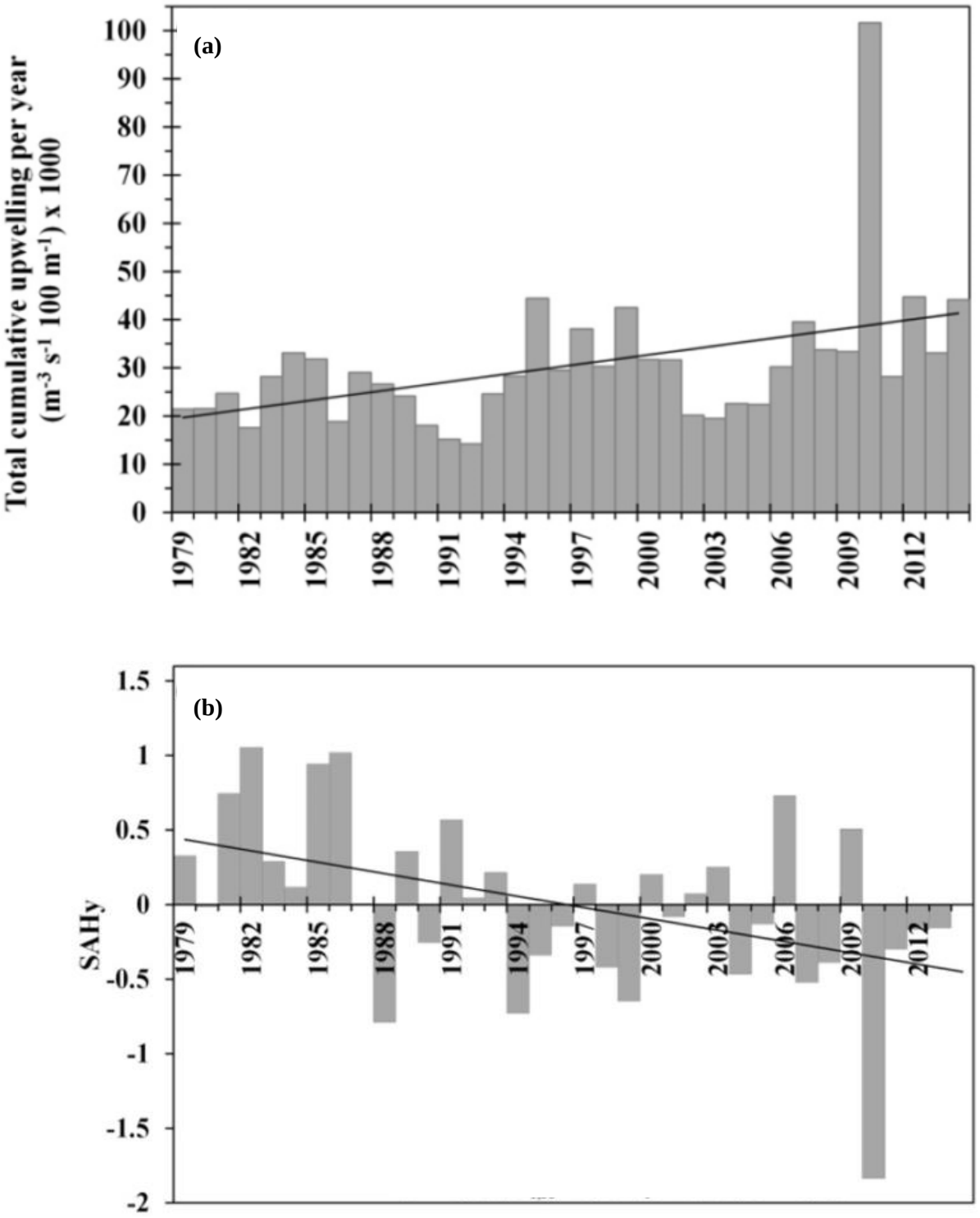

Fig. 2.9: *(a) Total Cumulative Upwelling (TCU) per year ($m^{-3}s^{-1}$ 100 m^{-1} × 1000) for the Agulhas Bank region (from 19–29°E) for the period 1979–2015 using daily averaged geostrophic wind data from the National Centre of Environmental Prediction – Department of Energy (NCEP-DOE) Reanalysis 2. (b) The meridional position (SAHy) anomaly of the South Atlantic high pressure system for the period 1979–2014 using monthly NCEP-DOE Reanalysis 2 sea level pressure. Solid black lines indicate significant linear trends (adapted from Lamont et al., 2017).*

the South Coast (**Fig. 2.10**) during El Niño (La Niña) in austral summer are weaker (stronger) and thus upwelling is weaker (stronger; Rouault, Pohl & Penven, 2010; Dufois & Rouault, 2012). The La Niña years of 2000/2001 and 2007/2008 (Dufois & Rouault, 2012) occurred around similar times as increases in upwelling-favourable winds along the South Coast observed by Blamey et al. (2012) and Lamont et al. (2018). However, while trends towards increasing upwelling-favourable winds along the South Coast have been observed, no trend towards more La Niña or El Niño years was found (Rouault, Pohl & Penven, 2010; Blamey et al., 2015).

During a positive (negative) SAM phase, the SLP over the Southern Ocean is above (below) average and over Antarctica is below (above) average, meaning that the westerly wind belt is located northwards (southwards) and wind speeds are below (above) average (Rouault, Pohl & Penven, 2010; Loveday, Penven & Reason, 2015). Studies have shown a trend towards a positive SAM phase since the 1950s (Hartmann et al., 2013; Loveday, Penven & Reason, 2015). The influence of ENSO has been significantly correlated with SST anomalies along the South Coast of South Africa during the austral summers and autumns of 1982-2008, while correlations between South Coast SST anomalies and SAM events are weakly significant during austral summers (Rouault, Pohl & Penven, 2010).

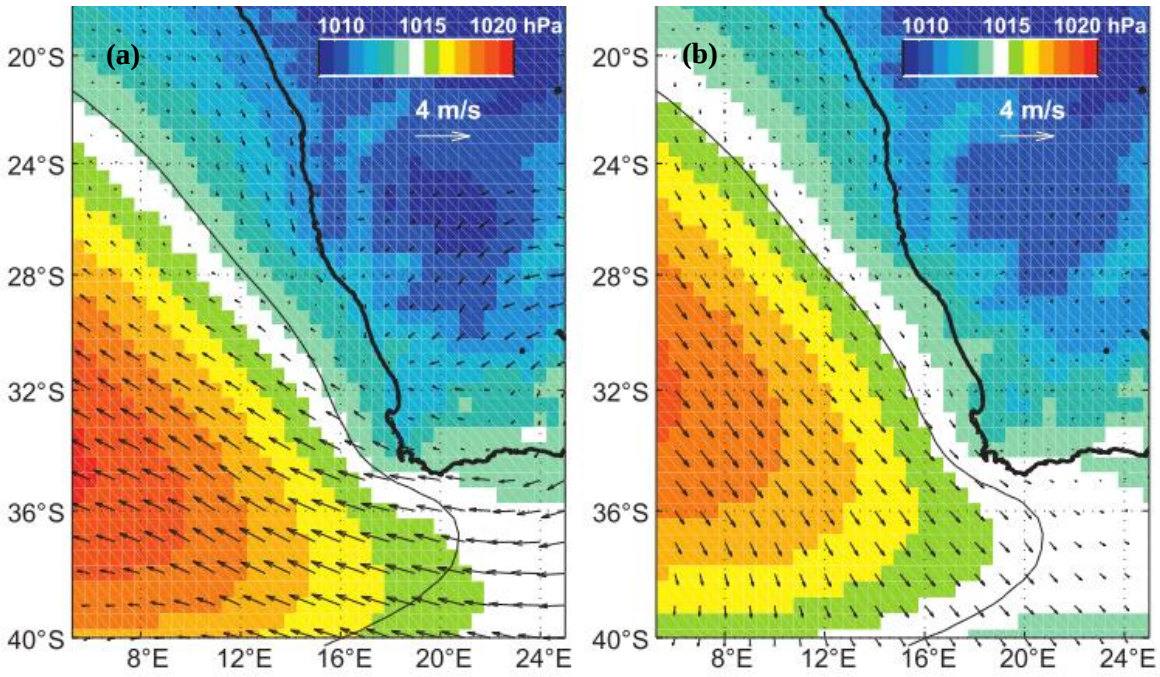

Fig. 2.10: *Summer average (December to February, 1981–2009) of sea level pressure (hPa) and monthly wind vector composites at 1000 hPa (m/s) during (a) La Niña years and (b) El Niño years, sourced form National Centre of Environmental Prediction (NCEP) reanalysis Climate Forecast System Reanalysis (CFSR). The black line shows the climatological 1015 hPa isobar during summer (from Dufois & Rouault 2012).*

2.4. Studying coastal waves:

2.4.1. Wave theory

A discussion of wave theory requires the definition of a number of terms: wave length, wave crest, wave trough, wave period, wave frequency and wave height (**Fig. 2.11**). Wave length is the distance between two successive points on a wave, such as between wave crests. Wave period is the time interval taken by two successive points on a wave to pass a fixed point. Wave frequency is the inverse of wave period in Hertz, defined as the number of wave crests that pass a fixed point in a second. Wave height is the vertical distance between the trough and the next crest (Trujillo & Thurman, 2014). When the varied ocean surface is observed, the highest waves tend to be the most noticeable; when measuring wave height, it has therefore become accepted to measure significant wave height (H_{m0}), which is defined as the average of the highest 1/3 of waves observed (Stewart, 2008; Akpinar & Kömürcü, 2012).

Surface gravity waves are referred to as deep-water waves (**Fig. 2.11**) if they travel through water much deeper than their wave lengths (Talley et al., 2011). Water particles in deep-water waves move in a circular motion. This motion exponentially decreases in diameter with depth until the base of the wave is reached, where no wave disturbances are present (Laing et al., 1998; Talley et al., 2011). Surface waves are referred to as shallow-water waves if they travel through water much shallower than their wave lengths. Instead of a circular motion, the particles move in elliptical paths (Talley et al., 2011). In practice, a phenomenon known as stokes drift occurs where the orbital motions of water particles in both types of waves do not return exactly to their original positions and instead slightly advance in the direction of wave propagation (Laing et al., 1998; Stewart, 2008).

i. <u>Wave generation and propagation:</u>

All waves are generated by an external force which disturbs the water particles out of their equilibrium state, while another force returns them back to their original position. For surface gravity waves generated by external force winds, the restoring force is gravity (Talley et al., 2011). As the wind blows across the ocean surface, it transfers energy into the surface, generating surface wind-waves. Wave energy and height are linked in the following expression:

$$E = \rho_w g H^2/8$$

where E is wave energy, ρ_w is water density, g is gravity and H is wave height (Laing et al., 1998; Hughes, 2016). Wind-waves are driven by local winds. They have short wave lengths and high wave frequencies (low wave periods) and travel at speeds slower than the forcing wind (Talley et al., 2011). Wind-waves grow exponentially (nonlinear growth) in height and increase in length with more energy input until the wave is too steep and breaks. Therefore, as local wind speeds, duration and fetch area (area affected by wind) increase, so will wave height and length (Laing et al., 1998).

Waves radiate out from areas of generation and propagate perpendicular to their wave crest (Laing et al., 1998). As waves propagate out and the fetch area and/or winds decrease, wave length increases and more uniformly symmetrical (sinusoidal-shaped) waves emerge, known as swell (Laing et al., 1998; Talley et al., 2011). Swell has a higher wave period (lower wave frequency) than wind-waves (Talley et al., 2011), and can propagate out of the fetch area and far across the ocean without additionally input of wind energy, while still retaining most of the original wave height and energy (Laing et al., 1998; Talley et al., 2011). Swell is thus remotely generated, mostly by storms. In deep water, swell waves leave the generation area before other wave types because long waves travel faster than short ones (Hanley, Belcher & Sullivan, 2010).

The open ocean surface is however forced by varying winds speeds and directions on multiple time and space scales, and thus waves with varying frequencies and lengths coexist. The sea surface is therefore often described as a spectrum of waves (Laing et al., 1998; Stewart, 2008; Talley et al., 2011). Usually the spectrum is described in terms of the above wave energy equation, i.e., as defined by wave frequency and energy with respect to wave height. A wave spectrum is a continuous curve connecting discrete frequencies with corresponding wave energy densities. Therefore, wave energy density-frequency spectrums usually describe the sea surface in terms of statistics (H_{m0}, peak wave period and direction) rather than absolute values. Given the height of a wave and the wind speed, the wave period can then be determined from the frequency part of the spectrum (Laing et al., 1998; Arnott, 2009). There are many different types of spectra used to model the sea surface. For example, the JOint North Sea WAve Project (JONSWAP) spectrum (developed by Hasselmann et al., 1973) is used to describe the energy density spectrum of different stages of wave growth under a constant wind in deep water.

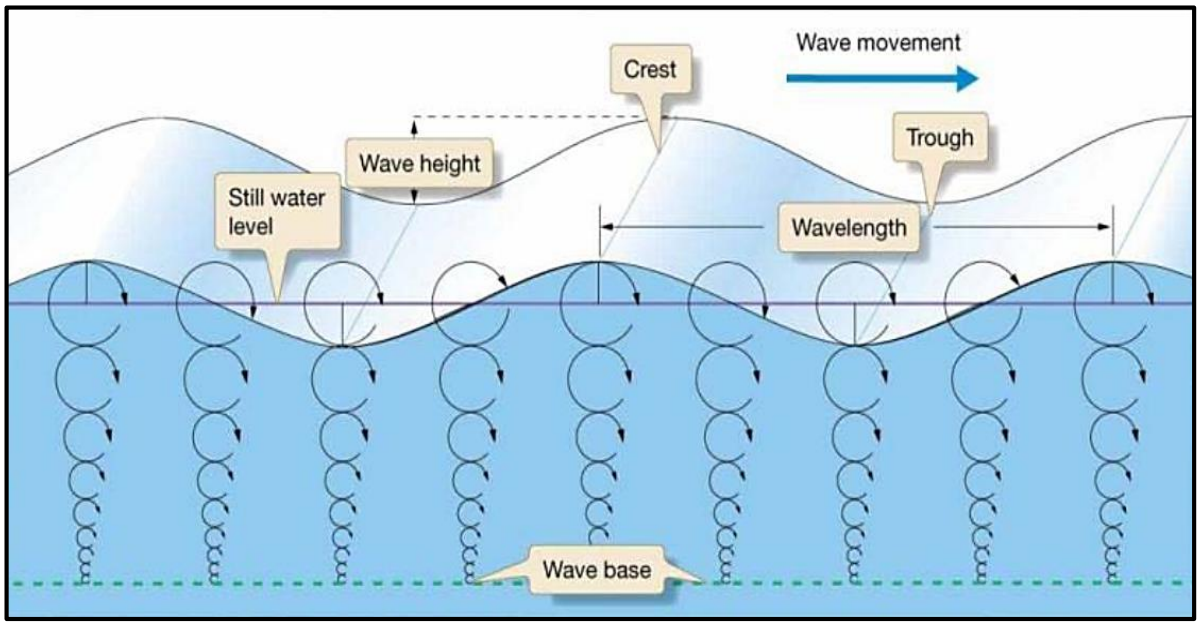

Fig. 2.11: *Schematic illustration of a linear, sinusoidal surface deep-water wave (from Trujillo & Thurman 2014).*

ii. From deep-water to the coast:

When deep-water waves propagate across shallow water, wave properties transform under the influence of shoaling, refraction, diffraction, reflection and bottom effects, and result in shallow-water waves (Laing et al., 1998). As deep-water waves encounter shallower depths, the base of the waves interacts with the sea floor, friction with the sea floor causes it to slow down, energy dissipates, and wave height decreases (Laing et al., 1998; Folley & Whittaker, 2009). Waves also shorten, thus becoming shallow-water waves but maintaining their original wave period and frequency (Laing et al., 1998; Stewart, 2008; Talley et al., 2011). This occurs before the surf zone, where wave-bottom interactions dominate (Laing et al., 1998).

Simultaneously, refraction can occur. If waves approach the coast at an angle (**Fig. 2.12 (a)**), the wave segments in deeper water will travel faster than the ones in shallower water. This results in refraction as wave fronts bend towards the shallower part to become more parallel with the coastline (Laing et al., 1998; Talley et al., 2011). On irregular coastlines, refraction unevenly distributes wave energy and thus wave heights along the shore. When refraction occurs in a bay, the lines of wave energy propagation (orthogonal lines) spread out along the shore (**Fig. 2.12 (b)**), diffusing wave energy and hence decreasing wave heights. The opposite is the case with refraction around shoreline extensions (for example headlands) where increased wave heights result from the focussing of wave energy along the shore (Laing et al., 1998; Stewart, 2008; Talley et al., 2011).

While the wave height initially decreases in shallow water, shoaling begins to occur close to the shoreline in the surf zone. This process refers to wave height starting to exponentially increase to conserve wave energy (Laing et al., 1998). After a certain point the wave's energy cannot be conserved any further, and the wave breaks to release the energy. The breaking point typically occurs when wave steepness (wave height/wave length) is larger than 1/7 and/or when the ratio of wave height to water depth ratio is 0.8 (Talley et al., 2011; Trujillo & Thurman, 2014). As a result of this energy loss, wave height decreases in the surf zone (Laing et al., 1998; Folley & Whittaker, 2009). As noted above, waves can also break after reaching a critical height through wind energy input. This is known as whitecapping. In deep water, where the sea floor does not interact with wave bases, whitecapping constitutes the primary mechanism for dissipating energy and height (Laing et al., 1998).

Diffraction and reflection are phenomena that can also occur at the coast when waves encounter obstructions. Diffraction, like refraction, is a process where the wave direction changes but in the case the translocation of energy along the wave crest to sections around and behind the obstruction, where of diffraction it is a result of physical obstruction by features such as headlands. The obstruction causes waves are lower (Laing et al., 1998). Reflection of incident waves and energy back to deep waters may occur off an obstacle or a beach (Laing et al., 1998; Talley et al., 2011).

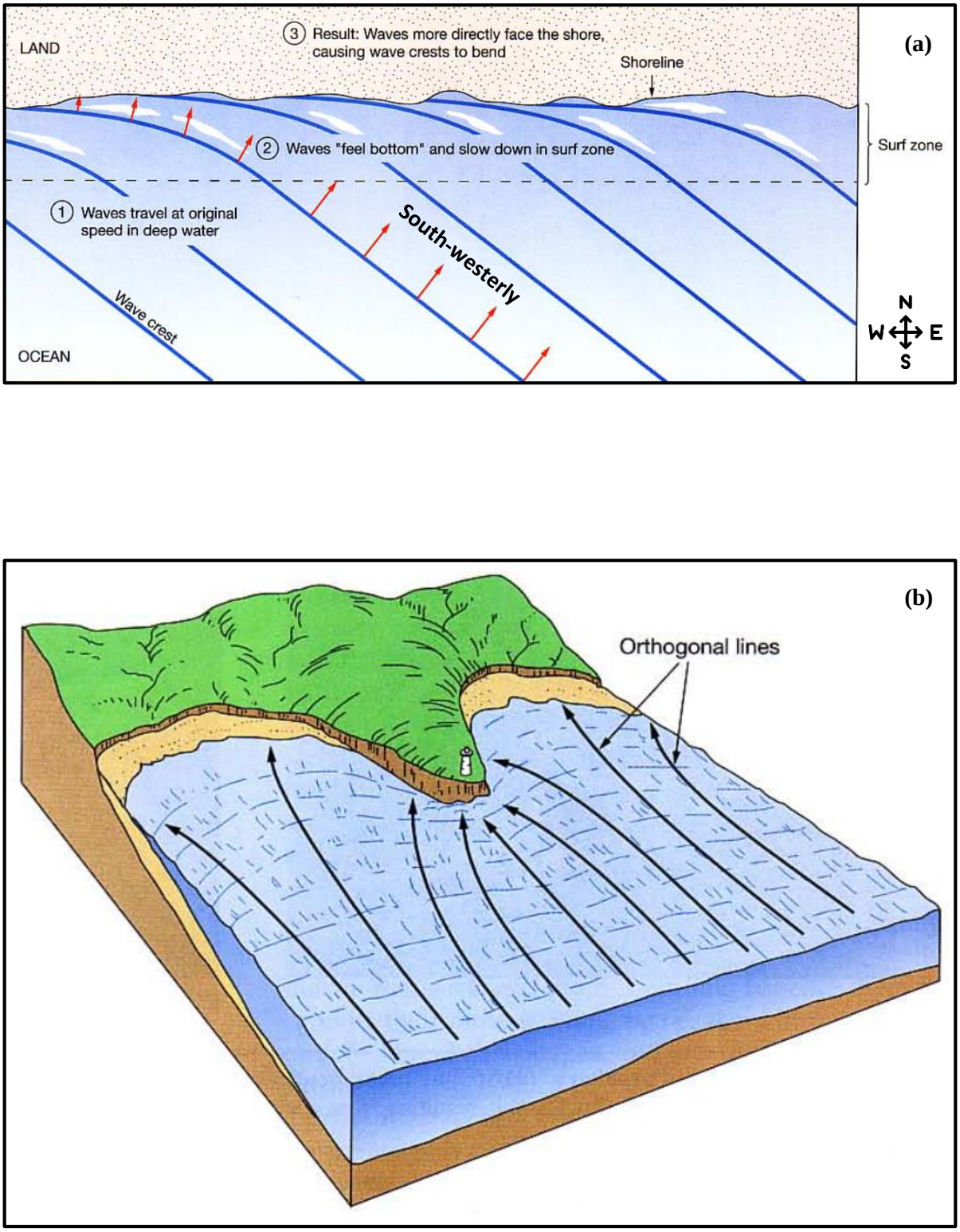

Fig. 2.12: *Wave refraction of (a) waves travelling at an angle to the shore, and of (b) waves interacting with an irregular coastline. Orthogonal lines indicate the lines of wave energy propagation (from Trujillo & Thurman 2014).*

iii. Waves at the coast:

Waves at the coast consist of both swell waves, which originate from far away, and wind-driven waves which originate closer to the coast (Laing et al., 1998). At distant coasts, swell arrives in narrow-band frequency sets, with the lowest frequency waves arriving first (Laing et al., 1998). Swell-generated coastal waves consist of fairly parallel lines of relatively uniform sinusoidal breakers (Trujillo & Thurman, 2014). They will most likely interact with the sea floor before wind-waves because they have longer wave periods (Arnott, 2009). Local wind-driven coastal waves are not well sorted at the coast, and consequently induce rougher and choppier coastal sea states. These waves are considered high-energy waves and are associated with strong winds (Arnott, 2009; Trujillo & Thurman, 2014). Consequently, wave heights at the coast can increase when wind-waves are produced and are superimposed onto swell (Arnott, 2009; Remya & Kumar, 2013). As noted above, this is known to occur as a result of onshore and offshore winds such as sea-land breezes (Sonu et al., 1973; Remya & Kumar, 2013).

2.4.2. Third-generation wave models:

Models are used to study geophysical systems because the large spatial and temporal scales involved often prevent researchers from carrying out sufficient experiments or observations (Casas-Prat & Sierra, 2010; Edwards, 2011). However, such model results are inherently uncertain because models cannot capture the full system; many components are not yet fully understood, observational data sets of boundary conditions are commonly incomplete or inaccurate, and available computational power is insufficient. Consequently, many components and processes are simplified, estimated and assumed (IPCC, 2001; McGuffie & Henderson-Sellers, 2005; Stewart, 2008). The spatial resolution of models is often limited by available data and computation time. Additionally, many model calculations are discretised into discrete spatial and temporal steps because the model equations do not have steady-state solutions. Processes of finer spatial and temporal resolution may therefore be ignored by model computations. Lastly, models are forced by either observational or modelled data; the former may suffer from gaps or short observational records, while the latter is inherently uncertain, as noted above. Consequently, the data used to force some models can enhance the uncertainty in their results. The repeated validation of model results by observational data is therefore desirable. Therefore, considering the above, models are currently one of the best numerical representation of the real world (McGuffie & Henderson-Sellers, 2005).

Numerical wave models use numerical computations to simulate waves based on wave theory principles (Thomas & Dwarakish, 2015). Third-generation numerical wave models are considered to offer more realistic simulations of natural wave systems than their predecessors (Arnott, 2009). Third-generation wave phase-average models can simulate the generation, evolution and dissipation of

nonlinear ocean surface waves over time and space domains by employing Eulerian energy or action balance equations (Booij, Ris & Holthuijsen, 1999). The WAve Model (WAM) model (developed by the WAve Model Development and Implementation (WAMDI) Group was the first third-generation model and provides the underlying structure of wave transformation models like WaveWatch III (developed by National Oceanic and Atmospheric Administration (NOAA)) and SWAN (developed by the Delft University of Technology) (WAMDI Group, 1988; Booij, Ris & Holthuijsen, 1999). Both the WAM and WaveWatch III models are better suited for deep or shelf waters, away from obstacles, because they cannot account for the diffraction and nonlinear wave propagation that may occur at the coast. Regardless, both models do account for some shallow-water processes such as wind generation, whitecapping, bottom dissipation and nonlinear quadruplet (deep-water) wave-wave interactions (Booij, Ris & Holthuijsen, 1999). More details on the WAM and WaveWatch III models are given by WAMDI Group (1988) and Booij, Ris & Holthuijsen (1999), respectively.

2.4.3. The Simulating WAves Nearshore (SWAN) model:

Unlike WAM and WAVEWATCH III, the SWAN model can simulate the transformation of waves from offshore to nearshore for shallow coastal regions with ambient currents (Booij, Ris & Holthuijsen, 1999; Folley & Whittaker, 2009; Thomas & Dwarakish, 2015). It accounts for wave energy propagation through third-generation model formulations of wave generation (energy transfer from wind to wave, and nonlinear quadruplet and triad wave-wave interactions which are characteristic of shallow waters) and dissipation (through whitecapping, bottom friction, depth-induced breaking and negative nonlinear triad wave-wave interactions), as well as non-dissipative processes (refraction and shoaling). The model is thus driven by both wave and wind boundary conditions. The inclusion of formulations for nonlinear triad wave-wave interactions and depth-induce breaking is new to these kinds of models (Booij, Ris & Holthuijsen, 1999; Thomas & Dwarakish, 2015). Details of the formulations in the SWAN model are given in Booij, Ris & Holthuijsen (1999).

The SWAN model is based on solving the Eulerian discrete spectral action balance equation that produces the evolution of the action density in time and space (Booij, Ris & Holthuijsen, 1999; Folley & Whittaker, 2009). This is implemented as implicit numerical propagation schemes based on finite differences, because explicit propagation schemes are unsuitable for use in coastal simulation (this approach is also new to this kind of wave model) (Booij, Ris & Holthuijsen, 1999). Action density is the energy density divided by wave frequency, and unlike energy density, it is conserved in the presence of currents and accounts for refraction (Booij, Ris & Holthuijsen, 1999; Folley & Whittaker, 2009). SWAN is therefore fully spectral in all directions and frequencies over any water depth and current field, and can account for wave energy propagation (Theron et al., 2014). Specific SWAN model outputs include the wave statistics (H_{m0}, peak wave period and direction) that correspond to the peak of the JONSWAP spectrum (Arnott, 2009).

SWAN model outputs for the coast of South Africa have been used and successfully validated at several sites using measurement data (Baloyi et al., 2009; Joubert & van Niekerk, 2013; Rossouw, Terblanche & Moes, 2013; Theron et al., 2014; Rossouw et al., 2015). For example, Baloyi et al. (2009) used the SWAN model to study sediment transport near the port of Ngqura in the south-eastward-facing Algoa Bay on the South African South-East Coast. SWAN model outputs (H_{m0}, peak wave period and direction) were validated against recordings from the Integrated Port Operation Support System (IPOSS) Waverider buoy (33.822528°S, 25.692778°E) over the period from the 1st of January to the 1st of May 2013. Model outputs agreed well with the buoy's data, and the model was considered adequate to simulate waves around Algoa Bay. The modelled waves travelled in southerly and south-westerly direction towards Algoa Bay during both January and July, and their height dissipated as they approached the shore. But during the July snapshot, the Bay on average contained waves with higher H_{m0} compared to the January map. On both maps, a wave height shadow is evident on the west side of the Bay (Baloyi et al., 2009).

CHAPTER 3: Data and Methods

3.1. Data background:

The available Simulating WAves Nearshore (SWAN) model wave outputs (significant wave height (H_{m0}), peak wave direction and period) used in this study were generated under the Department of Environmental Affairs and the Council for Scientific and Industrial Research (DEA-CSIR) South African Coastal Vulnerability Assessment phase 2 project, for the period of 1997-01-30 to 2013-12-01, forced by wind (wind direction and speed) and wave (H_{m0}, peak wave direction and period) model outputs from NCEP, produced by the WaveWatch III model (hereafter, 'the NCEP model'). In this case, the SWAN model was run within the DELFT3D numerical model suite (Theron et al., 2014). The SWAN model wave outputs created in the DEA-CSIR project were developed by, firstly, collecting high resolution bathymetry data from the South African Navy Hydrographic office (SANHO) standard bathymetry charts, as well as any other detailed bathymetric surveys available. Numerical model nested grids of 1 km and 0.5 km were set up for about 20 modelled areas, covering about 100 km of the South African shoreline. The SWAN model wave output locations were predetermined at the 7 m and 15 m isobaths (depth contours) in each modelled area, at distances of 0.5 km from each other (Theron et al., 2014).

After the bathymetry data was collected, each modelled area was forced by various combinations of the wind and wave model outputs from the nearest NCEP model grid point, resulting in a range of nearshore high-resolution wave conditions for the corresponding modelled area. For each modelled area, the resultant wave conditions were plotted on scatter plots, from which occurrences of values were sampled at varying frequencies (discrete conditions) depending on concentrations observed on the scatter plot (higher concentration, higher sampling frequency). For each modelled area, using the sampled input wave conditions and corresponding wave outputs, transformation coefficient tables (look-up tables of representative conditions) were created. These tables were then used to convert the 17 years of wind and wave model outputs from the corresponding NCEP model grid point into SWAN H_{m0}, peak period and wave direction nearshore time series for each SWAN output location within the corresponding modelled area. These tables can thus be used to determine which offshore conditions along the South African coastline will result in which adjacent nearshore wave conditions (Theron et al., 2014).

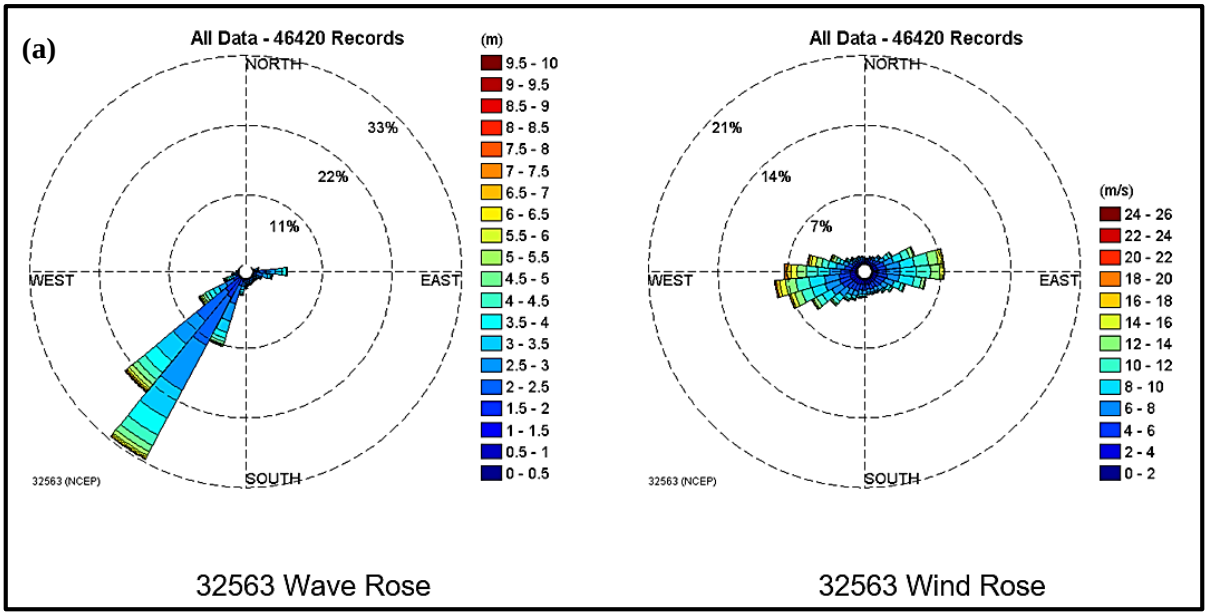

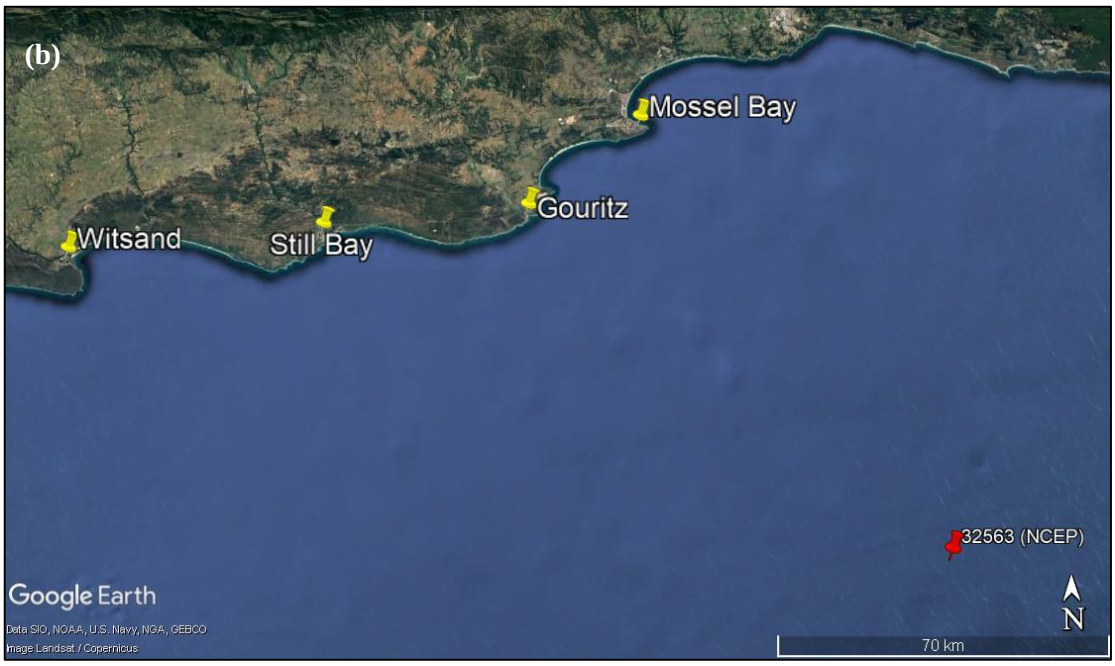

Fig. 3.1: *(a) The wave and wind roses of the 32563 National Centre of Environmental Prediction (NCEP) numerical data point (22.5ºE, 35ºS). Wind and wave model outputs from this point drives the nearshore local-scale Simulating WAves Nearshore (SWAN) model wave outputs over 17 years (1997-01-30 to 2013-12-01) for the Mossel Bay and Still Bay (including Witsand and Gouritz) modelled areas in the Department of Environmental Affairs and the Council for Scientific and Industrial Research (DEA-CSIR) project. The roses indicate direction (North, South, East, West) and magnitude (colour bar), and frequency of occurrence of magnitudes and directions (dashed circles) (from Theron et al., 2014). (b) The locations of the traditional handline fishing towns along the South Coast of South Africa and the 32563 NCEP data point that are of interest for this study.*

The specific SWAN model wave outputs analysed in this study came from the Still Bay and Mossel Bay modelled areas (SBMA and MBMA), which were forced by NCEP model wind and wave outputs from the 32563 NCEP grid point, located at 22.5ºE and 35ºS, about 100 km offshore of the South Coast (**Fig. 3.1**). Within the SBMA and the MBMA, eight SWAN wave outputs were extracted from four fishing towns known to contain the launch sites used by the South Coast traditional handline fishers – Witsand and Still Bay in the SBMA, Gouritz and Mossel Bay in the MBMA (**Figs. 3.1-3.3**). These eight SWAN wave outputs came from four of the 7 m and four adjacent 15 m isobath SWAN model outputs near the main launch site or slip way used in each fishing town. Hereafter, the eight model outputs per fishing town are referred to as the 'study sites'. These study sites were chosen because the nearshore local-scale wave conditions near the launch sites are expected to be well correlated with fisher's decisions on whether they can launch their boats and return safely to shore (i.e., contributing to the number of possible sea-days). In the case of Witsand and Gouritz, the study sites are near river mouths, while the actual launch sites are in the river estuaries. The small waves in the rivers are considered a negligible factor when considering launching boats. Since river mouth conditions are influenced by the nearshore waves, exiting the river mouth is, however, a deciding factor with regard to launching. The Still Bay and Mossel Bay model sites are located near local harbours from which the boats launch. All four sites were therefore considered acceptable choices for providing information on the South Coast nearshore local-scale wave climate.

The SWAN model produces three different simulated wave time series per model output: (1) wind-waves, (2) swell and (3) combined wind-waves and swell. In this study the (3) combined wind-waves and swell are analysed because they represent total wave climate, one of the factors which affect fishers' decision to launch. Before SWAN and NCEP model outputs could be analysed, both had to be corrected because missing values and duplicated timesteps are not accepted by the Empirical Mode Decomposition (EMD) method used in this study. The duplicated timesteps originate from NCEP model outputs, where two midnight timesteps (00h00 and 24h00) exist for the first day of each month for the period of February 1997 to December 2010. As a result, the SWAN model outputs included duplicated midnight timesteps, as well as missing values. The 00h00 timestep was removed from the NCEP and SWAN model outputs analysed in this study because it is part of the model 'spin up' for the day runs, making the 24h00 timestep more reliable. Since the EMD method only works on continuous time series, the missing values in SWAN model outputs had to be interpolated from the value preceding and following it. As none of the data gaps exceeded a length of one timestep, there were no abrupt changes in values and linear interpolation was therefore considered appropriate. The corrected NCEP (hereafter, 'NCEP time series') and SWAN time series consisted 3-hourly timesteps from 1997-01-30-03h00 to 2013-11-30-24h00. Additionally, before any analysis, the SWAN time series of each wave parameter was spatially averaged across the study sites (**Figs. 3.2-3.3**). This provides a single average time series of each SWAN wave parameter per study site (hereafter, 'SWAN time series').

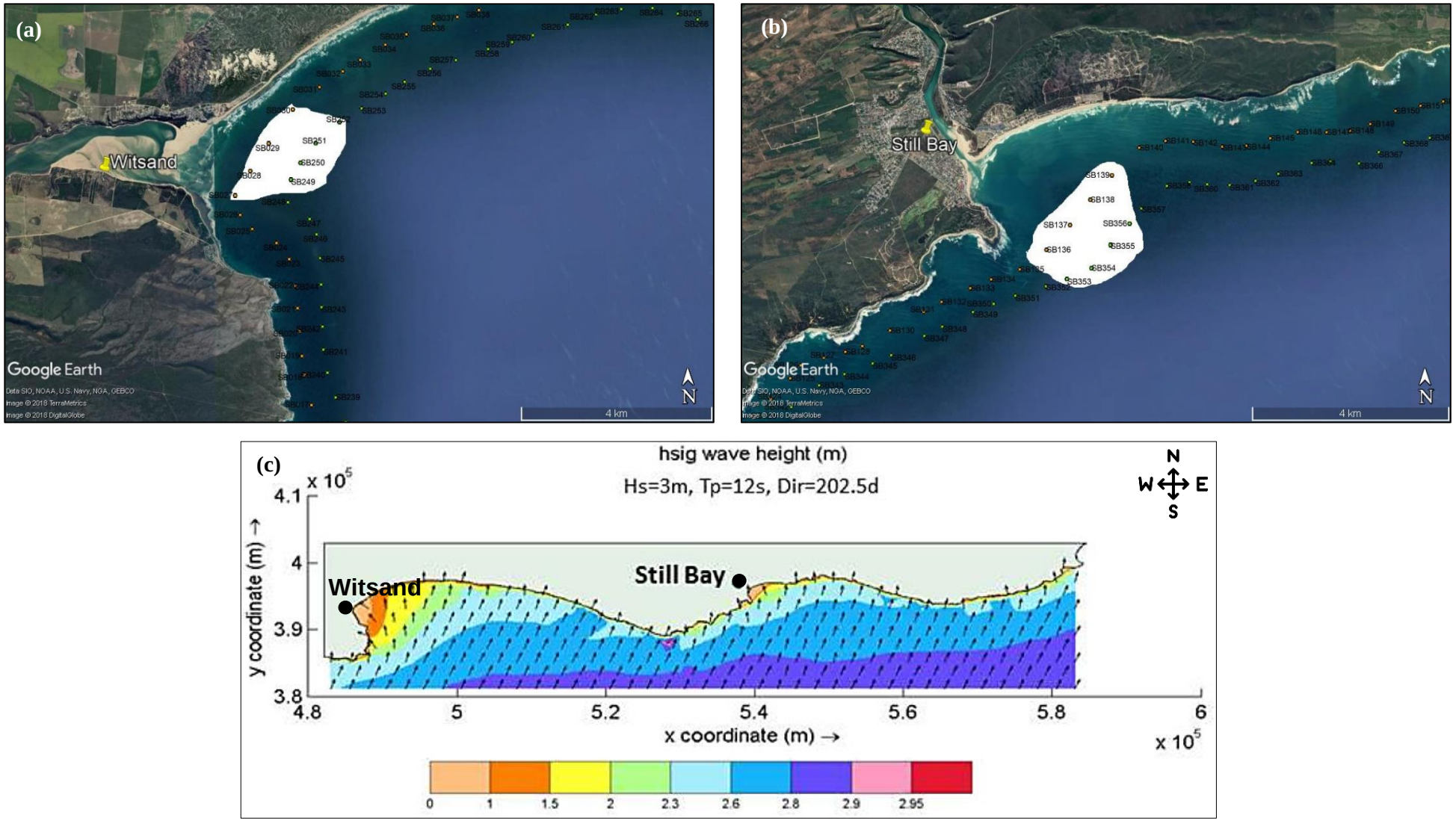

Fig. 3.2: *The eight Simulating WAves Nearshore (SWAN) model outputs representing the study sites of (a) Witsand and (b) Still Bay within the Still Bay modelled area (SBMA), outlined by white shapes. SWAN model outputs along the 7 m and 15 m isobaths are indicated by orange and green dots, respectively. (c) SBMA vector plot of significant wave height (H_{m0}, colour contours) and wave direction (arrows) with a forcing of a 3 m high (Hs) and 12 s period (Tp) swell, approaching at an angle of 202.5° from true north (adapted from Theron et al., 2014).*

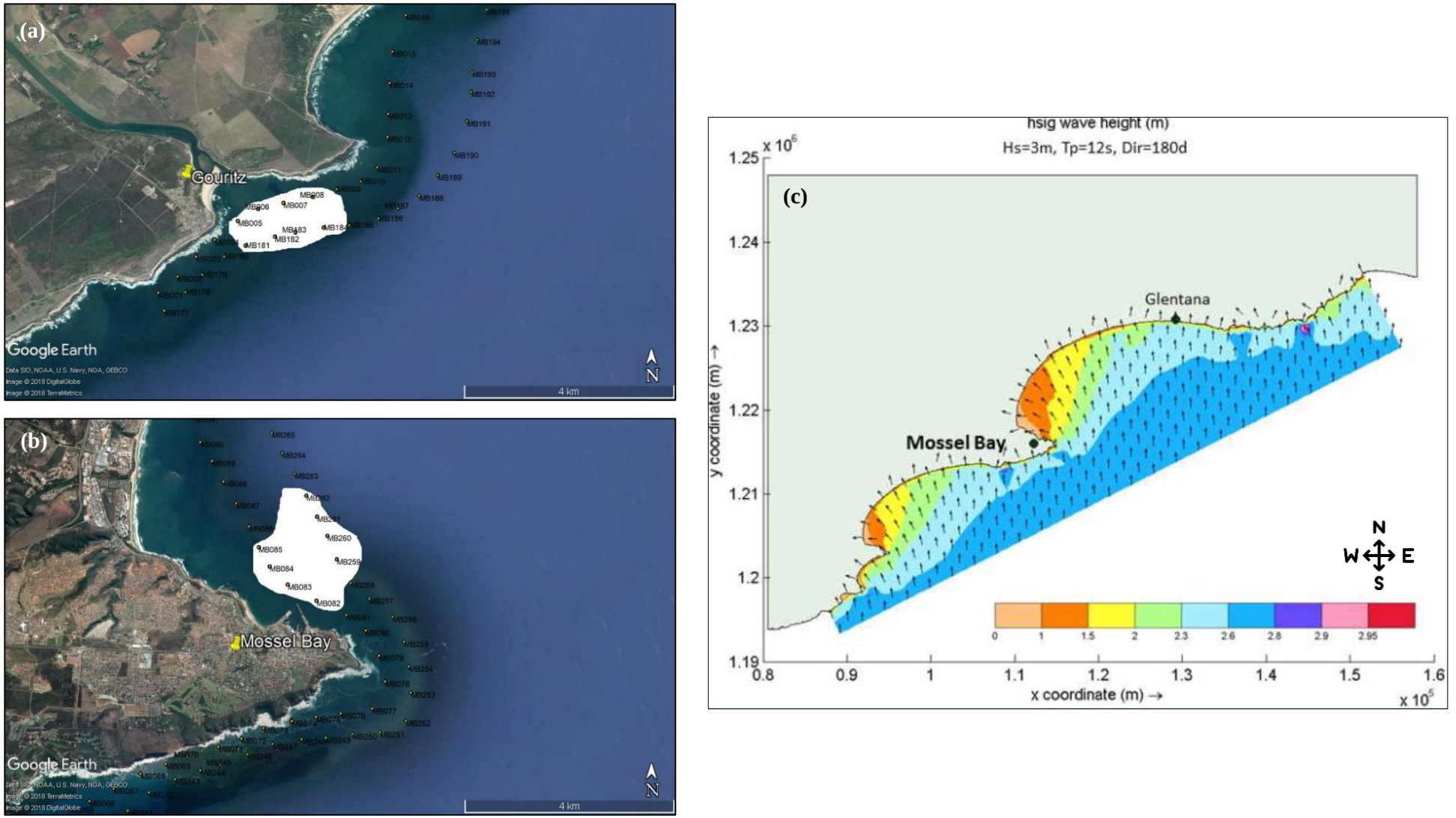

Fig. 3.3: *The eight Simulating WAves Nearshore (SWAN) model outputs representing the study sites of (a) Gouritz and (b) Mossel Bay within the Mossel Bay modelled area (MBMA), outlined by white shapes. SWAN model outputs along the 7 m and 15 m isobaths are indicated by orange and green dots, respectively. (c) MBMA vector plot of significant wave height (H_{m0}, colour contours) and wave direction (arrows) with a forcing of a 3 m high (Hs) and 12 s period (Tp) swell, approaching at an angle of 180º from true north (adapted from Theron et al., 2014).*

The NCEP and SWAN time series analyses were performed using the full time series and/or only the summer periods of each variable. Summer was chosen as a focus for the study because it is the time when Kob will move inshore, and therefore defines the main fishing season. The full time series comprises of all model outputs from 1997-01-30-03h00 to 2013-11-30-24h00 (hereafter, 'full time series or period'), while summer period refers to the three month southern hemisphere summer period (December to February (Ward, 2018)) of each year within the full time series. Summer, for example in 1997, is defined as December 1997, January 1998, and February 1998. Since the time series ends in November 2013, the summer of 2013 is not included in the summer time series, which thus consists only of the summer months of 1997–2012. In line with Ward (2018), southern hemisphere autumn months are March to May, winter months are June to August, and spring months are September to November. Furthermore, 'austral summer' is considered to last from October to March and 'austral winter' from April to September, likewise in line with Ward (2018).

3.2. Data validation and discrepancies:

The 32563 NCEP H_{m0} model outputs were recently validated against Jason-2 satellite altimetry data and the FA platform buoy (Barnes, 2018). Barnes (2018) found the statistical comparisons (bias, root mean square error, slope of line of best fit passing through origin, scatter index, Will-mott index of agreement) between the satellite-and-NCEP datasets and buoy-and-NCEP datasets show 'good agreement' with one another (details in Barnes (2018) study). The 32563 NCEP model outputs used in this study are, therefore, considered to accurately reproduce the wave climate offshore of the South Coast of South Africa.

The SWAN model outputs of the DEA-CSIR project were validated using measurements obtained from the CSIR Waverider buoys (Theron et al., 2014). The only available buoys were located near Slangkop (18°10.6'E, 34°7.6'S offshore of Kommetjie), near Port of Ngqura in Algoa Bay (25°43'E, 33°50'S), and offshore of the Port of East London (27°55'E, 33°2'S). A comparison was also performed between measured data at Slangkop and two output locations near St Helena Bay. This was deemed acceptable because the Slangkop location well simulated the general wave climate for the entire South-West Coast (Theron et al., 2014). SWAN outputs agree well with the measured data along the South African coast within the southern Benguela, with Slangkop outputs showing better agreement than East London due to the NCEP model simulating wave conditions of the South Atlantic Ocean better than those along the East Coast. NCEP model wave condition simulation discrepancies between the West and East Coast are attributed to the added influence of the Agulhas current off the East Coast and the higher resolution of wind conditions over the West Coast region (Theron et al., 2014).

Discrepancies may also arise due to assumptions made in the production of the SWAN model outputs and those inherent in the model itself. The SWAN model run performed in the DEA-CSIR project did not accounted for the influence of flow on waves (for example, currents), nor for diffraction; as for the WAM and NCEP models, the area over which simulations are performed must be located a few wavelengths away from vertical protruding obstacles such as harbours (Booij, Ris & Holthuijsen, 1999; Thomas & Dwarakish, 2015). The SWAN model was set up in stationary mode, meaning that a uniform offshore NCEP wind field (specific to each NCEP point) was forced across the entire corresponding SWAN modelled area for the entire duration of each timestep (in this case 3 hours). It is therefore assumed that the time taken for waves produced by these winds to propagate from the boundary to the shore is shorter than the time taken for offshore wind conditions to change.

As a result of the assumption of the JONSWAP spectrum used in the simulation, the SWAN model usually overestimates the energy of developing waves with low frequencies (long periods) for very short distances from the shore, because wave conditions are simplified by using an *a priori* wave spectrum (Booij, Ris & Holthuijsen, 1999; Thomas & Dwarakish, 2015). In other words, forcing the SWAN model with a uniform wind field produces nearshore waves that do not contain the full spectrum of wind-waves. However, for most of the modelled areas of the Theron et al. (2014) study, this is a fairly reasonable assumption to make because most of the South African coastline is very exposed and therefore, the application of a uniform wind field is accurate because the resulting wind-waves are fairly similar across the area as no obstructions are present to influence the waves, besides the bathymetry very close to the shore (Joubert & van Niekerk, 2013). Additionally, despite the fact that uniform winds are used, Theron et al. (2014) in their validation show that the SWAN models provide a reasonably accurate representation of the wave conditions along the South Coast. Overall the SWAN model has been considered to be working acceptably well along the South African coast (Theron et al., 2014).

3.3. Data analysis:

3.3.1. General wind and swell characteristics:

Synoptic-scale wind roses as well as offshore synoptic-scale and nearshore local-scale wave roses were created in MATLAB (version: 9.1.0.441655 (R2016b)) to characterise the general wind and swell characteristics of the South Coast in terms of direction and magnitude. NCEP model outputs used to force SBMA and MBMA were used to create full and summer time series synoptic-scale wind roses and offshore synoptic-scale wave roses. SWAN model outputs per study site were used to create full and summer nearshore local-scale wave roses for each study site. The following wind rose parameters were used: maximum circle frequency 21%, number of circle frequencies 3, number of directions 36. Wave roses used the same parameters except for a maximum circle frequency of 75%.

To derive an overview of the summer synoptic-scale wind climate and the nearshore local-scale wave climate of the South Coast, normalised Probability Density Functions (PDFs) and histograms of summer NCEP wind speed, summer SWAN peak period and summer SWAN H_{m0} were produced in MATLAB (version: 9.1.0.441655 (R2016b)) for each study site. Both representations show the relative density of a given value of the parameter of interest, indicating parameter distributions and central tendencies. The PDF type used in this study determines the underlying normal distribution. The histogram type used here is known as a PDF estimate histogram where the area of each bar is the relative frequency of the corresponding class, and the sum of the bar areas is less than or equal to 1. The histogram provides a discretization of the continuous PDF.

The statistical difference between the study sites, in terms of their peak periods and their H_{m0}'s, were tested in MATLAB using a two-sample t-test function ('ttest2'). Therefore, six tests were run between two study sites peak periods and six tests were run between two study sites H_{m0}'s. Assumptions made here were that the variable (either peak period or H_{m0}) of both study sites being tested have the same mean and variance (although unknown), both are normally distributed, and that each value of the variable given is sampled independently. Results are in **Appendix A**. The test showed whether or not the two variables tested have the same mean and variance, the PDF distributions show that the time series are normally distributed, and each value was sampled per time series (i.e., independently).

3.3.2. Daily variability:

Since fishers use the morning sea state (around 06h00) as one of the factors in deciding whether they can return safely in the afternoon (around 15h00), the daily variability of wave climate is an important component. The change and variability of the difference between SWAN H_{m0}'s at 06h00 and 15h00 during the summer time series were analysed per year from 1997–2012 and study site. Additionally, the same H_{m0} daily difference summer time series were used to produce annual boxplots from 1997–2012 per study site due to the available summer months. Boxplots are an effective way to visualise the distribution of data.

3.3.3. Empirical Mode Decomposition (EMD):

Variability and trends of the nearshore local-scale wave climate were analysed using the EMD method (Huang et al., 1998). EMD has previously been used to analyse nonlinear and nonstationary time series such as coastal sea surface level (Huang et al., 1998; Ezer & Corlett, 2012; Ezer et al., 2013; Ezer, Haigh & Woodworth, 2016), sea level pressure (Wu & Huang, 2009), shallow water turbulent velocity (Schmitt et al., 2009), and SWAN nearshore wave energy (Ching-Piao et al., 2012). It uses a sifting process to decompose a nonlinear and nonstationary time series into the underlying trend and simple components known as the Intrinsic Mode Functions (IMFs) (Huang et al., 2003; Sharpley &

Vatchev, 2006). True IMFs are monocomponent (linear and stationary) signals of varying oscillations of the original time series, that exhibit the following properties: (1) the mean envelope of the local maxima and minima (local extrema) of the function is (close to) zero; and (2) the number of extrema and zero crossings is equal or differs by one at most (Sharpley & Vatchev, 2006). The decomposition is based on the data themselves and is therefore very adaptive and efficient (Huang et al., 2003; Wang et al., 2012).

The decomposition sifting method starts by extracting the first IMF (the fastest oscillation) from the original time series (example in **Fig. 3.4 (a)**). This is done by (1) identifying the local extrema of the time series, (2) then interpolating (cubic spline) between local extrema to create the upper and lower envelope of the time series, (3) from which the mean envelope (the first IMF) is calculated (**Fig. 3.4 (b)**). This is subtracted from the original time series, and a residual with a slower oscillation remains (**Fig. 3.4 (c)**). However, this first extracted IMF may not necessarily be a true IMF. Therefore, steps 1-3 are repeated on the residual (**Fig. 3.5 (a, b)**) until its properties meet the criteria for a true IMF (**Fig. 3.5 (c)**). Subsequent IMF of decreasing oscillation speed are then determined from the remaining residual by reapplying the sifting process (Huang et al., 1998, 2003).

Eventually there remains a residual with only one set of extrema from which no more IMFs can be extracted. This remaining residual (the non-IMF component) can either be a constant or a trend if it is still different from zero (Huang et al., 1998, 2003). After the EMD method has been applied, the results will be a non-IMF component and a finite and often small number of IMFs, each with their own frequency spectrum that is often related to a specific physical process (Huang et al., 1998, 2003; Wang et al., 2014). The number of IMFs is determined by the data record length and the amount of variability within it (Ezer, Haigh & Woodworth, 2016). However, sometimes the embedded modes of data may exhibit mode mixing. This can occur either when a single IMF contains more than one signal and therefore more than a single time scale, or when a single scale appears in more than one IMF (Junsheng et al. 2006; Wang et al. 2012). When mode mixing is observed, the noise-assisted data analysis method by Wu & Huang (2009) called Ensemble EMD (EEMD) can be used instead (Wang et al. 2012).

In current study EMD was applied to the SWAN nearshore local-scale H_{m0} full time series of each study site using the EEMD function in MATLAB (version: 9.1.0.441655 (R2016b)) to produce H_{m0} modes of variability (hereafter, 'modes') and trends. The EEMD function was set to produce EMD results because no mode mixing was observed in the individual EMD modes produced per study site. EMD decomposed the average H_{m0} time series for each study site into 16 true IMFs, including the original time series (mode 1), the EMD modes (modes 2–15) and the trend (mode 16).

i. Fast Fourier Transformation (FFT):

The length of the cycle of the variability of each EMD H_{m0} mode was determined using the Fast Fourier Transformation (FFT) in MATLAB (version: 9.1.0.441655 (R2016b)), developed by Cooley &

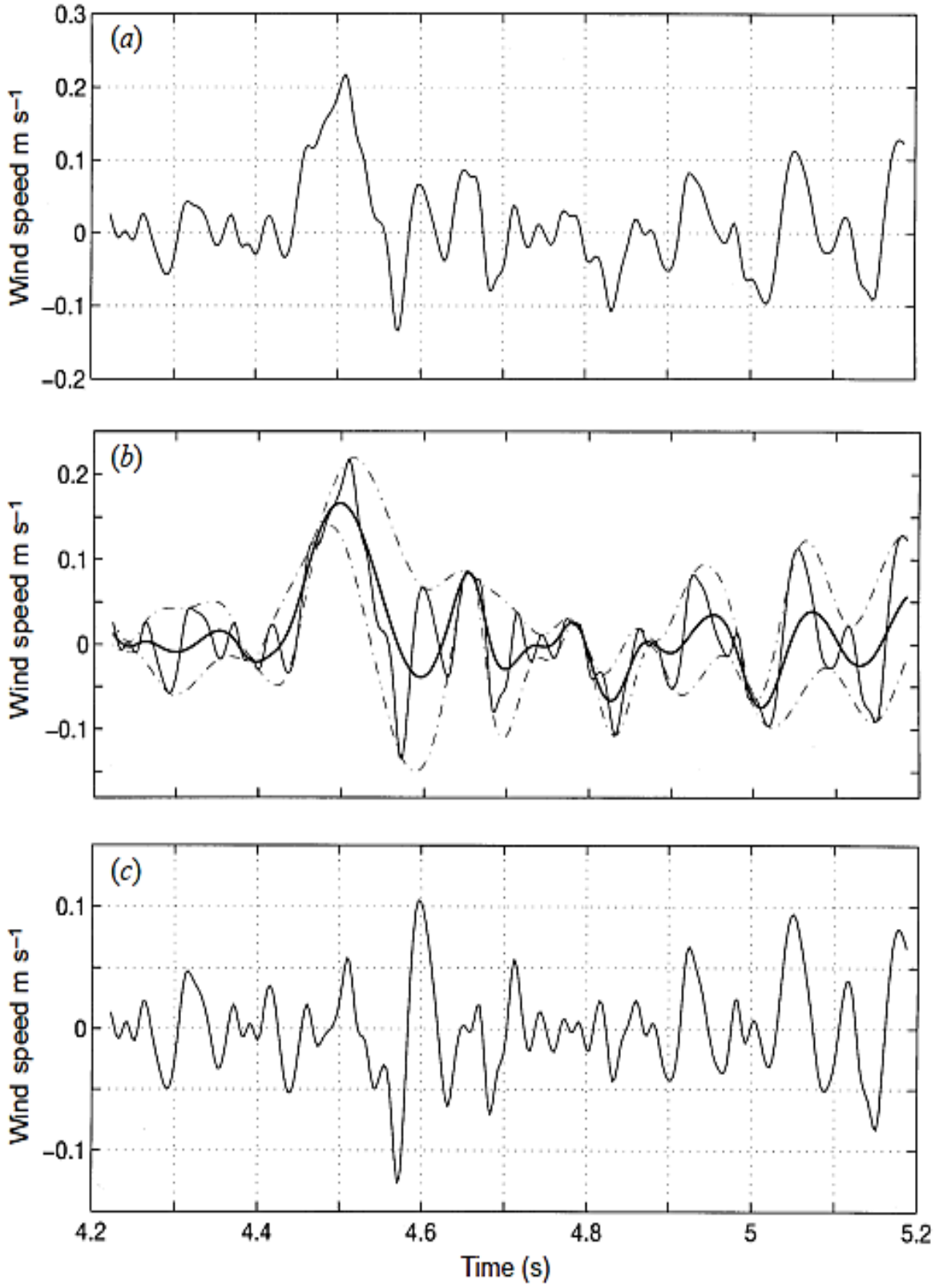

Fig. 3.4: *(a) A random original time series of wind speed subjected to the sifting process of Empirical Mode Decomposition (EMD), where (b) the maximin and minimum envelopes are determined through cubic spline interpolation, the mean envelope is calculated and then subtracted from the original time series, leaving (c) the residual (from Huang et al., 1998).*

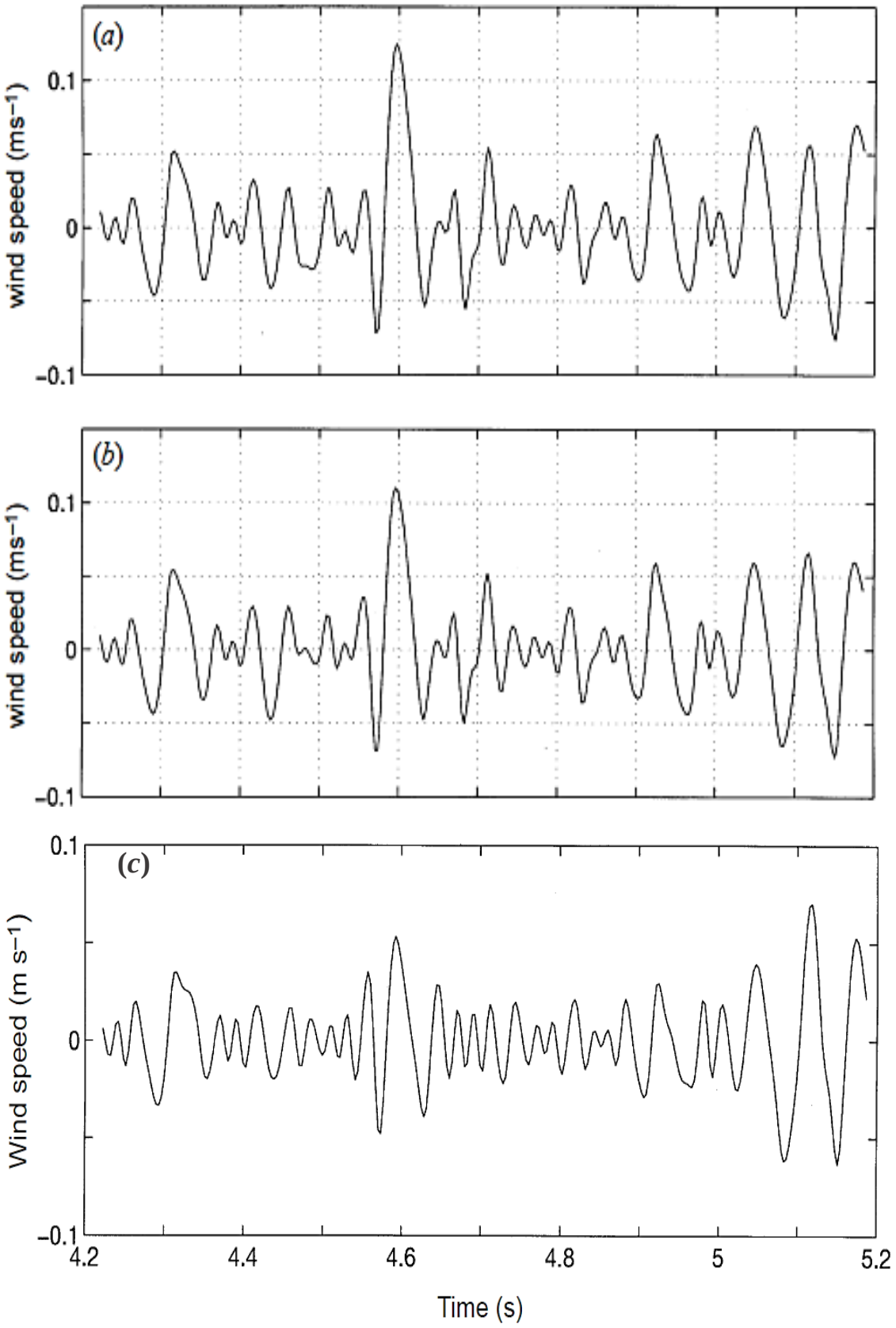

Fig. 3.5: *(a) The residual remaining after one and (b) two more sifting processes have been applied to the residual in Fig. 3.4 (c). (c) The final first true Intrinsic Mode Function (IMF) after sifting has concluded. This IMF will be the new 'original' time series from which the next highest frequency component is extracted (adapted from Huang et al., 1998).*

Tukey (1965). The FFT is a widely used and faster way of computing the Discrete Fourier Transform (DFT), which involves the transformation of the time domain into its frequency domain (Brigham & Morrow, 1967; Cochran et al., 1967; Cooley, Lewis & Welch, 1969; Donnelly, 2006). The frequency domain of a time series can be displayed as either an amplitude spectrum or a power spectrum (Donnelly, 2006). The FFT reduces not only the computational time requirements but also the number of rounding errors associated with DFT (Cochran et al., 1967). The FFT has, in some cases, successfully analysed coastal environment data (Hardman-Mountford et al., 2003; Bressan & Tinti, 2016; Armenio, De Serio & Mossa, 2017).

The FFT provided the frequency and power spectrum of each EMD H_{m0} mode of each study site in this study, from which their dominant frequency could be determined by finding the corresponding frequency of the peak of their power spectrum (hereafter, 'peak frequency'). The peak frequencies were then recorded and the lengths of the cycles (hereafter, 'timescales') of the variability of each EMD H_{m0} mode for each study site was calculated (**Appendix B)**. The table in **Appendix B** additionally indicates the groupings of the various timescales of variability, including that of the EMD H_{m0} modes considered to have interannual variability.

Considering that the observed changes reported by fishers in the region exist on interannual timescales, the analyses of interannual H_{m0} variability and trends were focussed on. The EMD H_{m0} modes considered to represent interannual variability (modes 12-15 per each study site) are hereafter referred to as 'H_{m0} interannual variability time series'; the EMD H_{m0} modes considered to represent interannual variability with a trend (modes 12-16 per each study site) are hereafter referred to as 'H_{m0} interannual and trend time series'; and lastly, the long term mean of the H_{m0} interannual and trend time series was subtracted from the H_{m0} interannual and trend time series, creating an 'the H_{m0} interannual anomaly time series' for each study site. The H_{m0} interannual variability time series was compared to the H_{m0} interannual and trend time series and to the H_{m0} interannual anomaly time series, for each study site.

ii. Regression models:

The significance of the EMD trends were determined by fitting regression models to the EMD H_{m0} trend time series of each study site, using the programme called Rstudio (version 1.1.442). The function 'lm()' allows for the least square's regression analyses. All tests performed here tested the significance of the slope of the trend compared to no slope with a significance level set at 0.05. Therefore, a trend in this study was considered significant when its p-value was below the significance level (**Appendix C**). The formula tested was that of a simple linear model 'Y~X', where Y is H_{m0} and X is time in this study. This model assumes that there is a linear relationship between X and Y, residual errors of the model fitted are normally distributed, residual errors of the model fitted have a constant variance, and the residual errors of the model fitted are independent of X.

Once results were achieved, the assumptions made by the linear models for each study sites trend time series were checked. Firstly, the time series was plotted with the corresponding estimated linear model line of each study site (**Appendix D**) to see how well the estimated linear model line visually fits the time series. Here, it is possible to already tell if the time series does not follow a linear relationship. But to be sure, diagnostic plots of the linear models for each study site were produced (**Appendices E & F**). There are four diagnostic plots – residual vs fitted, normal Q-Q, scale-location, and residuals vs leverage.

The residual vs fitted plot indicates that there is a linear relationship between the variables if the red line runs horizontal through the plot, without a distinct pattern. However, if the red line does not run horizontal through the plot and rather in a more distinct pattern, the relationship is non-linear and was not explained by the model fitted (i.e., residuals were left out). The normal Q-Q plot indicates that the residual errors are normally distributed if the residuals on the plot follow the grey dashed line. However, if the residuals do not follow the grey dashed line well, then the time series is not normally distributed. Note that the residuals hardly ever follow the grey line perfectly but does not mean that the residual errors distribution is not fairly normal. The scale-location plot indicates that the variance of the residual errors is constant by showing a horizontal red line with residual points spread equally on either side of the line. However, if the red line does not run horizontal through the plot and the values are not equally spread from the red line, the residual errors variance is not constant. The residuals vs leverage plot indicates the extreme values of the time series (outliers) that influence the regression results when they are included or excluded (if any). If values are found in the upper right or lower right corners, outside of the cook distance red dashed lines, they are influential against the regression line (i.e., the regression results will be largely altered if the outliers are excluded from the analysis). All diagnostic plots indicate on their plots the top three most extreme time series values by labelling them with the row number in which they sit in the data set. These three values, however, may not be outliers (i.e., affects the interpretation of the model). If all assumptions are met, the results of the linear regression model are accepted (**Appendix C**).

If the residual vs fitted plot indicates a non-linear relationship between the variables, the simple solution is to then apply either a X^2 (quadratic) or log(X) (logarithmic) to the non-linear time series least squares model formula instead. If a non-linear regression model follows the time series better and the multiple R-squared value (the percentage of variance that the model explains) is higher, then the non-linear regression model fits the time series better than the linear model and the non-linear model statistical results are more acceptable (**Appendix C**). However, if the residual vs fitted plot indicates a linear relationship between the variables but two or more of the other diagnostic plots show problems, further analysis should be applied, such as fitting a quadratic or logarithmic model to the time series. Then again, if a non-linear regression model follows the time series better and the multiple R-squared

value is higher, then the non-linear regression model fits the time series better than the linear model and the non-linear model statistical results are more acceptable (**Appendix C**).

Statistically significant detection of trends is also dependent on the amount of data available. For example, even if there is a lot of scattering around a small slope but there are a lot of data, the slope can still be significant (Bryhn & Dimberg, 2011). It is therefore desirable to have a small amount as possible of missing data (IPCC, 2001). Additionally, a short-period within a time series may show the absence or even the inverse of a trend detected in a longer period, as short-period trends are very sensitive to start and end values (Hartmann et al., 2013; Stocker et al., 2013). For example, while the global surface temperature trends of the 15-year periods starting from 1995 and 1996 showed temperature increases of 0.13 and 0.14°C per decade, the period from 1997 showed only 0.07°C (Stocker et al., 2013). This is because of the natural climate variability within a time series that can sometimes exaggerate or dampen the long-term trend. Short-period trends are therefore generally considered less reliable than long term trends (longer than ~50 years) (Hartmann et al., 2013; Stocker et al., 2013).

3.3.4. Sequential Regime Shift Detection (SRSD):

The SRSD method (Rodionov, 2004) was applied to the 1998 to 2012 annual averages of the H_{m0} interannual anomaly time series of each study site – 1997 and 2013 had to be left out because of incomplete data. Studies of the southern Benguela have shown that the marine system is subject to regime shifts (Howard et al., 2007; Blamey et al., 2012, 2015). SRSD (formally known as the Sequential T-test Algorithm for analysing Regime Shifts (STARS) method, developed by Rodionov (2004) for the Pacific Decadal Oscillation and North Pacific ecosystems, has already been used for detecting regime shifts in the southern Benguela (Howard et al., 2007; Blamey et al., 2012, 2015; Jarre et al., 2015). The method tests the likelihood of a regime shift occurring for each data point in the form of anomalies or absolute values (the RSI) (Rodionov, 2004; Blamey et al., 2012). The detailed seven step process is given by Rodionov (2004).

While SRSD is a widely accepted method, regime shift detection robustness is strengthened when multiple regime shift detecting methods are used on multiple different variables within the system of interest because the type of method used can influence the shift detected (Blamey et al., 2012). However, Blamey et al. (2012) considered the SRSD to be advantageous to the other regime shift detection methods used in their study (change point analysis and Chow breakpoint test) because SRSD performed better close to the end of a time series. Therefore, only the SRSD method was used for analyses in this study.

Most regime shift analyses, including SRSD, cannot distinguish between an actual regime shift and 'red noise' (autocorrelation) in raw ('straight') data (Rodionov, 2004; Blamey et al., 2012). To solve this problem, Rodionov (2006) developed a method to prewhiten the data (remove the red noise, if any) prior to applying SRSD. This is done using either the Mariott-Pope and Kendall (MPK) method

or the Inverse Proportionality with 4 corrections (IP4) method to estimate a first-order autoregressive model (AR1) which models red noise by subsampling the data (Blamey et al., 2012). IP4 occasionally outperforms MPK when smaller subsample sizes are used. IP4 was therefore considered the preferable option by both Howard et al. (2007) and Blamey et al. (2012), and therefore, analyses with red noise estimation in the current study used the IP4 method with a subsample of six.

However, both Howard et al. (2007) and Blamey et al. (2012) determined that pre-whitening data led to the detection of fewer and lower magnitude regime shifts when applied to a known situation compared to alternative shift detection methodology. Therefore, it can at times be overly conservative. Additionally, Howard et al. (2007) found that the timing of biological observations was uncorrelated to results of SRSD on pre-whitened data but not of the straight data. Therefore, the current study performed the SRSD analyses with (pre-whitened data) and without (straight data) red noise estimation, but focusses on the analyses without red noise estimation.

The SRSD method requires the prior determination of three parameters which can affect the RSI value: (1) the cut-off length (l) is the minimum length of an intact regime that can be detected, in years; (2) the Huber's weight (H_w) helps to control the effect of outliers on the average value of the regime shift by controlling the weight assigned to them; and (3) the significance level (α) is the threshold at which the Student's t-test finds a significant difference between the mean values (or variances) of the two regimes. This is usually done through sensitivity analyses by running a few preliminary, experimental SRSD analyses with varying parameter values on both straight and pre whitened data (Rodionov, 2006; Howard et al., 2007; Blamey et al., 2012). The default parameter settings for the current study were based on the sensitivity analyses performed in this study.

The parameter settings for the sensitivity analyses were based on the Howard et al. (2007) and Blamey et al. (2012) studies. Both studies found that the Huber value (1, 3, 6) had little effect on the results, and the default $H = 1$ was deemed adequate for analysis. Therefore, the $H = 1$ was used for the sensitivity analyses. Both studies found that analyses with longer cut-off lengths detected slightly (almost negligibly) fewer regime shifts, and that a length of $l = 10$ was sufficient to assess decadal scale oceanic variability (Blamey et al., 2012). Therefore, the length of $l = 10$ was used for the sensitivity analyses, as well as the length of $l = 7$ since the time series used is only of 12 years. Both studies indicated that more regime shifts were detected at $a = 10\%$ than $a = 5\%$. However, even though the $a = 10\%$ was established as sufficient, especially because it compensated for the large interannual variability in both biological and environmental data (Howard et al., 2007), the sensitivity analyses also included the $a = 5\%$. Sensitivity testing was performed using various combinations of the above settings, on both straight and pre-whitened data. Such as in the Howard et al. (2007) and Blamey et al. (2012) studies, shifts detected in the same year under 70% or more of the settings during both the straight and pre-whitened analyses were considered 'robust'. Shifts detected between 60-70% of the

model settings only during straight analyses were considered ‘possible’, and only during pre-whitened analyses were considered ‘pre-whitened’ shifts. Sensitivity results are shown in **Appendix G**.

3.3.5. Seasonal and daily cycles:

The monthly and hourly climatologies of the H_{m0} SWAN full time series, as well as those of the H_{m0} periods defined by regime shifts determined by SRSD, were analysed for each study site. Monthly climatologies are the average values per month over the years of interest, while hourly climatologies are the same but for average values per hour. The monthly time scale runs from June (start of winter) to May (end of autumn) so that the main summer fishing season in is not split. The hourly time scale runs from 03h00 to 24h00 because of the three-hourly timestep and the removal of the duplicated midnight point at 00h00 (eliminating the first 3-hr period).

CHAPTER 4: Results

4.1. General wind and swell characteristics:

The characteristics of the synoptic-scale wind and the offshore synoptic-scale swell of the South African South Coast are shown in **Fig. 4.1** and in **Appendix H**. The average annual winds (**Appendix H (a)**) are predominantly from the west or east, with the strongest wind speeds predominantly coming from the west. The average summer winds (**Fig. 4.1 (a)**) are predominantly from the east. The average annual offshore (**Appendix H (b)**) and average summer offshore synoptic-scale waves are predominantly from the southwest, the latter having lower H_{m0}'s. The average nearshore local-scale wave characteristics shown in **Fig. 4.2** and **Appendix I** are specific to the study sites. The Witsand and Mossel Bay study sites both have average annual (**Appendix I (a, d)**) and average summer (**Fig. 4.2 (a, d)**) waves predominantly from the southeast. The only difference between annual and summer averages is a slight increase in the number of easterly waves in summer at both Witsand and Mossel Bay. On the other hand, the Still Bay and Gouritz study sites both have average annual H_{m0} ranges (**Appendix I (b, c)**) that are slightly larger than in summer (**Fig. 4.2 (b, c)**); however, both are predominantly from the south.

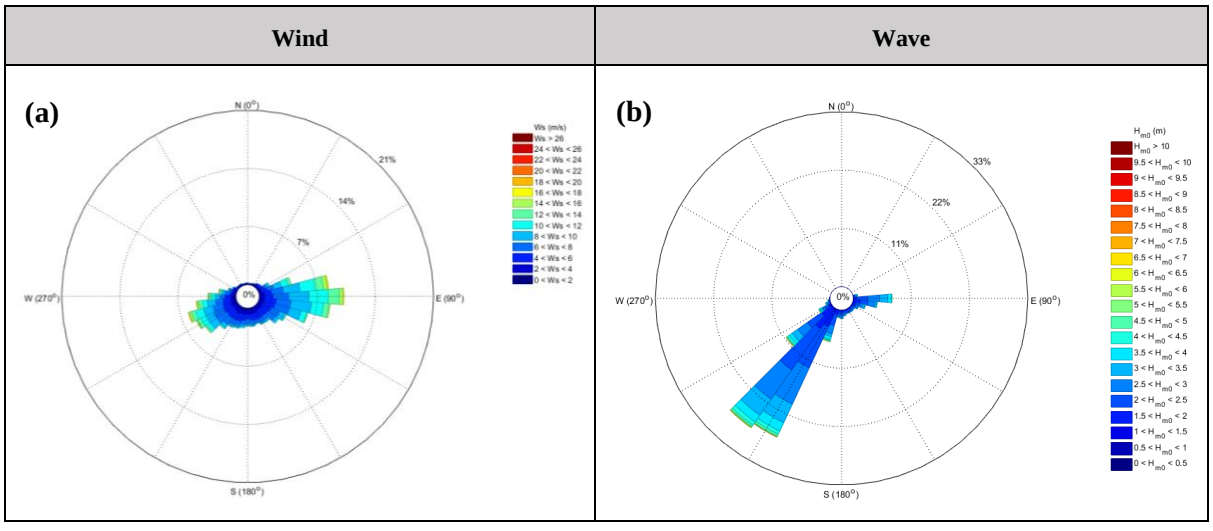

Fig. 4.1: *Coarse resolution National Centre of Environmental Prediction (NCEP) summer (a) synoptic-scale wind and (b) offshore synoptic-scale wave roses (summer months of 1997–2012). Wind rose shows the direction (degrees, º) frequency (percentage, %) and magnitude (colour bar) of wind speeds (Ws, m/s), while wave rose shows the directional frequency and magnitude of significant wave height (H_{m0}, m).*

The South Coast synoptic-scale wind speed distributions are shown in **Fig. 4.3 (a)**. The estimated average summer synoptic-scale wind speed mean is 7.2 m/s and the standard deviation (SD) is +/-3.3 m/s. The estimated average nearshore local-scale wave climate distributions of the study sites are shown in **Figs. 4.3 (b, c)**. Similar to the general nearshore local-scale wave characteristics (**Fig. 4.2** and **Appendix I**), wave distributions are similar between Witsand and Mossel Bay, and between Still Bay and Gouritz. Witsand and Mossel Bay both show a slight peak of low summer peak periods (about 5 s) (**Fig. 4.3 (b)**), which is not evident for Still Bay and Gouritz. This could be indicative of some additional and local local-scale driver of smaller peak periods during summer, specific to only Witsand and Mossel Bay.

For the estimated average summer peak periods (**Fig. 4.3 (b)**), Witsand and Mossel Bay show lower means (9.46 s; 9.70 s) and higher SDs (+/- 2.61 s; +/- 2.43 s) compared to Still Bay and Gouritz (10.08 s +/-2.05 s; 10.08 s +/- 2.03 s), i.e., they show slightly more variability. For the estimated average summer (**Fig. 4.3 (c)**) H_{m0}, Witsand and Mossel Bay show lower means (0.99 m; 1.08 m) and SDs (+/- 0.43 m; +/- 0.42 m) than Still Bay and Gouritz (1.80 m +/- 4.9 m; 1.83 m +/- 5.1 m). The differences

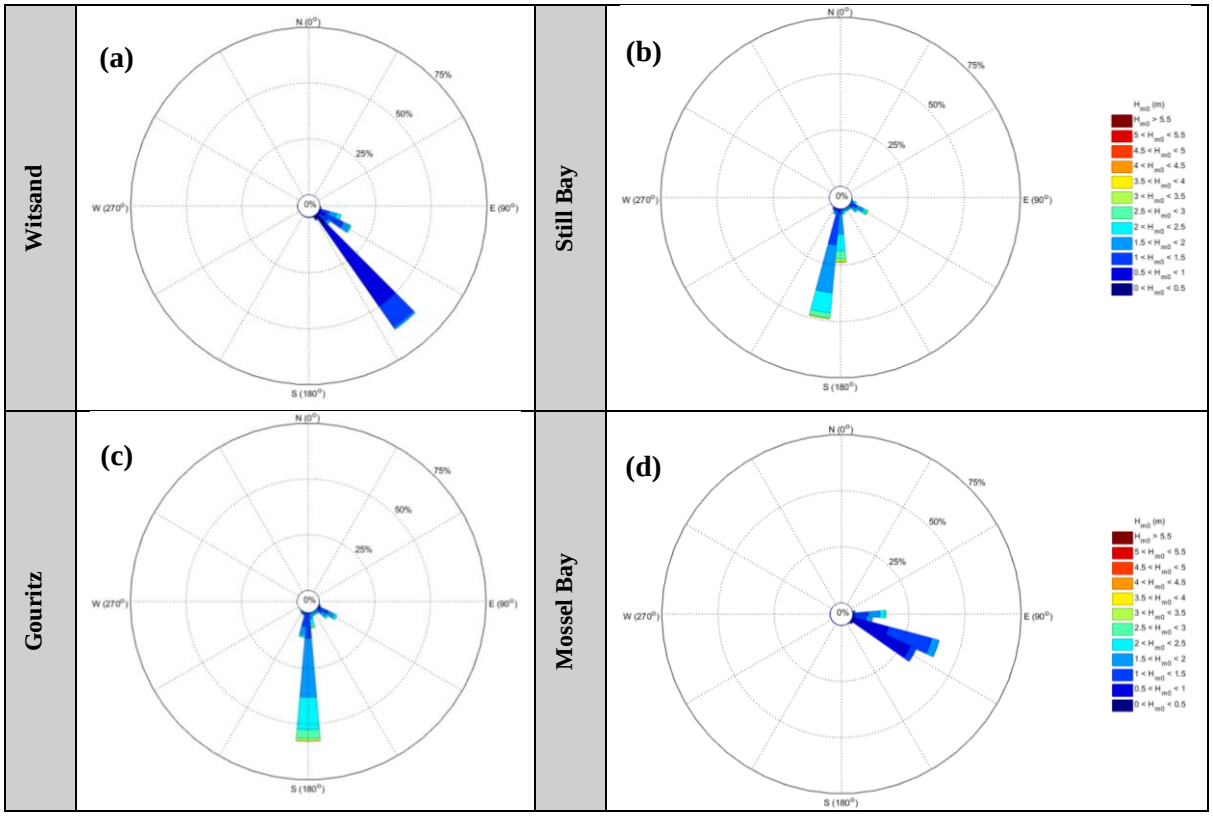

Fig. 4.2: *Average high resolution Simulating WAves Nearshore (SWAN) summer nearshore local-scale wave roses (summer months of 1997–2012) for the study sites at (a) Witsand, (b) Still Bay, (c) Gouritz, and (d) Mossel Bay. Wind roses show the direction (degrees, °) frequency (percentage, %) and magnitude (colour bar) of wind speeds (Ws, m/s). Wave roses show the directional frequency and magnitude of significant wave height (H_{m0}, m).*

between all study sites in terms of peak period and H_{m0} are all significant (**Appendix A**), besides for the difference between Still Bay and Gouritz peak periods. This suggests that the estimated average summer peak period means of Still Bay and Gouritz are fairly similar in magnitude.

4.2. Sub-daily trends and variability of the nearshore environment:

The summer sub-daily difference between the 06h00 (morning) and 15h00 (afternoon) SWAN nearshore local-scale H_{m0}'s per year (1997–2012) are represented as annual time series for Still Bay (**Fig. 4.4**) and the other study sites (**Appendix J**). While the previous results for nearshore local-scale

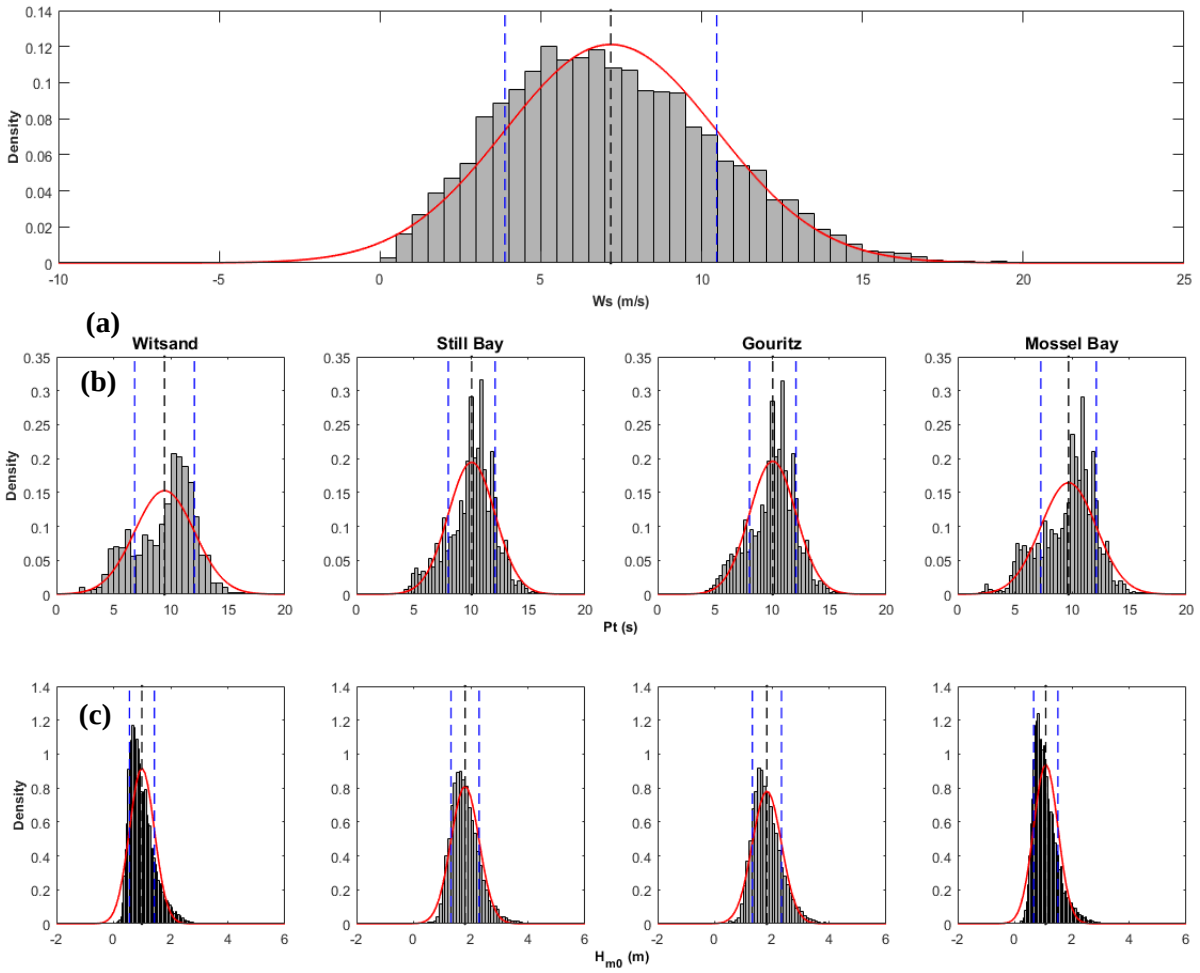

Fig. 4.3: *Normalised Probability Density Functions (PDFs; red line) and PDF estimated histograms (grey bars) of the average (a) coarse resolution National Centre of Environmental Prediction (NCEP) synoptic-scale wind speeds (Ws, m/s), and of the average (b) high resolution Simulating WAves Nearshore (SWAN) nearshore local-scale peak periods (Pt, s) and (c) high resolution SWAN nearshore local-scale significant wave heights (H_{m0}'s, m) for the four study sites (Witsand, Still Bay, Gouritz, and Mossel Bay) during summer months of 1997–2012. Plots show the density (y-axis) of the estimated PDFs of Ws, Pt, or H_{m0} (x-axis). The black dashed line represents the average and the blue dashed lines represent one standard deviation (SD) from the average.*

wave characteristics (**Figs. 4.2** and **4.3 (b, c)**, and **Appendix I**) show a certain grouping of the study sites, this is not apparent here (**Fig. 4.4** and **Appendix J**). While no intra- or inter-annual trends towards increasing or decreasing differences were observed for any study site, all sites show high summer sub-daily difference variability. Furthermore, all study sites show more positive than negative values each year, indicating that larger waves occur more frequently during the afternoon than the morning during summer. This is confirmed by **Fig. 4.5** where the information in **Fig. 4.4** and **Appendix J** are summarised into annual boxplots for each study site; all show positive means. The smallest means for each study site occur during the 2006 summer. This indicates that during that period, afternoon H_{m0}'s are mostly similar to morning wave heights. **Fig. 4.5** shows that all study sites have outliers in summer sub-daily difference merely ranging from ~0.5 m to 1 m. Consequently, the average summer sub-daily difference for each year is very small and shows no trend over time at all study sites.

The spread of the summer data (distance between the most extreme outliers) differs from year to year for each study site. The smallest spread of data occurs during the 1998 summer for Still Bay and Gouritz (**Fig. 4.5 (b, c)**), as well as during the 2006 summer for Witsand and Mossel Bay (**Fig. 4.5 (a, d)**). Post-2006, all study sites show a larger summer sub-daily variability of differences between morning and afternoon H_{m0}'s in general, compared to the 1997–2006 period; however, no trends in differences are observed. Additionally, Still Bay and Gouritz (**Fig. 4.5 (b, c)**) seem to experience larger outliers than Witsand and Mossel Bay (**Fig. 4.5 (a, d)**), particularly during this more variable period. Therefore, during post-2006 to 2014 Still Bay and Gouritz (**Fig. 4.5 (b, c)**) experience a larger spread of differences between summer morning and afternoon H_{m0}'s than the other two sites (**Fig. 4.5 (a, d)**).

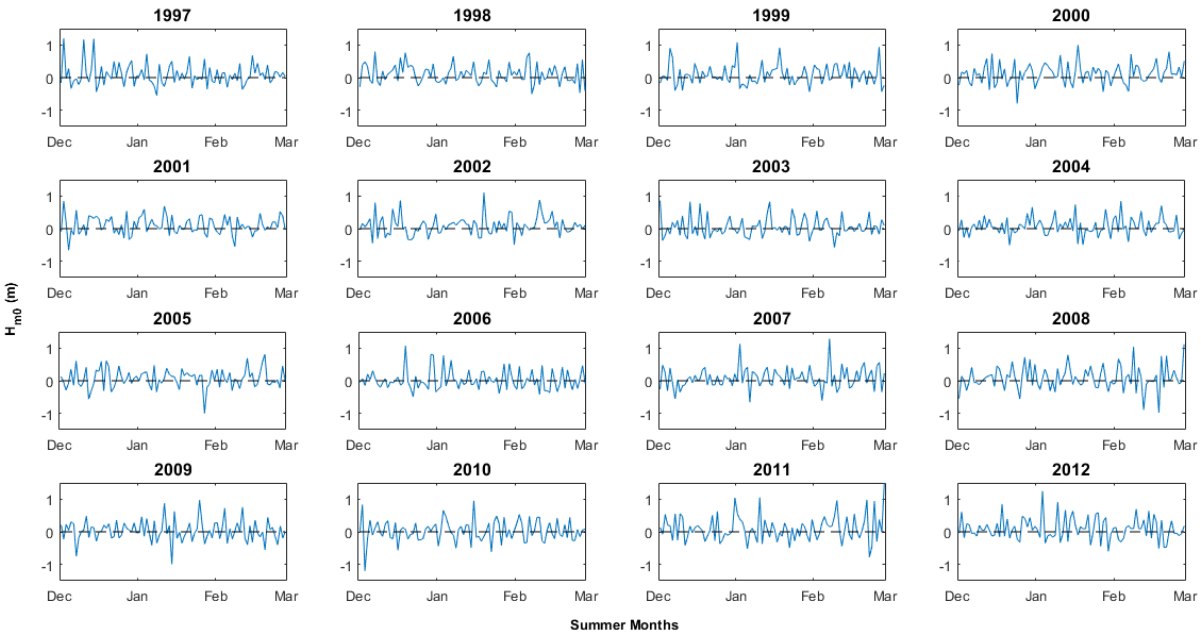

Fig. 4.4: *Annual time series of the summer (summer months per year for 1997–2012) daily differences between nearshore local-scale significant wave height (H_{m0}) at 06h00 and 15h00 for Still Bay. The 'difference' was the H_{m0} value at 06h00 subtracted from the value at 15h00. Positive values indicate that the afternoon H_{m0} values are larger than the morning H_{m0} values, while negative values indicate the inverse.*

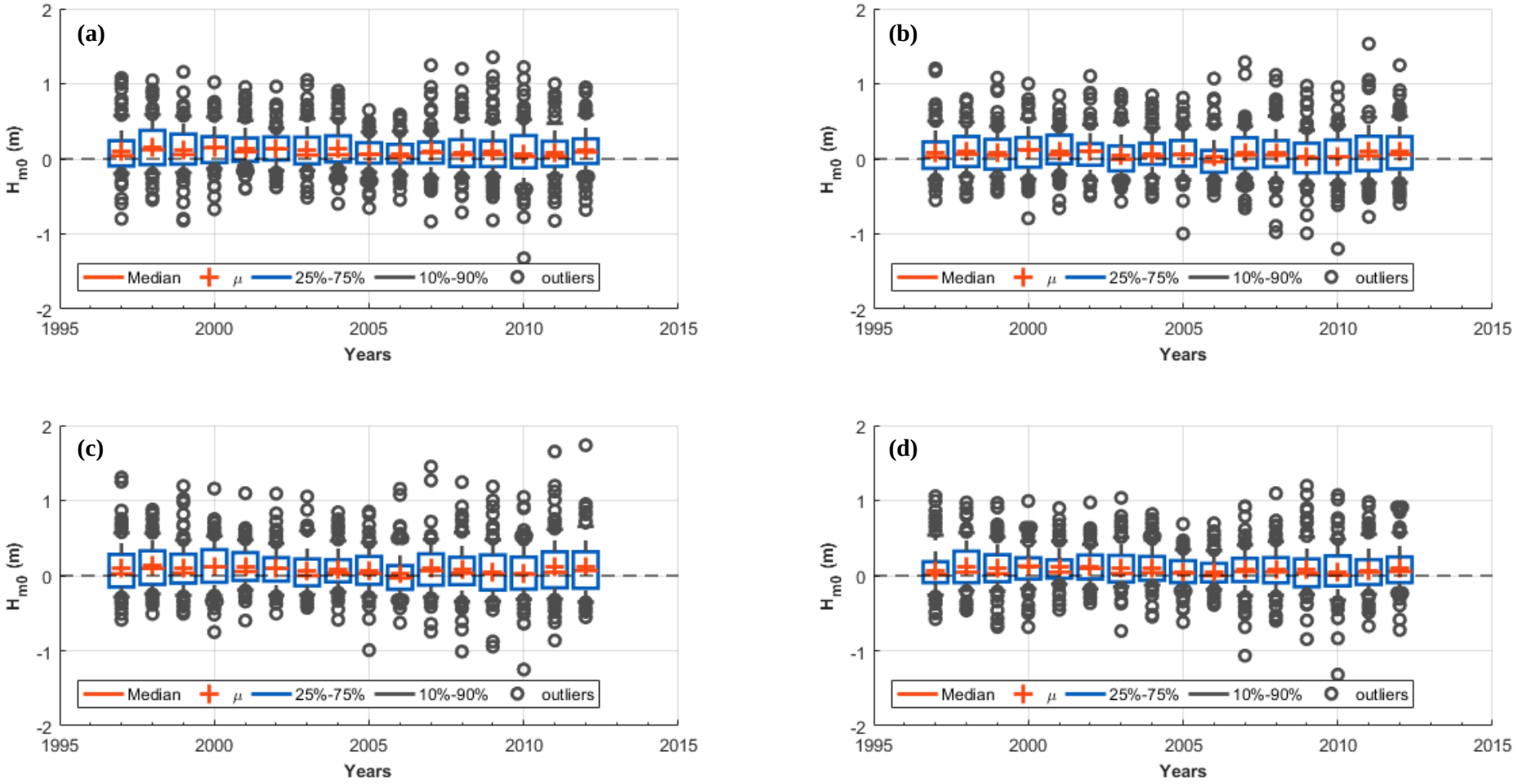

Fig. 4.5: *Annual boxplots of the summer (summer months per year for 1997–2012) daily differences between nearshore local-scale significant wave height (H_{m0}) at 06h00 and 15h00 for (a) Witsand, (b) Still Bay, (c) Gouritz, and (d) Mossel Bay. The 'difference' was the H_{m0} value at 06h00 subtracted from the value at 15h00. Positive values indicate that the afternoon H_{m0} values are larger than the morning H_{m0} values, while negative values indicate the inverse. Blue box: upper (75% of data) to lower (25% of data) quartile, encompassing the interquartile range (50% of data). Horizontal red line: median of box; red cross: mean. Whiskers: data outside the interquartile range which is from 10% to 90%. Data outside this 80% range are considered outliers (black outlined dots).*

4.3. Long-term trends and variabilities of the nearshore environment:

Fig. 4.6 shows relevant results of EMD application to the full SWAN nearshore local-scale H_{m0} time series, specifically those for the combined group of EMD interannual varibility of each study site (12-15 modes) and their trends (mode 16). All study sites show an increase in H_{m0} of about 0.15–0.21 m, depending on study site (details in **Table 1**) over the full period (**Fig. 4.6 (a)**). After plotting the linear regression lines on the EMD H_{m0} trend time series for each study site (**Appendix D**), it was clear than the model did not fit well (the red linear regression model line did not follow the time series close enough) for Still Bay, Gouritz and Mossel Bay. However, the linear model seemed to fit the Witsand time series well. Furthermore, the diagnostic plots for the linear models (**Appendix E**) indicated that Witsand residual errors follow a linear relationship, while the other study sites are not; the Witsand residual errors distribution is more normal than the other study sites; the Witsand residual errors variance is fairly constant and only slightly increasing along the x-axis, while the variance is not constant at all for the other study sites; and none of the study sites have any influential values. Therefore, it was decided to apply non-linear (quadratic and logarithmic) regression models to Still Bay, Gouritz and Mossel Bay, as well as Witsand for consistency.

Plots of the non-linear regression model lines and the study sites time series indicated that the linear and logarithmic models followed the Witsand time series best, while the quadratic model followed Still Bay, Gouritz and Mossel Bay time series the best (**Appendix D**). The latter was confirmed by the diagnostic plots of the quadratic models for Still Bay, Gouritz and Mossel Bay (**Appendix F**), which showed that their non-linear relationships were explained by the quadratic models fitted, the residual variances are definitely constant, and the there are no influential values present in the time series. Lastly, the multiple r-squared value for the linear model fitted to Witsand and for the quadratic model fitted to Still Bay, Gouritz and Mossel Bay were the highest compared to the other models fitted to the study sites time series (see **Appendix C**). Therefore, the regression model results from the linear model for Witsand and those from the quadratic models for Still Bay, Gouritz and Mossel Bay were the most acceptable, and showed that the slopes for each time series are significant. Therefore, the trends observed in the EMD H_{m0} time series for each plot are significant., indicating a positive trend towards higher H_{m0}'s. As shown previously, values for Witsand and Mossel Bay are about 1 m lower than Still Bay and Gouritz over this period (**Table 1**).

With the H_{m0} interannual varibility included in the trend time series (**Fig. 4.6 (b)**), the same groupings of study sites emerge as seen before (**Fig. 4.6 (a)**). However, each study site shows greater variability (**Fig. 4.6 (b)**). The degree of the trend's impact on the interannual variability at each site can be observed when the trend is excluded and the interannual variability remains (**Fig. 4.6 (c)**). For example, when the trend is included (**Fig. 4.6 (b)**), Witsand and Mossel Bay experience a period of higher H_{m0}'s during 2013 compared to the period 2003–2006. However, both the periods experienced

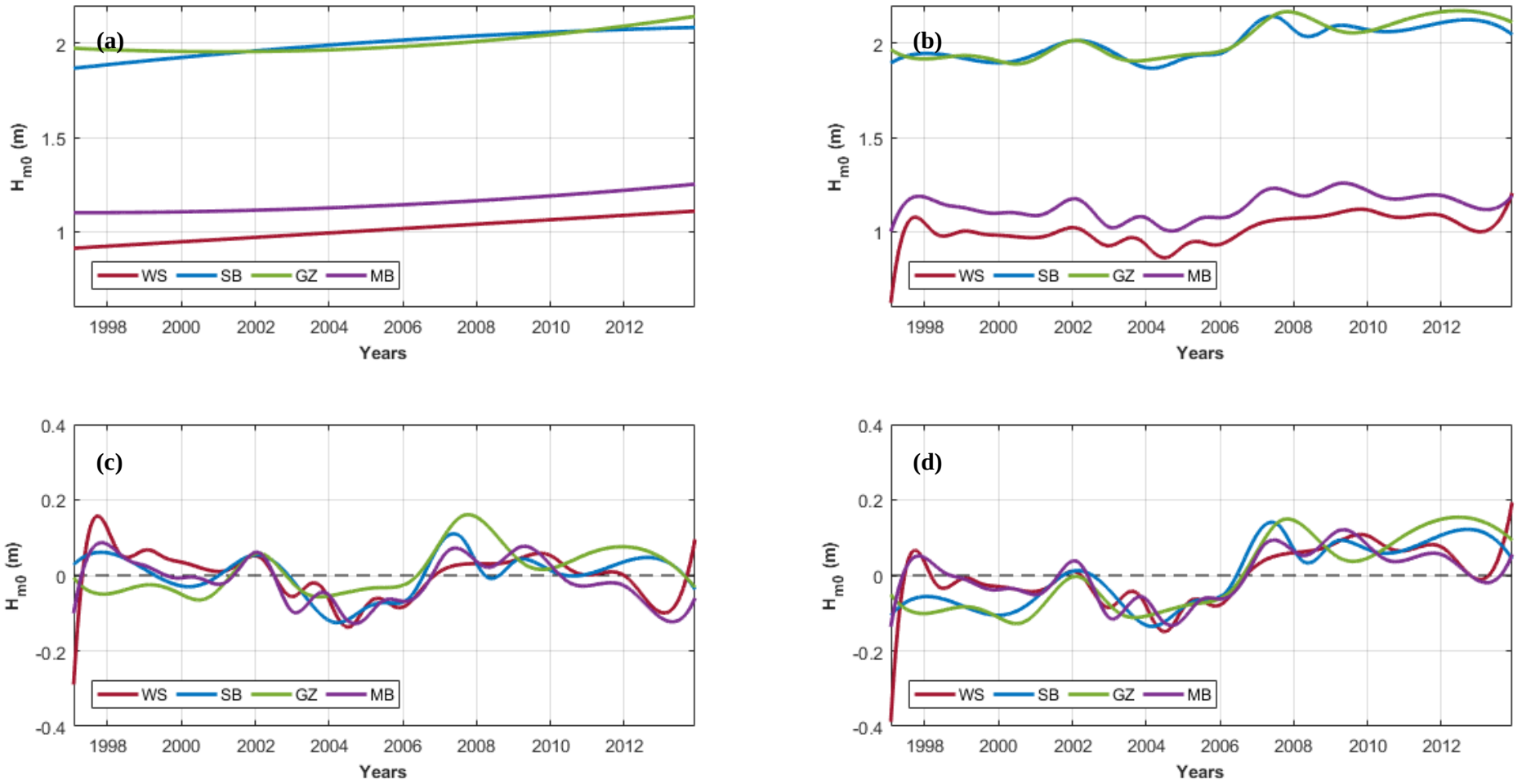

Fig. 4.6: *Empirical Mode Decomposition (EMD) results for Witsand (WS, red time series), Still Bay (SB, blue time series), Gouritz (GZ, green time series), and Mossel Bay (MB, purple time series) nearshore local-scale significant wave height (H_{m0}) full time series (1997-01-30-03h00 to 2013-11-30-24h00). (a) Trend time series (mode 16) for each study site. (b) and (c) Interannual variability time series with the trend (modes 12-16) and without the trend (modes 12-15) time series, respectively, for each study site. (c) Positive (negative) values indicate periods of interannual higher (lower) H_{m0} values compared to the trend. (d) H_{m0} interannual anomaly time series; positive (negative) values indicate periods of interannual higher (lower) H_{m0} values compared to the long-term average.*

Table 1: *Nearshore local-scale significant wave heights (H_{m0}) at the start and end of the trend time series and difference between values (H_{m0} increase), after applying Empirical Mode Decomposition (EMD), per study site.*

Study site	H_{m0} start	H_{m0} end	H_{m0} increase
Witsand	*0.91 m*	*1.11 m*	*0.20 m*
Still Bay	*1.87 m*	*2.08 m*	*0.21 m*
Gouritz	*1.97 m*	*2.14 m*	*0.17 m*
Mossel Bay	*1.10 m*	*1.25 m*	*0.15 m*

similar magnitudes of H_{m0}'s when the trend is excluded (**Fig. 4.6 (c)**). Therefore, the trend of increasing H_{m0} values at each study site could be exaggerating the underlying interannual variability.

Whether an overall increasing trend causes H_{m0}'s at each study site to be higher than normal towards the end of the time series can be determined by looking at the H_{m0} interannual anomaly time series for each study site (**Fig. 4.6 (d)**). Between 1999 and mid-2006 (except for the period mid 2001-mid 2002) all study sites generally experience lower than usual H_{m0}, whereas post mid-2006, there is a they all generally experience higher than usual H_{m0}. The Sequential Regime Shift Detection (SRSD) analysis sensitivity analyses indicated that shifts in the H_{m0} interannual anomaly time series were detected during 2006 for all study sites. However, the Witsand shift was considered possible only on straight data. The other study sites showed robust shifts for 2006 but only Gouritz was considered robust on both straight and pre-whitened data, while Still Bay and Mossel Bay were considered robust on only straight data. Furthermore, this shift was mostly detected under α = 10% and l = 7. The other robust shift detected was for Witsand during 2012 but only on pre-whitened data (for all combinations), while a possible shift was detected on straight data for 2007 (for only α = 5%). Therefore, following this analyses, only the shifts detected with H = 1, α = 10% and l = 7 on straight data were presented here (**Fig. 4.7**). The shift detected during 2006 at all the study sites indicates that before and after 2006, the study sites possibly experienced two different sea state periods which may have altered seasonality and sub-daily sea states. This is explored in **Fig. 4.8**.

Monthly (**Fig. 4.8 (a)**) and hourly (**Fig. 4.8 (b)**) climatologies of the full SWAN nearshore, local-scale nearshore local-scale H_{m0} time series and the regime shift H_{m0} time series of lower and higher waves (i.e., start of the full SWAN nearshore time series to end of 2005, and start of 2006 to end of the full time series, respectively) show the same groupings of study sites as seen before (**Fig. 4.6 (a, b)**). Only Still Bay and Gouritz show distinct seasonal cycles for all three time periods, where their H_{m0}'s peak at the end of winter or start of spring (maximum H_{m0}) and trough during summer (minimum H_{m0}) (**Fig. 4.8 (a)**). On the other hand, Witsand and Mossel Bay do not show a distinct seasonal cycle (**Fig. 4.8 (a)**). On the other hand, all study sites sub-daily cycles show similar timing and degrees of oscillation, while magnitudes differ with respect to the study site (**Fig. 4.8 (b)**). Specifically, at all study sites, H_{m0}'s start increasing (slightly) after 15h00 by about 0.3 m, then start decreasing after 21h00 by the same amount until about 06h00 (**Fig. 4.8 (b)**).

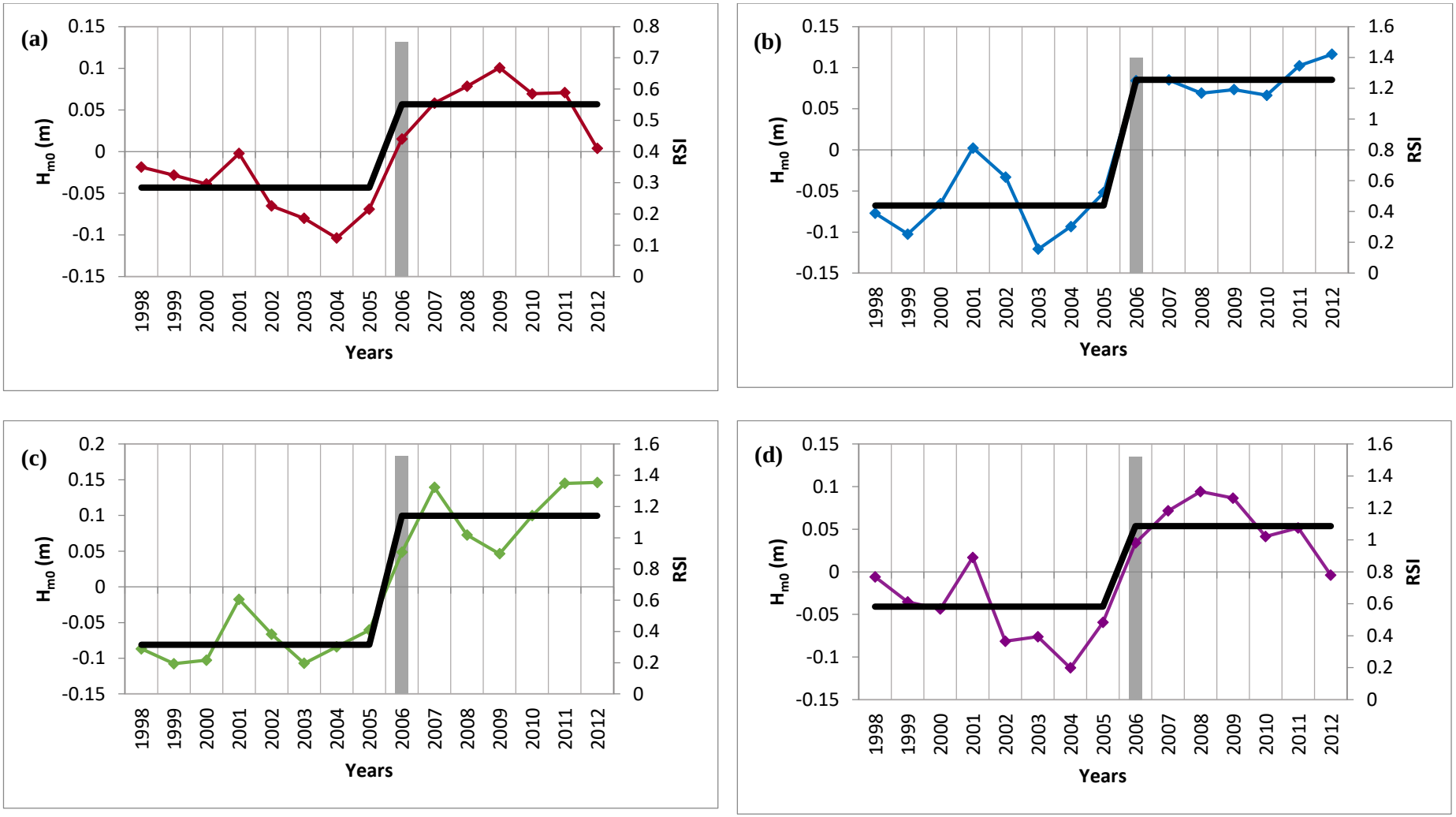

Fig. 4.7: *Sequential Regime Shift Detection (SRSD) analysis results without red noise estimation of the average nearshore local-scale significant wave height (H_{m0}) interannual anomaly time series (1997-01-30-03h00 to 2013-11-30-24h00) for (a) Witsand, (b) Still Bay, (c) Gouritz, and (d) Mossel Bay. Coloured time series are average H_{m0} anomaly time series, black time series are SRSD weighted means time series. The grey bar indicates time and magnitude of the Regime Shift Index (RSI).*

For both the seasonal and sub-daily H_{m0} SWAN nearshore local-scale time series (**Fig. 4.8 (a)** and **(b)**), the full time series of each study site is below the higher H_{m0} period time series and above the lower H_{m0} period time series of that study site. The only other noticeable difference between the various time periods is one in the timing of maximum (during winter) and minimum (during summer) H_{m0}'s of the seasonal cycles of Still Bay and Gouritz (**Fig. 4.8 (a)**). Specifically, compared to their full H_{m0} seasonal time series, their winter H_{m0}'s start later during their higher H_{m0} period, and their summer H_{m0}'s start later during their lower H_{m0} period.

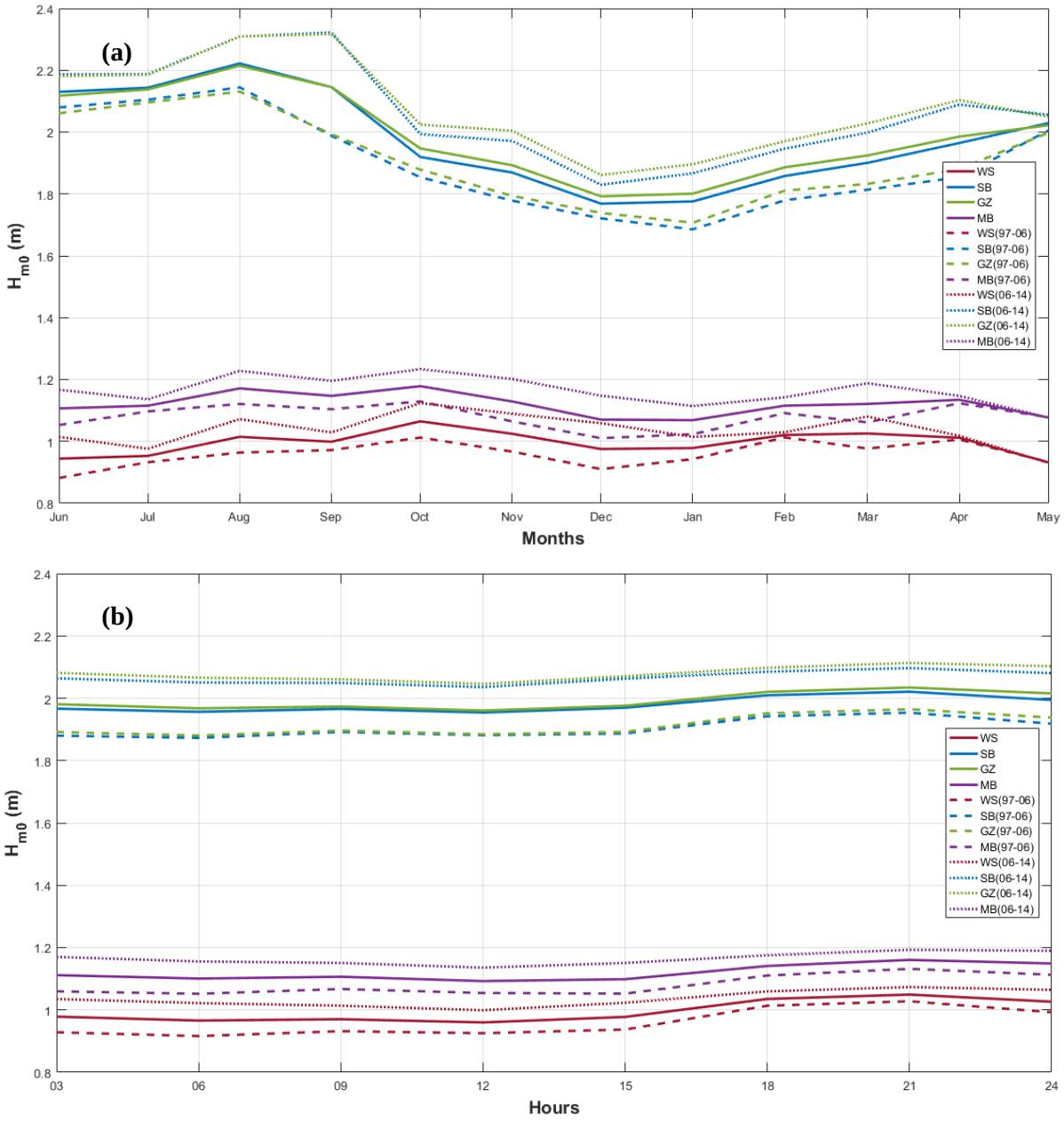

Fig. 4.8: *Mean monthly (a) and hourly (b) climatology's of the nearshore local-scale significant wave height (H_{m0}) full time series (solid line), the start of the full time series to the end of 2005 (1997-01-30-03h00 to 2005-12-31-21h00; dashed line) and the start of 2006 to the end of the full time series (2005-12-31-24h00 to 2013-11-30-24h00; dotted line) for each study site (Witsand, Still Bay, Gouritz, Mossel Bay; blue, red, yellow, green time series).*

CHAPTER 5: Discussion and Conclusion

This study aimed to assess possible changes of nearshore local-scale sea state in terms of wave climate along the South Coast as relevant to the traditional handline fishers there, based on analyses of Simulating WAves Nearshore (SWAN) model outputs. This study was part of a wider assessment looking at changes in climate along the South Coast region and bridging the gap between the South Coast environmental data and the South Coast traditional handline fisher's knowledge.

5.1. Discussion of data and methods:

5.1.1. Data:

The data time series used in this study is less than 14 years long. This is considered very short for any trend analyses, including climate change. Additionally, different trends or degrees of trends may arise due to different time series lengths (Hartmann et al., 2013; Stocker et al., 2013). The accessible record length was however considered adequate in the present case because the South Coast fishers observe variability on many different temporal scales, including daily. Additionally, fishers recall of past climate conditions only goes back a few decades (Gammage, Jarre & Mather, 2017a). Therefore, while the NCEP and subsequently the SWAN models could have been forced over longer time periods for this project, this was not necessary to meet the objectives of the present study.

The wave model outputs used in this study were produced by forcing the SWAN model with NCEP model outputs. While models are a good numerical representations of the real environment, many simplifications, estimations and assumptions are involved (IPCC, 2001; McGuffie & Henderson-Sellers, 2005; Stewart, 2008). For example, the NCEP grid resolution is comparatively coarse (1^{o}) and therefore cannot resolve some local-scale wind or wave dynamics. Additionally, NCEP swell and wave conditions were assumed as being saturated (fully developed) across the SWAN modelled area. When using NCEP model outputs as boundary conditions, some of these limitations are carried over to the SWAN model outputs.

Simulated wave heights from the 32563 NCEP model data point used in this study (22.5^{o}E, 35^{o}S) were recently validated against the FA platform data and the Jason-2 altimetry satellite (Barnes, 2018). It is important to known that the NCEP model works as well as the SWAN model it is forcing because the NCEP model outputs are the boundary conditions which determine the SWAN model outputs. The SWAN model has been shown to be able to downscale coarse resolution NCEP boundary

conditions to the nearshore environments and capture local-scale wave climates as impacted by local topography along the South African coastline (Baloyi et al., 2009; Joubert & van Niekerk, 2013; Theron et al., 2014; Rossouw et al., 2015). Additionally, the SWAN model could justifiably be run in stationary mode because the South and West Coasts of South Africa are exposed to similar large-scale winds and thus similar large-scale wave conditions (Rossouw, 1989; Rossouw, Terblanche & Moes, 2013). Finally, offshore synoptic-scale waves mostly consist of fully developed swell that approach the South African coastline with most of their wave characteristics still intact (Laing et al., 1998; Cooper, 2001; Talley et al., 2011; Rossouw, Terblanche & Moes, 2013). It can therefore be assumed that the SWAN model in stationary mode provides reliable information about local-scale wave conditions along the South Coast when using reliable, coarse resolution NCEP wave and wind forcings.

Spatially averaging the corrected SWAN wave time series (significant wave height (H_{m0}), peak period and wave direction) over each of the four South Coast study sites, was considered acceptable, as the objective of this study was to determine the average nearshore wave climates close to the main launch sites used by the South Coast traditional handline fishers'. Additionally, this spatial averaging is in line with the fishers' climate knowledge which focussed on the ability to launch and stay out in the adjacent fishing grounds (Duggan, Green & Jarre, 2014).

It must be acknowledged that analysing H_{m0} alone does not provide a complete picture of the nearshore local-scale sea state. Nevertheless wave height is one of the most commonly used parameters to describe the sea state in terms of wave climate (Akpinar & Kömürcü, 2012). This is because wave energy, which is relevant to wave dissipation at the coast, is proportional to wave height, making wave height a useful indicator of wave energy, the latter requiring several additional parameters to calculate (Laing et al., 1998; Hughes, 2016). While H_{m0} is an indirect measure of wave height, it is considered the best measure of the wave height of a generally variable sea surface as experienced by an observer (Stewart, 2008; Akpinar & Kömürcü, 2012). Hereafter, the H_{m0} data will be referred to as wave height.

5.1.2. Methods:

The Empirical Mode Decomposition (EMD) method has been used on nonlinear and nonstationary marine time series such as sea surface level (Huang et al., 1998; Ezer & Corlett, 2012; Ezer et al., 2013; Ezer, Haigh & Woodworth, 2016), sea level pressure (Wu & Huang, 2009), shallow water turbulent velocity (Schmitt et al., 2009) and SWAN nearshore wave energy (Ching-Piao et al., 2012). To my knowledge it has however not yet been used for research on nearshore local-scale wave height. In the current study, EMD successfully separated the corrected SWAN wave height time series into the timescales of wave height variability of the nearshore close to the launch sites. While some of the studies mentioned above use the Ensemble EMD method (Wu & Huang, 2009; Ezer, Haigh & Woodworth, 2016) to address mode mixing (Wu & Huang, 2009; Wang et al., 2012), no mode mixing was evident in the resultant modes of this study.

While most of the above studies use the Hilbert transform to post-process EMD or EEMD results (Huang et al., 1998; Schmitt et al., 2009), the Fast Fourier Transform (FFT) was preferred in this study. The FFT method provides the dominant frequency of the entire mode time series which is of interest for this study (Donnelly, 2006). FFT has been used in conjunction with EMD on non-environmental data such as wind turbine current signals (Lin & Chen, 2012). While using FFT for post-processing of EMD results is not common with respect to environmental (let alone marine) data, FFT on its own has been successfully used for frequency spectrum analyses on coastal environmental data (Hardman-Mountford et al., 2003; Bressan & Tinti, 2016; Armenio, De Serio & Mossa, 2017). The combination of the two methods here yielded adequate results for this study.

Linear regression analyses were considered a suitable method to test for trends because it is a widely accepted way to detect, and estimate the statistical significance of, linear environmental trends in historical data over time (Hartmann et al., 2013). However, findings as indicated in the results, most time series were not linear when the model's assumptions were checked. This was solved by fitting quadratic formula to the linear model, transforming the model into a non-linear and thus ensuring statistical results are more acceptable. Again, the non-linear models' abilities were checked and confirmed to fit the time series well and thus suitable to draw conclusion from its results. However, statistical significance of trends observed in this study should be treated with due caution since the length of the time series is only 14 years. With such a short time series, detected trends must be considered uncertain in terms of representing long-term change over time; as noted, short trends are strongly influenced by the start and end data of the period (Hartmann et al., 2013; Stocker et al., 2013). Taking this into consideration, it is likely acceptable to consider significant trends detected in this study as *possible* trends or *tendencies* over the study's time period (1997–2014).

The Sequential Regime Shift Detection (SRSD) method was effective at detecting a regime shift in wave height anomalies. While the robustness of regime shift detection is considered strengthened when more than one detection method is used on more than one variable, Blamey et al. (2012) found SRSD to be adequate for determining *possible* regime shifts by itself. While SRSD was applied to both straight and pre-whitened data, the current study focussed on the former. This decision was based on Howard et al. (2007) who found that the timing of biological observations correlated to the SRSD analyses on straight data but not on pre-whitened data. Similar to the study of Ward (2018), where *possible* South Coast wind regime shifts were determined in this way, straight analysis was thus considered suitable for accurately detecting the timing of *possible* regime shifts in the present study. The parameters used to detect the regime shift were determined by the sensitivity analyses performed in this study, where the various values of the parameters chosen were based on earlier work that also investigated the southern Benguela marine environment (Howard et al., 2007; Blamey et al., 2012).

In summary, the length of the corrected time series is considered adequate for correlation with fishers' perspectives and thus the objectives of this thesis. The NCEP-forced corrected SWAN model

data analysed in this study is considered to constitute reliable information on coastal region of the South Coast. Spatial averaging is considered adequate for general nearshore wave analysis and H_{m0} for sea state analysis as required for this study. EMD and FFT can be effectively combined to determine the periods of variability embedded in the corrected wave height data. Regression analyses of linear and non-linear time series provides adequate information about their *tendencies*. Use of SRSD in this study is based on the sensitivity analyses performed in this study, past studies results using the method on similar data, and it thus is considered suitable for detecting *possible* regime shifts.

5.2. Discussion of results:

5.2.1. General wind and wave characteristics:

The wind results discussed here represent the synoptic-scale winds over the South Coast region. The general synoptic-scale annual and summer (December to February) wind (**Fig. 4.1 (a)** and **Appendix H (a)**) and wave (**Fig. 4.1 (b)** and **Appendix H (b)**) directions along the South Coast over the period of 1997–2014 agree with synoptic-scale atmospheric circulation patterns (Schumann, in press; Blanke et al., 2009) and offshore synoptic-scale wave climates (Rossouw, 1989; Theron et al., 2010; Rossouw, Terblanche & Moes, 2013) observed over the Agulhas Bank. This qualitative comparison with existing literature indicates that the NCEP model effectively simulates the average synoptic-scale wind and the average offshore synoptic-scale wave directions off the South Coast of South Africa.

The average changes in wave height and direction observed from offshore (**Fig. 4.1 (b)** and **Appendix H (b)**) to nearshore (**Fig. 4.2** and **Appendix I**) in this study agree with the known effects of refraction and bottom friction in shallow waters. As offshore waves propagate through shallower coastal waters, wave bases start to encounter the sea floor, bottom friction begins decelerating the wave, and wave height starts to decrease (Laing et al., 1998; Folley & Whittaker, 2009). Since waves travel faster in deeper water, the north end of the south-westerly approaching wave fronts, which encounters the shallow coastal waters of the South Coast first, will slow down compared to the south end; this therefore refracts towards the coast, and the wave front approaches from a more southerly direction (see **Fig. 2.12 (a)**) (Laing et al., 1998; Talley et al., 2011). Taken together, these processes acting on approaching waves result in lower wave heights and more southerly waves (compared to south-westerly) at the study sites.

Refraction in bays also spreads the wave energy out along the coastline, further decreasing wave height along the coast (Laing et al., 1998; Stewart, 2008; Talley et al., 2011). Consequently, the waves entering the embayments of Witsand and Mossel Bay experience more energy dissipation and thus are lower in height when they reach the nearshore waters than those of Still Bay and Gouritz.

Furthermore, depending on the shape of the local coastline and the direction of the incoming swell, local bathymetry may cause wave heights to decrease in sheltered coastal waters waves. In the south-eastward-facing bays of Witsand and Mossel Bay (**Fig. 3.2 (a)** and **Fig. 3.3 (b)**), study sites (launch sites) are located near the main launch sites on the west side of the embayments. Here wave heights are low because of the sheltering effect of the local headlands from the predominantly south-westerly-approaching swell. In contrast, the nearshore study sites at Still Bay and Gouritz are more directly exposed to these swell because the local coastline is flatter (fewer embayments or headlands) and southward-facing (**Fig. 3.2 (b)** and **Fig. 3.3 (a)**). Thus, the fishers in Witsand and Mossel Bay may find it easier to leave and return to the nearshore; however this excludes any problems encountered at river mouths (Witsand and Gouritz) or in the river itself (Ward, 2018; Gammage, 2015; Gammage, Jarre & Mather, 2017b), as well as the effects of the breakwaters of the Still Bay and Mossel Bay harbours.

The predominance of swell (about 10 s) along the South African coasts as shown in Cooper (2001) and Rossouw et al. (2013) is also evident in this study for the South Coast during summer of the period 1997–2014 (**Fig. 4.3 (b)**). The peak of shorter period waves observed only in Witsand and Mossel Bay are hypothesised to be local-scale easterly wind-waves driven by local easterly NCEP synoptic-scale wind inputs, which are mostly observed during summer (**Fig. 4.2 (a, d)**). The south-eastward-facing Witsand and Mossel Bay could be more directly exposed to these synoptic-scale easterly winds and subsequent local-scale easterly low peak period wind-waves than the southward-facing Still Bay and Gouritz. Consequently, when easterlies blow, fishers in Witsand and Mossel Bay may have a harder time going out to sea compared to those in Still Bay and Gouritz because easterly wind-waves could be superimposed on the dominant south-westerly swell. However, the synoptic-scale winds forcing the local-scale wind-waves are likely to be over-exaggerated in the model because it is run in stationary mode and the synoptic-scale winds are saturated across the SWAN grid; i.e., the synoptic-scale winds for each timestep blow for the entire duration of time step (three hours), which is probably an overestimation. Additionally, the seasonality of the synoptic-scale winds and of wave direction was not analysed in this study due to time constraints and thus conclusions drawn about it are uncertain.

Synoptic-scale sub-daily sea-land breezes, which have been observed and studied along the South African coast, could be driving the local-scale sub-daily wave height cycle observed in this study in **Fig. 4.8 (b)** (Preston-Whyte, 1969; Tyson & Preston-Whyte, 1972; Schumann, Illenberger & Goschen, 1991). Maximum afternoon sea breezes have globally been found to be consistent with higher afternoon coastal wave heights (Sonu et al., 1973; Remya & Kumar, 2013). While nearshore local-scale wave height from the morning to the afternoon generally increases along the South Coast, the increase is very small (**Fig. 4.8 (b)**). This is expected because, as noted, the South Coast is swell-dominated (Cooper, 2001; Rossouw et al., 2013), and the produced sub-daily wind-waves are therefore less pronounced, as evidenced by the lower ‘chop’ peak. In addition, because sub-daily sea-land breezes are limited by fetch area in terms of duration, the sub-daily waves generated mostly likely are small.

Furthermore, since these analyses were performed using annual data, the degree of oscillation within the sub-daily cycles could be dampened. Lastly, the NCEP model resolution may be too coarse to capture the local sub-daily winds and thus the SWAN model results may not always capture wind-waves induced by land-sea breezes.

The average local-scale seasonal wave height cycle along the South Coast in **Fig. 4.8 (a)** is consistent with the swell seasonal cycle observed over the Agulhas Bank, where average synoptic-scale wind speeds and wave heights (and subsequently nearshore local-scale wave heights) are strongest and highest during winter (Rossouw, 1989; Rossouw, Terblanche & Moes, 2013). Therefore, over the study period the fishers most likely were able to leave and return to the nearshore more easily during summer, which coincides with the main fishing season. However, because of the exposure of the Still Bay and Gouritz study sites to the approaching swell, these study sites show a much stronger seasonal cycle than those in the sheltered areas at Witsand and Mossel Bay.

In the above analyses, Witsands and Mossel Bay seem to experience similar wave conditions, while Still Bay and Gouritz do experience the same/similar wave conditions. The statistical test of significance difference in mean of summer average peak periods and H_{m0} indicated that only Still Bay and Gouritz summer average mean peak periods are not different from one another. This indicates that the wave conditions of Still Bay and Gouritz are more similar to one another, than the wave conditions of Witsand and Mossel Bay to one another. Furthermore, this confirms that the wave conditions between Witsand and Still Bay, Witsand and Goutiz, Still Bay and Mossel Bay, Goutitz and Mossel bay are not similar to one another.

5.2.2. Wave height variability and tendency:

The increase in variability of the sub-daily wave height post-2006, particularly at Still Bay and Gouritz (**Fig. 4.5**), could be due to the stronger exposure of these two study sites to the influences of the average synoptic-scale summer sub-daily variability, while Witsand and Mossel Bay are more sheltered by headlands. The timing of this increase in variability is in line with the results of Blamey et al. (2012), who found a 2007 shift towards more monthly upwelling variability at Cape Agulhas, part of the same coastal subsystem. Additionally, Ward (2018) found a 2006/2007 regime shift towards higher variability in the annual (June to May) offshore synoptic-scale westerly-easterly wind component at the same NCEP point used in this study. The South Coast marine system therefore may have been was more variable during summer months and on a sub-daily scale from about 2006/2007 until 2014. Consequently, uncertainty in fishers' assessment of whether the afternoon return would be as easy as the morning departure may have increased, particularly for Still Bay and Gouritz during 2006.

The increase in variability of summer sub-daily wave height difference post-2006 across the South Coast (**Fig. 4.5**) corresponds to the timing of the distinct change (**Fig. 4.6 (d)**) and regime shift (**Fig. 4.7**) from an abnormal low to an abnormal high mean wave height observed during 2006. This

mid- to late 2000s shift agrees with Lamont et al. (2018), who found more upwelling during 2007 along the Agulhas Bank coast. Ward (2018) also showed a 2006/2007 regime shift towards more offshore synoptic-scale easterly mean winds during austral summer (October to March) at the same NCEP point as used in this study. While the present study did not investigate if the observed wave height shift is specific to a season or if it occurs throughout the year, the observed seasonal shifts in the offshore synoptic-scale NCEP-sourced winds (Ward, 2018) could be driving the increase in mean height and variability of nearshore local-scale South Coast waves post-2006.

The influence of the summer offshore synoptic-scale NCEP wind speeds on local-scale wave height along the South Coast is again confirmed by the observed increasing number of extreme wind days (Ward, 2018) and wave height significant positive tendencies (**Fig. 4.6 (a)** and **Appendix C**), even though the period over which the wind tendency is observed is longer (1979 to 2015) than the present study's period (1997 to 2014) and that the winds analysed were only those of austral summer. Other studies have similarly found recent increasing trends across the Agulhas Bank towards stronger westerly winds, as a result of trends towards positive SAM phases (Hartmann et al., 2013; Loveday, Penven & Reason, 2015), and more frequent upwelling-favourable winds, as a result of the southward shifting of the South Atlantic High-Pressure System (SAH) (Lamont et al., 2018). Since the offshore synoptic-scale wind speeds of the South Coast show an increasing trend and remotely produced swell waves have been observed to dominate the South African coast, it is expected that this wind speed trend would manifest in the synoptic-scale NCEP swell heights and subsequently in the nearshore local-scale SWAN swell heights along the South Coast. However, again it must be mentioned here that while the present study did not investigate if the observed wave height trend is specific to a season or if it occurs throughout the year, the observed seasonal trend in the offshore synoptic-scale NCEP-sourced winds (Ward, 2018) could be driving the positive linear tendency towards higher nearshore local-scale South Coast waves.

The magnitudes of wave heights during the lower wave height period from 1997 to 2007 and the higher wave height period from 2007 to 2014 are reflected in the magnitudes of the sub-daily and monthly cycles. The timing of the monthly cycles differs from the average monthly cycle while the average sub-daily cycle is unchanged (**Fig. 4.8**). The following discussion pertains only to Still Bay and Gouritz, as the seasonal cycle was not strong enough for analysis at the more sheltered Witsand and Mossel Bay sites. During the lower wave height period (1997–2007), wave heights linked with summer conditions (lower waves) arrived later during the year. In contrast, wave heights linked with winter conditions (lower waves) arrived later during the higher wave height period (2007–2014). Thus summer waves lasted for a shortened period during 1997–2007 but for a longer period during 2007–2014.

The recent statements by the South Coast fishers about increasing variability in the 'normal' wind regimes (shifts between south-easterly and south-westerly winds) (Duggan, 2012; Gammage, 2015; Gammage, Jarre & Mather, 2017a) could be linked to the recent increase in summer sub-daily

wave height variability (post-2006) that was observed in this study (**Fig. 4.5**). Furthermore, the significant tendency towards higher nearshore South Coast waves observed in this study (**Fig. 4.6 (a)** and **Appendix C**) agrees with fishers' observations of a deteriorating sea state (Duggan, 2012; Gammage, 2015). Lastly, the longer duration of summer wave conditions towards from 2007-2014 observed in the current study (**Fig. 4.8**) could be linked to the fishers' observations of prolonged summer wind conditions (Duggan, 2012). However, the earlier period from 1997–2007 corresponds to the other fisher observation that summer wind conditions have been arriving later than normal (Duggan, 2012).

5.3. Discussion of future work:

Vermaaklikheid (between Witsand and Still Bay) is another fishing settlement along the South Coast which is also part of the SCIFR research project. This location might be investigated in the future in line with the work presented in this study. Given the results of the current study, it is expected that nearshore local-scale wave conditions at Vermaaklikheid may resemble those at Still Bay due to its southward-facing flatter shoreline but may incorporate features similar to Witsand because of the sites' close proximity. A longer time series would help make the statistics in this study more robust, particularly when testing the significance of observed wave height tendencies. While regime shift analyses were not the focus of this study, more and different regime shift detection analyses could be applied to the data to verify the possible shifts detected by SRSD. Performing correlation analyses between modes of variability and interannual wave height variability may be a more robust way to compare the years known to experience interannual variability to the years observed in this study which show interannual variability. Analysing the wave data separately in terms of driving forces (swell versus wind-driven) would help determine the degree of influence of the offshore synoptic-scale NCEP winds at the study sites; this may be important in the case of the low peak periods that were observed at Witsand and Mossel Bay but not at Still Bay and Gouritz. The discrepancies between sea state seasonal analyses and fishers observations highlights the need for specificity in interpreting observations both on the part of the fishers and of the scientists. Specifically, analyses of the onset of the first South-Easter event of the season, and changes in the frequency and duration of those events during summer would be useful. Additionally, continued efforts to improve conversations with fishers in the region may enhance mutual understanding of the changes discerned by fishers and researchers, and make detected correlations more robust.

5.4. Conclusion:

An understanding of multiple high resolution environmental factors contributing to sea state conditions along the South Coast of South Africa can help to contextualise and correctly interpret fishers' observations. Sea state is not driven by a single external force but by a combination of many forces, and fishers' observations of a deteriorating sea state and higher climate variability are not simply based on environmental factors. Analysing sea state conditions in terms of wave climate similar to Ward (2018) and analyses of wind conditions (which influence wave conditions) can advance the quantified understanding of the environment the fishers observe first hand.

The NCEP model was found to accurately resolve the average synoptic-scale wind and the average offshore synoptic-scale wave directions off the South Coast of South Africa, and thus provide accurate boundary conditions for the nearshore local-scale sea state simulations of the SWAN model. The shape and bathymetry of the South Coast coastline impacts the nearshore local-scale sea state in terms of wave height, wave direction, and sub-daily and seasonal variability. Coastal areas within south-eastward-facing bays with headlands on the west side were more sheltered from approaching south-westerly swell , and thus on average experienced lower waves from the southeast and a weaker seasonal cycle. This is in contrast to more exposed coastal areas such as the flatter (with fewer embayments or headlands) southward-facing areas along the South Coast, where the seasonal cycle on average is strong with more southerly, higher waves. Additionally, the south-eastward-facing embayments appear to experience low peak period waves, which is attributed to the focussing of nearshore local-scale summer easterly wind-waves (shorter period waves compared to swell) driven by the local synoptic-scale scale summer easterly winds. There remains some uncertainty regarding this last conclusion, as the seasonality of the synoptic-scale winds and of the waves directions was not analysed in this study. Additionally, the synoptic-scale winds and thus local-scale wave heights are likely to be over-exaggerated as the model was run in stationary mode.

The presence of slightly higher afternoon than morning waves along the South Coast was confirmed for the summer months and could possibly be induced by local sub-daily winds such as synoptic-scale scale sea-breezes. This additional height is expected to be small as a result of the swell dominating over the wind-waves and that the fetch area is limited in terms of the duration of sea breezes. Additionally, difference could also be small because looking at annual data may dampen season sub-daily cycles (if any) and the NCEP model's resolution may be too coarse to capture all land-sea breezes. High sub-daily variability was also observed; this became increasingly more pronounced post-2006 and particularly so for the more exposed sites. The timing of this increase in variability along the South Coast agrees both with other studies of upwelling and wind variability (Ward, 2018; Blamey et al., 2012), and with local fishers' observations of increasing climate variability (Duggan, 2012; Gammage, Jarre & Mather, 2017a). For the sites that showed strong seasonality in wave heights, rougher seas

occurred in winter than in summer, as expected in line with seasonality of the synoptic-scale scale swell over the Agulhas Bank. The duration of summer conditions appears to have lengthened post-2006, again agreeing with fishers' observations. Fishers' observations about later arrivals of summer conditions (Duggan, 2012), which will include the arrival of Kob in the inshore, do not however agree with findings of this study which observed summer waves to arrive earlier in the latter abnormal wave height period (post-2006 to 2014).

Since swell dominates along the coast, the trends and variability seen in the offshore synoptic-scale winds (and thus swell) are reflected in terms of wave height along the entire South Coast. Specifically, increasing nearshore local-scale wave heights observed in this study correspond to the observed offshore synoptic-scale austral summer wind (i.e., upwelling favourable winds) trends found in other studies (Ward, 2018; Lamont et al., 2017). However, again this cannot be stated with certainty because the present study did not analyse offshore synoptic-scale waves trends or variability. Additionally, the 2006 regime shift towards higher wave heights is consistent with the increase in summer sub-daily wave height variability observed in the current study, as well as regime shifts towards increasing mean upwelling (Lamont et al., 2018) and offshore synoptic-scale austral summer easterly winds (Ward, 2018) along the South Coast reported by other studies. Such increasing trends and interannual variability in sea state agree with the observed deterioration in sea state reported by the fishers (Duggan, 2012; Gammage, 2015; Gammage, Jarre & Mather, 2017a).

In conclusion SWAN model outputs are an appropriate tool to analyse nearshore local-scale wave climate at the South Coast as relevant to handline fishers. However, discrepancies between reports and study findings still exist; in this case with respect to shifts in seasonality. Future sea state studies may focus on this issue and include separate analyses of wind-waves vs swell, as well as a more in depth intra-seasonal analysis of wave height and direction.

References:

Ahrens, C.D. & Henson, R. 2016. *Essentials of meteorology: An invitation to the atmosphere, 8th edition*.

Akpinar, A. & Kömürcü, M.I. 2012. Wave energy potential along the south-east coasts of the Black Sea. *Energy*. 42:289–302. DOI: 10.1016/j.energy.2012.03.057.

Armenio, E., De Serio, F. & Mossa, M. 2017. Analysis of data characterizing tide and current fluxes in coastal basins. *Hydrology and Earth System Sciences*. 21(7):3441–3454. DOI: 10.5194/hess-21-3441-2017.

Arnott, R.D. 2009. *Introduction to Coastal Processes & Geomorphology*. DOI: 10.2112/1551-5036(2006)22[1589:BR]2.0.CO;2.

Baloyi, J., Mahlathi, C.D., Wessels, G.J.C., Ubbink, O. & Smit, J.E. 2009. Numerical study of the resultant sediment transport near the Port of Ngqura due to the blockage of a sediment bypass. In *13th International Conference on Heat Transfer, Fluid Mechanics and Thermodynamics*. 940–949.

Barnes, J. 2018. Altimetry comparison backward wave recreation and extreme wave analysis of NCEP data: Cape Point to Richards Bay. Master of Engineering (Civil). University of Stellenbosch.

Blamey, L.K., Howard, J.A.E., Agenbag, J. & Jarre, A. 2012. Regime-shifts in the southern Benguela shelf and inshore region. *Progress in Oceanography*. 106:80–95. DOI: 10.1016/j.pocean.2012.07.001.

Blamey, L.K., Shannon, L.J., Bolton, J.J., Crawford, R.J.M., Dufois, F., Evers-King, H., Griffiths, C.L., Hutchings, L., et al. 2015. Ecosystem change in the southern Benguela and the underlying processes. *Journal of Marine Systems*. 144:9–29. DOI: 10.1016/j.jmarsys.2014.11.006.

Blanke, B., Penven, P., Roy, C., Chang, N. & Kokoszka, F. 2009. Ocean variability over the Agulhas Bank and its dynamical connection with the southern Benguela upwelling system. *Journal of Geophysical Research: Oceans*. 114:C12028. DOI: 10.1029/2009JC005358.

Booij, N., Ris, R.C. & Holthuijsen, L.H. 1999. A third-generation wave model for coastal regions: 1. Model description and validation. *Journal of Geophysical Research*. 104(C4):7649–7666. DOI: 10.1029/98JC02622.

Bressan, L. & Tinti, S. 2016. Statistical properties of coastal long waves analysed through sea-level time-gradient functions: Exemplary analysis of the Siracusa, Italy, tide-gauge data. *Natural Hazards and Earth System Sciences*. 16(1):223–237. DOI: 10.5194/nhess-16-223-2016.

Brigham, E.O. & Morrow, R.E. 1967. The fast Fourier transform. *IEEE Spectrum*. 4(12):63–

70. DOI: 10.1109/MSPEC.1967.5217220.

Bryhn, A.C. & Dimberg, P.H. 2011. An operational definition of a statistically meaningful trend. *PLoS ONE*. 6(4):1–9. DOI: 10.1371/journal.pone.0019241.

Casas-Prat, M. & Sierra, J.P. 2010. Trend analysis of the wave storminess: The wave direction. *Natural Hazards and Earth System Science*. 10:2327–2340. DOI: 10.5194/nhess-10-2327-2010.

Ching-Piao, T., Ching-Her, H., Chien, H. & Hao-Yuan, C. 2012. Study on the wave climate variation to the renewable wave energy assessment. *Renewable Energy*. 38:50–61. DOI: 10.1016/j.renene.2011.06.041.

Cochran, W.T., Cooley, J.W., Favin, D.L., Helms, H.D., Kaenel, R. a., Lang, W.W., Maling, G.C.. J., Nelson, D.E., et al. 1967. What is the fast Fourier transform? *Proceedings of the IEEE*. 55(10):1664–1674. DOI: 10.1109/PROC.1967.5957.

Conversi, A., Dakos, V., Gardmark, A., Ling, S., Folke, C., Mumby, P.J., Greene, C., Edwards, M., et al. 2014. A holistic view of marine regime shifts. *Philosophical Transactions of the Royal Society B: Biological Sciences*. 370(20130279):1–8. DOI: 10.1098/rstb.2013.0279.

Cooley, J.W. & Tukey, J.W. 1965. An Algorithm for the Machine Calculation of Complex Fourier Series. *Mathematics of Computation*. 19(90):297–301. DOI: 10.2307/2003354.

Cooley, J., Lewis, P. & Welch, P. 1969. The fast Fourier transform and its applications. *IEEE Transactions on Education*. 12(1):27–34.

Cooper, J. 2001. Geomorphological variability among microtidal estuaries from the wave-dominated South African coast. *Geomorphology*. 40:99–122. DOI: 10.1016/S0169-555X(01)00039-3.

Department of Agriculture Forestry and Fisheries. 2012. Policy for the Small Scale Fisheries Sector in South Africa. (10505):56.

Donnelly, D. 2006. The fast Fourier and Hilbert-Huang transforms: A comparison. *International Journal of Computers, Communications & Control*. I(4):45–52. DOI: 10.1109/CESA.2006.4281628.

Dufois, F. & Rouault, M. 2012. Sea surface temperature in False Bay (South Africa): Towards a better understanding of its seasonal and inter-annual variability. *Continental Shelf Research*. 43:24–35. DOI: 10.1016/j.csr.2012.04.009.

Duggan, G.L. 2012. In the realm of the Kob Kings: Rethinking knowledges and dialogue in a small-scale fishery. Master of Social Science. Univeristy of Cape Town.

Duggan, G.L., Green, L.J.F. & Jarre, A. 2014. “Thinking like a fish”: Adaptive strategies for coping with vulnerability and variability emerging from a relational engagement with kob. *Maritime*

Studies. 13(4):1–21. DOI: 10.1186/2212-9790-13-4.

Edwards, P.N. 2011. History of climate modeling. *Wiley Interdisciplinary Reviews: Climate Change*. 2(1):128–139. DOI: 10.1002/wcc.95.

Ezer, T. & Corlett, W.B. 2012. Is sea level rise accelerating in the Chesapeake Bay? A demonstration of a novel new approach for analyzing sea level data. *Geophysical Research Letters*. 39(L19605):1–6. DOI: 10.1029/2012GL053435.

Ezer, T., Atkinson, L.P., Corlett, W.B. & Blanco, J.L. 2013. Gulf Stream's induced sea level rise and variability along the U.S. mid-Atlantic coast. *Journal of Geophysical Research: Oceans*. 118:685–697. DOI: 10.1002/jgrc.20091.

Ezer, T., Haigh, I.D. & Woodworth, P.L. 2016. Nonlinear sea-level trends and long-term variability on western European coasts. *Journal of Coastal Research*. 320:744–755. DOI: 10.2112/JCOASTRES-D-15-00165.1.

Folley, M. & Whittaker, T.J.T. 2009. Analysis of the nearshore wave energy resource. *Renewable Energy*. 34:1709–1715. DOI: 10.1016/j.renene.2009.01.003.

Gammage, L.C. 2015. Considering one's option when the fish leave: a case study of the traditional commercial handline fishery of the Southern Cape. Masters of Science. University of Cape Town.

Gammage, L.C., Jarre, A. & Mather, C. 2017a. A case study from the southern Cape linefishery 1 : The difficulty of fishing in a changing world. *South African Journal of Science*. 113(5/6):1–8. DOI: 10.17159/ sajs.2017/20160252.

Gammage, L.C., Jarre, A. & Mather, C. 2017b. A case study from the southern Cape linefishery 2: Considering one's options when the fish leave. *South African Journal of Science*. 113(5/6):1–10.

Griffiths, M.H. 2000. Long-term trends in catch and effort of commercial linefish off South Africa's Cape Province: snapshots of the 20 th century. *South African Journal of Marine Science*. 22:81–110. DOI: 10.2989/025776100784125663.

Hardman-Mountford, N.J., Richardson, A.J., Agenbag, J.J., Hagen, E., Nykjaer, L., Shillington, F.A. & Villacastin, C. 2003. Ocean climate of the South East Atlantic observed from satellite data and wind models. *Progress in Oceanography*. 59:181–221. DOI: 10.1016/j.pocean.2003.10.001.

Hartmann, D.J., Klein Tank, A.M.G., Rusticucci, M., Alexander, L. V., Brönnimann, S., Charabi, Y.A.R., Dentener, F.J., Dlugokencky, E.J., et al. 2013. Observations: atmosphere and surface. In *Climate change 2013: The physical science basis. Contribution of Working Group I to the Fifth Assessment Report of the Intergovernmental Panel on Climate Change*. T.F. Stocker, D. Qin, G.-K. Plattner, M. Tignor, S.K. Allen, J. Boschung, A. Nauels, Y. Xia, V. Bex, & P.M. Midgley, Eds.

Cambridge University Press, Cambridge, United Kingdom and New York, NY, USA. 159–254. DOI: 10.1017/CBO9781107415324.008.

Hasselmann, K., Barnett, T.P., Bouws, E., Carlson, H., Cartwright, D.E., Enke, K., Ewing, J.A., Gienapp, H., et al. 1973. Measurements of wind-wave growth and swell decay during the Joint North Sea Wave Project (JONSWAP). *Ergnzungsheft zur Deutschen Hydrographischen Zeitschrift Reihe*. (12). DOI: citeulike-article-id:2710264.

Howard, J.A.E., Jarre, A., Clark, A.E. & Moloney, C.L. 2007. Application of the sequential t-test algorithm for analysing regime shifts to the southern Benguela ecosystem. *African Journal of Marine Science*. 29(3):437–451. DOI: 10.2989/AJMS.2007.29.3.11.341.

Huang, N.E., Shen, Z., Long, S.R., Wu, M.C., Shih, H.H., Zheng, Q., Yen, N.-C., Tung, C.C., et al. 1998. The empirical mode decomposition and the Hilbert spectrum for nonlinear and non-stationary time series analysis. *Proceedings of the Royal Society London A: Mathematical, Physical and Engineering Sciences*. 454(1971):903–995. DOI: 10.1098/rspa.1998.0193.

Huang, N.E., Wu, M.-L., Qu, W., Long, S.R. & Shen, S.S.P. 2003. Applications of Hilbert-Huang transform to non-stationary financial time series analysis. *Applied Stochastic Models in Business and Industry*. 19:245–268. DOI: 10.1002/asmb.501.

Hughes, M. 2016. *Coastal waves, water levels, beach dynamics and climate change*. CoastAdapt, National Climate Change Adaptation Research Facility, Gold Coast.

Hutchings, L., Beckley, L.E., Griffiths, M.H., Roberts, M.J., Sundby, S. & van der Lingen, C. 2002. Spawning on the edge: spawning grounds and nursery areas around the southern African coastline. *Marine and Freshwater Research*. 53:307–318. DOI: 10.1071/MF01147.

Hutchings, L., van der Lingen, C.D., Shannon, L.J., Crawford, R.J.M., Verheye, H.M.S., Bartholomae, C.H., van der Plas, A.K., Louw, D., et al. 2009. The Benguela Current: An ecosystem of four components. *Progress in Oceanography*. 83:15–32. DOI: 10.1016/j.pocean.2009.07.046.

IPCC. 2001. *Climate change 2001: The scientific basis. Contribution of Working Group I to the Third Assessment Report of the Intergovernmental Panel on Climate Change*. J.T. Houghton, Y. Ding, D.J. Griggs, M. Noguer, van der L.P. J, X. Dai, K. Maskell, & C.A. Johnson, Eds. Cambridge University Press, Cambridge, United Kingdom and New York, NY, USA. DOI: 10.1256/004316502320517344.

IPCC. 2014. *Climate change 2014: Synthesis report. Contribution of Working Groups I, II and III to the Fifth Assessment Report of the Intergovernmental Panel on Climate Change*. IPCC, Geneva, Switzerland. DOI: 10.1017/CBO9781107415324.004.

Jarre, A., Hutchings, L., Kirkman, S.P., Kreiner, A., Tchipalanga, P.C.M., Kainge, P., Uanivi,

U., van der Plas, A.K., et al. 2015. Synthesis: climate effects on biodiversity, abundance and distribution of marine organisms in the Benguela. *Fisheries Oceanography*. 24(S1):122–149. DOI: 10.1111/fog.12086.

Joubert, J.R. & van Niekerk, J.L. 2013. *South African wave energy resource data: A case study*.

Kruger, A.C., Goliger, A.M., Retief, J. V. & Sekele, S. 2010. Strong wind climatic zones in South Africa. *Wind and Structures, An International Journal*. 13(1):37–55. DOI: 10.12989/was.2010.13.1.037.

Laing, A.K., Gemmill, W., Magnusson, A.K., Burroughs, L., Reistad, M., Khandekar, M., Holthuijsen, L., Ewing, J.A., et al. 1998. *Guide to wave analysis and forecasting*. second ed. E. Bouws, L. Draper, A.K. Laing, D.J.T. Carter, L. Eide, & J.A. Battjes, Eds. Geneva, Switzerland: World Meteorological Organization.

Lamont, T., García-Reyes, M., Bograd, S.J., van der Lingen, C.D. & Sydeman, W.J. 2018. Upwelling indices for comparative ecosystem studies: Variability in the Benguela Upwelling System. *Journal of Marine Systems*. 188:3–16. DOI: 10.1016/j.jmarsys.2017.05.007.

Lin, D.-F. & Chen, P.-H. 2012. Fault recognition of wind turbine using EMD analysis and FFT classification. In *Third International Conference on Digital Manufacturing & Automation Fault*. Taiwan. 414–417. DOI: 10.1109/ICDMA.2012.99.

Loveday, B.R., Penven, P. & Reason, C.J.C. 2015. Southern Annular Mode and westerly-wind-driven changes in Indian-Atlantic exchange mechanisms. *Geophysical Research Letters*. 42:4912–4921. DOI: 10.1002/2015GL064256.

Lutjeharms, J.R.E. 2006. The ocean environment off southeastern Africa: A review. *South African Journal of Science*. 102:419–426.

Lutjeharms, J.R.E., Cooper, J. & Roberts, M. 2000. Upwelling at the inshore edge of the Agulhas Current. *Continental Shelf Research*. 20:737–761.

McGuffie, K. & Henderson-Sellers, A. 2005. Chapter 1: Climate. In *A climate modelling primer, 3rd edition*. John Wiley & Sons, Ltd. 1–46.

Miller, S.T.K., Keim, B.D., Tabolt, R.W. & Mao, H. 2003. Sea breeze: Structure, forecasting, and impacts. *Reviews of Geophysics*. 41(3). DOI: 10.1029/2003RG000124.

Pauly, D. & Christensen, V. 1995. Primary production required to sustain global fisheries. *Nature*. 374:255–257.

Petersen, S., Paterson, B., Basson, J., Moroff, N., Roux, J.-P., Augustyn, J. & D'Almeida, G. 2010. *Tracking the implementation of an Ecosystem Approach to Fisheries in Southern Africa. WWF*

South Africa report series - 2010/Marine/001.

Preston-Whyte, R.A. 1969. Sea breeze studies in Natal. *South African Geographical Journal*. 51(1):38–49. DOI: 10.1080/03736245.1969.10559447.

Raemaekers, S. & Sowman, M. 2015. *Community-level socio-ecological vulnerability assessments in the Benguela current large marine ecosystem*. Rome.

Reason, C.J.C., Landman, W. & Tennant, W. 2006. Seasonal to decadal prediction of southern African climate and its links with variability of the Atlantic ocean. *Bulletin of the American Meteorological Society*. 87(7):941–955. DOI: 10.1175/BAMS-87-7-941.

Remya, P.G. & Kumar, R. 2013. Impact of diurnal variation of winds on coastal waves off south east coast of India. *The International Journal of Ocean and Climate Systems*. 4(3):171–179. DOI: 10.1260/1759-3131.4.3.171.

Rodionov, S.N. 2004. A sequential algorithm for testing climate regime shifts. *Geophysical Research Letters*. 31(L09204):1–4. DOI: 10.1029/2004GL019448.

Rodionov, S.N. 2006. Use of prewhitening in climate regime shift detection. *Geophysical Research Letters*. 33(L12707):1–4. DOI: 10.1029/2006GL025904.

Rossouw, J. 1989. Design waves for the South African coastline. Doctorate of Philosophy. University of Stellenbosch.

Rossouw, M., Terblanche, L. & Moes, J. 2013. *General characteristics of long waves around the South African coast*. Stellnebosch.

Rossouw, M., Rautenbach, C., Page, P. & Harribhai, J. 2015. Deriving nearshore wave climate data along the South African coast. In *11th International Symposium for GIS and Computer Cartography for Coastal Zones Management*.

Rouault, M., Pohl, B. & Penven, P. 2010. Coastal oceanic climate change and variability from 1982 to 2009 around South Africa. *African Journal of Marine Science*. 32(2):237–246. DOI: 10.2989/1814232X.2010.501563.

Roy, C., Van Der Lingen, C.D., Coetzee, J.C. & Lutjeharms, J.R.E. 2007. Abrupt environmental shift associated with changes in the distribution of Cape anchovy *Engraulis encrasicolus* spawners in the southern Benguela. *African Journal of Marine Science*. 29(3):309–319. DOI: 10.2989/AJMS.2007.29.3.1.331.

Schmitt, F.G., Huang, Y., Lu, Z., Liu, Y. & Fernandez, N. 2009. Analysis of velocity fluctuations and their intermittency properties in the surf zone using empirical mode decomposition. *Journal of Marine Systems*. 77:473–481. DOI: 10.1016/j.jmarsys.2008.11.012.

Schumann, E.H. (in press). Interannual wind variability on the south and east coasts of South Africa. *Journal of Geophysical Research*. 97(D18):20.397-20.403. DOI: 10.1029/92JD02215.

Schumann, E.H. 1999. Wind-driven mixed layer and coastal upwelling processes off the south coast of South Africa. *Journal of Marine Research*. 57:671–691. DOI: 10.1357/002224099321549639.

Schumann, E.H., Illenberger, W.K. & Goschen, W.S. 1991. Surface winds over Algoa Bay, South Africa. *South African Journal of Science*. 87:202–207.

Sharpley, R.C. & Vatchev, V. 2006. Analysis of the intrinsic mode functions. *Constructive Approximation*. 24:17–47. DOI: 10.1007/s00365-005-0603-z.

Sink, K.J., Holness, S., Harris, L., Majiedt, P., Atkinson, L., Robinson, T., Kirkman, S., Hutchings, L., et al. 2012. *National biodiversity assessment 2011: Technical report, Volume 4: Marine and coastal component*. Pretoria.

Sonu, C.J., Murray, S.P., Hsu, S.A., Suhayda, J.N. & Waddell, E. 1973. Sea breeze and coastal processes. *EOS transactions, American Geophysical Union*. 54(9):820–833.

Sowman, M. 2006. Subsistence and small-scale fisheries in South Africa: A ten-year review. *Marine Policy*. 30(1):60–73. DOI: 10.1016/j.marpol.2005.06.014.

Stewart, R.H. 2008. *An introduction to physical oceanography*. Texas. DOI: 10.1119/1.18716.

Stocker, T.F., Dahe, Q., Plattner, G.-K., Alexander, L. V., Allen, S.K., Bindoff, N.L., Bréon, F.-M., Church, J.A., et al. 2013. Technical summary. In *Climate change 2013: The physical science basis. Contribution of Working Group I to the Fifth Assessment Report of the Intergovernmental Panel on Climate Change*. T.F. Stocker, D. Qin, G.-K. Plattner, M. Tignor, S.K. Allen, J. Boschung, A. Nauels, Y. Xia, V. Bex, & P.M. Midgley, Eds. Cambridge, United Kingdom and New York, NY, USA: Cambridge University Press. 33–115. DOI: 10.1017/ CBO9781107415324.005.

Talley, L.D., Pickard, G.L., Emery, W.J. & Swift, J.H. 2011. Gravity waves, tides, and coastal oceanography. In *Descriptive Physical Oceanography*. Elsevier Ltd. 223–244. DOI: 10.1016/B978-0-7506-4552-2.10020-4.

Theron, A., Rossouw, M., Barwell, L., Maherry, A., Diedericks, G. & de Wet, P. 2010. Quantification of risks to coastal areas and development : wave run-up and erosion. In *Science real and relevent conference 2010*. V. NE20–PA–F. 1–16.

Theron, A., Rossouw, M., Rautenbach, C., Page, P., Harribhai, J., Maherry, A. & von Saint Ange, U. 2014. *MetOcean conditions & vulnerability - Medium resolution wave climate & run-up (South African coastal vulnerability assessment DEA - CSIR : Phase 2)*. Cape Town.

Thomas, T.J. & Dwarakish, G.S. 2015. Numerical wave modelling – A review. *Aquatic*

Procedia. 4:443–448. DOI: 10.1016/j.aqpro.2015.02.059.

Trujillo, A.P. & Thurman, H. V. 2014. Waves and water dynamics. In *Essentials of oceanography (11th Edition)*. Pearson Education, Inc.

Tyson, P.D. & Preston-Whyte, R.A. 1972. Observations of regional topographically-induced wind systems in Natal. *Journal of Applied Meteorology*. 643–650.

Visser, N. 2015. The origins of the present: economic conflicts in the fisheries of the South African south coast, circa 1910 to 1950. *Maritime Studies*. 14(9):1–31. DOI: 10.1186/s40152-015-0029-6.

WAMDI Group. 1988. The WAM model—A third generation ocean wave prediction model. *Journal of Physical Oceanography*. 18:1775–1810. DOI: 10.1175/1520-0485(1988)018<1775:TWMTGO>2.0.CO;2.

Wang, T., Zhang, M., Yu, Q. & Zhang, H. 2012. Comparing the applications of EMD and EEMD on time-frequency analysis of seismic signal. *Journal of Applied Geophysics*. 83:29–34. DOI: 10.1016/j.jappgeo.2012.05.002.

Wang, Y.H., Yeh, C.H., Young, H.W.V., Hu, K. & Lo, M.T. 2014. On the computational complexity of the empirical mode decomposition algorithm. *Physica A: Statistical Mechanics and its Applications*. 400:159–167. DOI: 10.1016/j.physa.2014.01.020.

Ward, C.D. 2018. Climate variability in social-ecological systems of the southern Cape: Integrating farming and fishing perspectives. Doctor of Philosophy. University of Cape Town.

Watermeyer, K.E., Hutchings, L., Jarre, A. & Shannon, L.J. 2016. Patterns of distribution and spatial indicators of ecosystem change based on key species in the southern Benguela. *PLoS ONE*. 11(7):1–22. DOI: 10.1371/journal.pone.0158734.

Winker, H., Kerwath, S.E. & Attwood, C.G. 2013. Comparison of two approaches to standardize catch-per-unit-effort for targeting behaviour in a multispecies hand-line fishery. *Fisheries Research*. 139:118–131. DOI: 10.1016/j.fishres.2012.10.014.

Winker, H., Kerwath, S.E. & Attwood, C.G. 2016. *Report on age-structured stock assessments and the simulation of the impact of various fisheries management options for the South African linefishery*.

Wu, Z. & Huang, N.E. 2009. Ensemble Empirical Mode Decomposition: A noise-assisted data analysis method. *Advances in Adaptive Data Analysis*. 1(1):1–41.

WWF. 2011. *Fisheries: Facts and trends South Africa*. Cape Town.

Appendices:

A. Statistical significance of differences between study sites peak period means and significant wave height means:

The statistical results of the two-tailed t-test performed in MATLAB between study sites peak period (pt) means and between their significant wave height (H_{m0}) means.

Peak period (pt) / significant wave height (*Hm0*)	**Data set 1**	**Data set 2**	**p-value**	**t-stat**	**Reject (1) / accept null hypothesis (0)**
pt	Witsand	Still Bay	2.5291e-91	-20.3555	1
pt	Witsand	Gouritz	8.2798e-91	-20.2963	1
pt	Witsand	Mossel Bay	7.2095e-14	-7.4885	1
pt	Still Bay	Gouritz	0.8874	0.1416	0
pt	Still Bay	Mossel Bay	8.1425e-38	12.8769	1
pt	Gouritz	Mossel Bay	2.4120e-37	12.7922	1
H_{m0}	Witsand	Still Bay	0	-133.7583	1
H_{m0}	Witsand	Gouritz	0	-135.1239	1
H_{m0}	Witsand	Mossel Bay	5.7366e-62	-16.6606	1
H_{m0}	Still Bay	Gouritz	8.6317e-05	-3.9268	1
H_{m0}	Still Bay	Mossel Bay	0	119.5793	1
H_{m0}	Gouritz	Mossel Bay	0	121.2310	1

B. Results of the Fast Fourier Transform (FFT) analysis of EMD H_{m0} modes 2–15:

This table shows the peak frequency for each EMD significant wave height (H_{m0}) mode of variability (modes 2–15) of for each study site. Cycle (Days): calculated daily cycles. Colours indicate several 'timescale' groupings. The variability time scale of interest in this study was that of the interannual (pink) time scale, i.e., > ~1 year. This was determined to consist of modes 12–15 for each study site. Although mode 11 for all study sites is on a time scale of a year or more, it does not represent a clear annual cycle and is thus not included in the interannual group.

Witsands				Still Bay				Gouritz				Mossel Bay			
Modes	*Peak Frequency*	*Cycle (Days)*	*Timescale*	*Modes*	*Peak Frequency*	*Cycle (Days)*	*Timescale*	*Modes*	*Peak Frequency*	*Cycle (Days)*	*Timescale*	*Modes*	*Peak Frequency*	*Cycle (Days)*	*Timescale*
2	12300	0.4999	half day	2	12300	0.4999	half day	2	12300	0.4999	half day	2	12300	0.4999	half day
3	6150	0.9998	daily	3	6150	0.9998	daily	3	6150	0.9998	daily	3	6150	0.9998	daily
4	1105	5.5647	5.6 daily	4	1175	5.2332	5.2 daily	4	908	6.7720	6.7 daily	4	1485	4.1407	4.1 daily
5	661	9.3026	9.3 daily	5	634	9.6987	9.7 daily	5	651	9.4455	9.4 daily	5	795	7.7346	7.7 daily
6	391	15.7263	15.7 daily	6	366	16.8005	16.8 daily	6	320	19.2156	19.2 dialy	6	466	13.1953	13.2 daily
7	251	24.4980	24.5 daily	7	194	31.6959	31.7 daily	7	251	24.4980	24.5 daily	7	210	29.2810	29.3 daily
8	118	52.1102	1.7 monthly	8	87	70.6782	2.4 monthly	8	118	52.1102	1.7 monthly	8	81	75.9136	2.5 monthly
9	45	136.6444	4.6 monthly	9	50	122.9800	4.1 monthly	9	37	166.1892	5.5 monthly	9	54	113.8704	3.8 monthly
10	20	307.4500	10.2 monthly	10	18	341.6111	11.4 monthly	10	18	341.6111	11.4 monthly	10	29	212.0345	7.1 monthly
11	14	439.2143	1.2 yearly	11	17	361.7059	12 monthly	11	12	512.4167	1.4 yearly	11	17	361.7059	12.1 monthly
12	9	683.2222	1.9 yearly	12	4	1.5373e+03	4.2 yearly	12	2	3.0745e+02	8.4 yearly	12	10	614.9000	1.7 yearly
13	4	1.5373e+03	4.2 yearly	13	4	1.5373e+03	4.2 yearly	13	3	2.0497e+03	5.6 yearly	13	3	2.0497e+03	5.6 yearly
14	2	3.0745e+02	8.4 yearly	14	2	3.0745e+02	8.4 yearly	14	2	3.0745e+02	8.4 yearly	14	2	3.0745e+02	8.4 yearly
15	2	3.0745e+02	8.4 yearly	15	2	3.0745e+02	8.4 yearly	15	2	3.0745e+02	8.4 yearly	15	2	3.0745e+02	8.4 yearly

Timescale Groups						
Subdaily	Daily	Subweekly	Fortnightly	Monhtly	Annual	Interannual

C. Regression results:

The following table shows the outputs of the regression models fitted to the EMD H_{m0} trend time series for each study site, performed in Rstudio (version 1.1.442). The model that best fit the time series per study site is shown (indicated next to the study site name). The highlighted values are important values in determining the fit of the model (multiple r-suqared) and the significance of the slope (p-value).

Witsand - linear model:

```
Call:
lm(formula = WS$Hm0 ~ WS$DateTime)

Residuals:
       Min         1Q     Median         3Q        Max
-4.999e-05 -5.376e-06  6.000e-09  5.371e-06  5.000e-05

Coefficients:
             Estimate Std. Error t value Pr(>|t|)
(Intercept) 5.973e-01  7.210e-07  828485   <2e-16 ***
WS$DateTime 3.700e-10  6.377e-16  580244   <2e-16 ***
---
Signif. codes:  0 ‘***’ 0.001 ‘**’ 0.01 ‘*’ 0.05 ‘.’ 0.1 ‘ ’ 1

Residual standard error: 2.169e-05 on 49189 degrees of freedom
Multiple R-squared:      1,    Adjusted R-squared:      1
F-statistic: 3.367e+11 on 1 and 49189 DF,  p-value: < 2.2e-16
```

Still Bay - quadratic model:

```
Call:
lm(formula = SB$Hm0 ~ SB$DateTime + SBdt2)

Residuals:
       Min         1Q     Median         3Q        Max
-4.998e-05 -2.498e-05 -1.900e-08  2.499e-05  5.011e-05

Coefficients:
              Estimate Std. Error t value Pr(>|t|)
(Intercept)  9.332e-01  1.027e-05   90871   <2e-16 ***
SB$DateTime  1.516e-09  1.852e-14   81827   <2e-16 ***
SBdt2       -3.695e-09  6.162e-14  -59960   <2e-16 ***
---
Signif. codes:  0 ‘***’ 0.001 ‘**’ 0.01 ‘*’ 0.05 ‘.’ 0.1 ‘ ’ 1

Residual standard error: 2.887e-05 on 43829 degrees of freedom
Multiple R-squared:      1, Adjusted R-squared:      1
F-statistic: 8.303e+10 on 2 and 43829 DF,  p-value: < 2.2e-16
```

Gouritz - quadratic model:

```
Call:
lm(formula = GZ$Hm0 ~ GZ$DateTime + GZdt2)

Residuals:
       Min         1Q     Median         3Q        Max
-5.015e-05 -2.577e-05 -1.900e-07  2.523e-05  5.097e-05

Coefficients:
              Estimate Std. Error t value Pr(>|t|)
(Intercept)  3.060e+00  1.032e-05  296428   <2e-16 ***
GZ$DateTime -2.253e-09  1.862e-14 -120992   <2e-16 ***
GZdt2        8.569e-09  6.195e-14  138324   <2e-16 ***
---
Signif. codes:  0 ‘***’ 0.001 ‘**’ 0.01 ‘*’ 0.05 ‘.’ 0.1 ‘ ’ 1

Residual standard error: 2.902e-05 on 43829 degrees of freedom
Multiple R-squared:      1, Adjusted R-squared:      1
F-statistic: 5.9e+10 on 2 and 43829 DF,  p-value: < 2.2e-16
```

Mossel Bay - quadratic model:

```
Call:
lm(formula = MB$Hm0 ~ MB$DateTime + MBdt2)

Residuals:
       Min         1Q     Median         3Q        Max
-5.010e-05 -2.495e-05 -7.100e-08  2.497e-05  5.021e-05

Coefficients:
              Estimate Std. Error t value Pr(>|t|)
(Intercept)  1.499e+00  1.027e-05  145965   <2e-16 ***
MB$DateTime -9.252e-10  1.852e-14  -49961   <2e-16 ***
MBdt2        4.029e-09  6.161e-14   65398   <2e-16 ***
---
Signif. codes:  0 ‘***’ 0.001 ‘**’ 0.01 ‘*’ 0.05 ‘.’ 0.1 ‘ ’ 1

Residual standard error: 2.886e-05 on 43829 degrees of freedom
Multiple R-squared:      1, Adjusted R-squared:      1
F-statistic: 4.179e+10 on 2 and 43829 DF,  p-value: < 2.2e-16
```

D. Regression analyses – scatter plots with estimated linear model line and best fitted model line:

The following shows two plots per study site, performed in Rstudio (version 1.1.442). Both plots show the EMD H_{m0} trend time series (black) with the linear model line (left column, red line) running through the one plot and the best fitting model line (column right, red line) running through the other plot.

<table>
<tr><td colspan="2">Witsand</td></tr>
<tr><td>Linear model</td><td>Best fit model - linear</td></tr>
<tr><td> 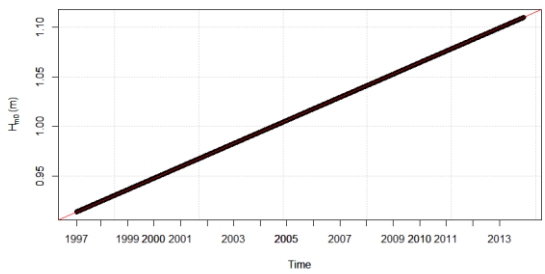
</td><td> 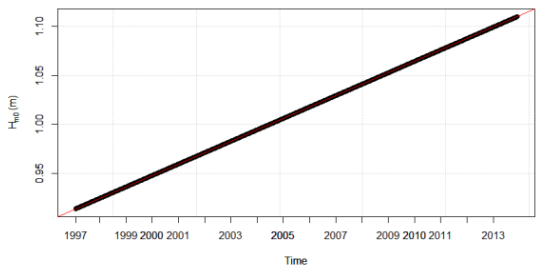
</td></tr>
<tr><td colspan="2">Still Bay</td></tr>
<tr><td>Linear model</td><td>Best fit model - quadratic</td></tr>
<tr><td> 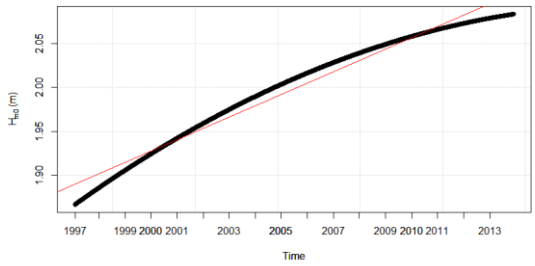
</td><td> 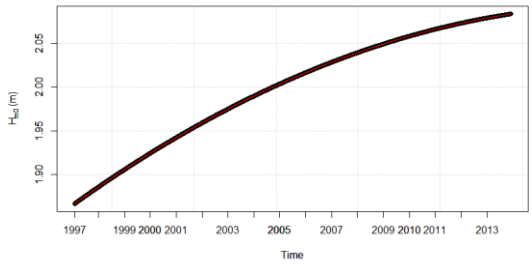
</td></tr>
<tr><td colspan="2">Gouritz</td></tr>
<tr><td>Linear model</td><td>Best fit model - quadratic</td></tr>
<tr><td> 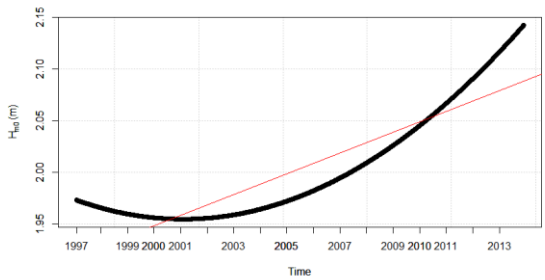
</td><td> 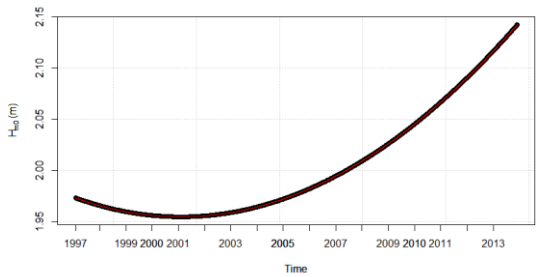
</td></tr>
</table>

Still Bay	
Linear model	Best fit model - quadratic
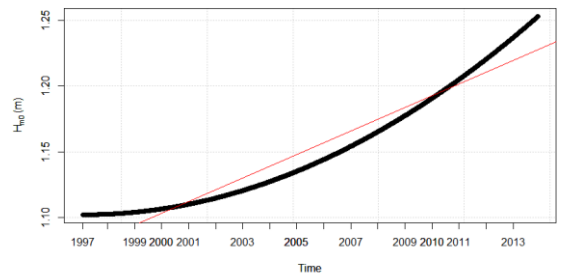	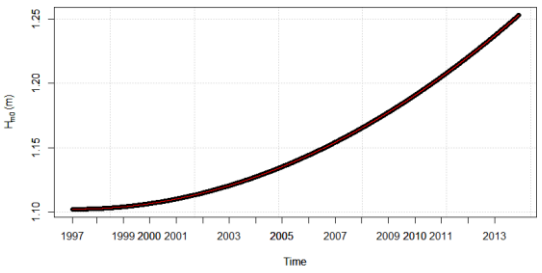

E. Regression analyses – diagnostic plots of the linear models:

The following plots show the diagnostic plots of the linear models fitted to the EMD H_{m0} trend time series for each study site, performed in Rstudio (version 1.1.442). Details of plots explained in section 3.3.3. ii.

Witsand

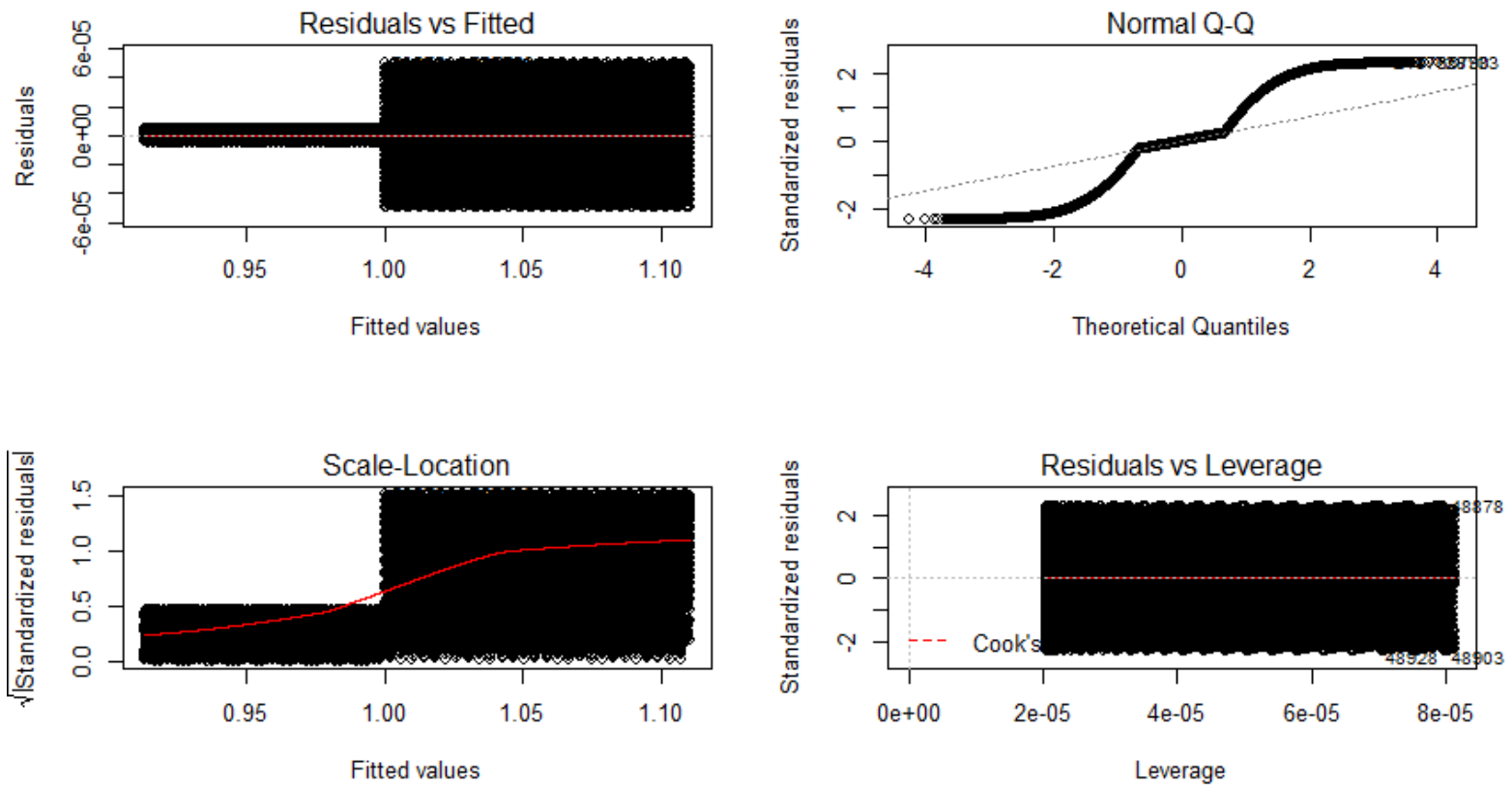

Still Bay

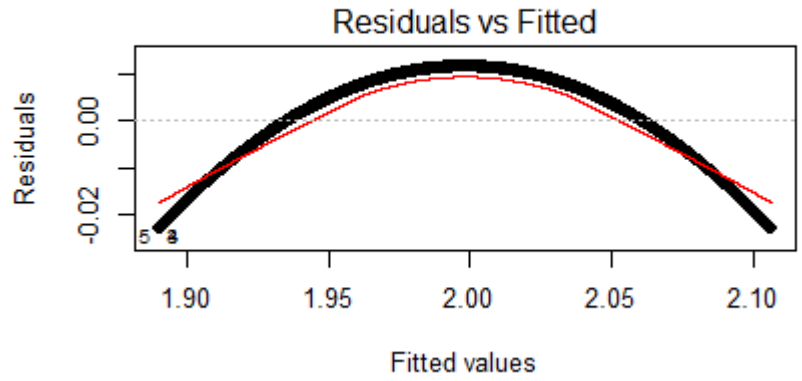
Residuals vs Fitted
Residuals
0.00
-0.02
1.90
1.95
2.00
2.05
2.10
Fitted values

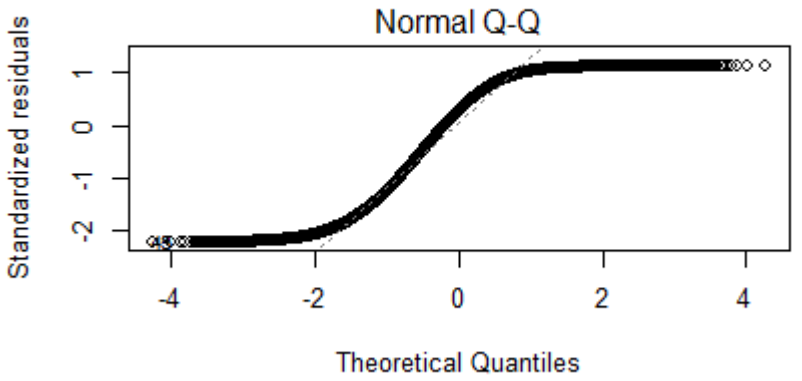
Normal Q-Q
Standardized residuals
1
0
-1
-2
-4
-2
0
2
4
Theoretical Quantiles

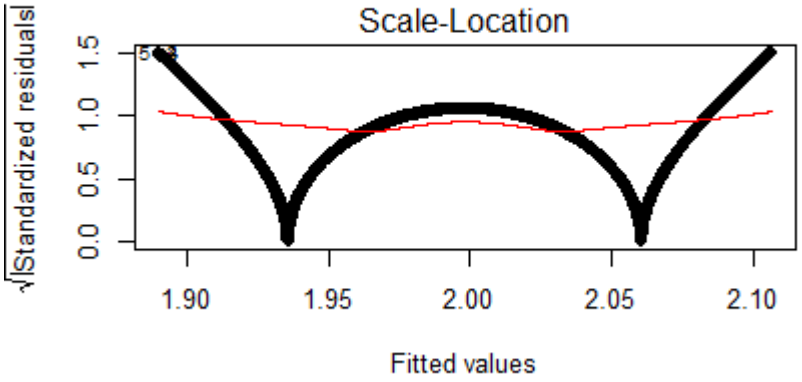
Scale-Location
√|Standardized residuals|
1.5
1.0
0.5
0.0
1.90
1.95
2.00
2.05
2.10
Fitted values

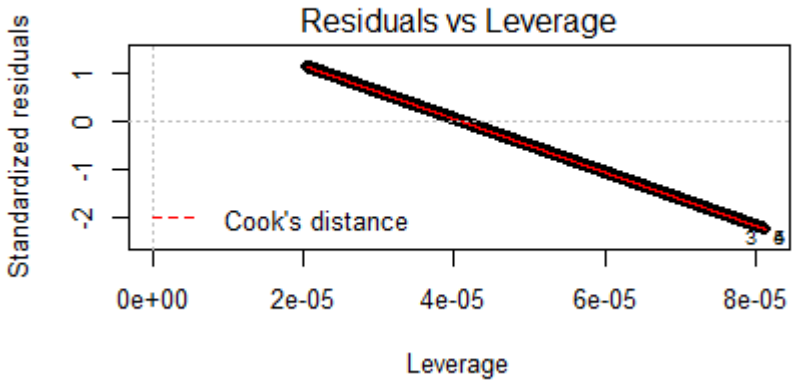
Residuals vs Leverage
Standardized residuals
1
0
-1
-2
Cook's distance
0e+00
2e-05
4e-05
6e-05
8e-05
Leverage

Gouritz

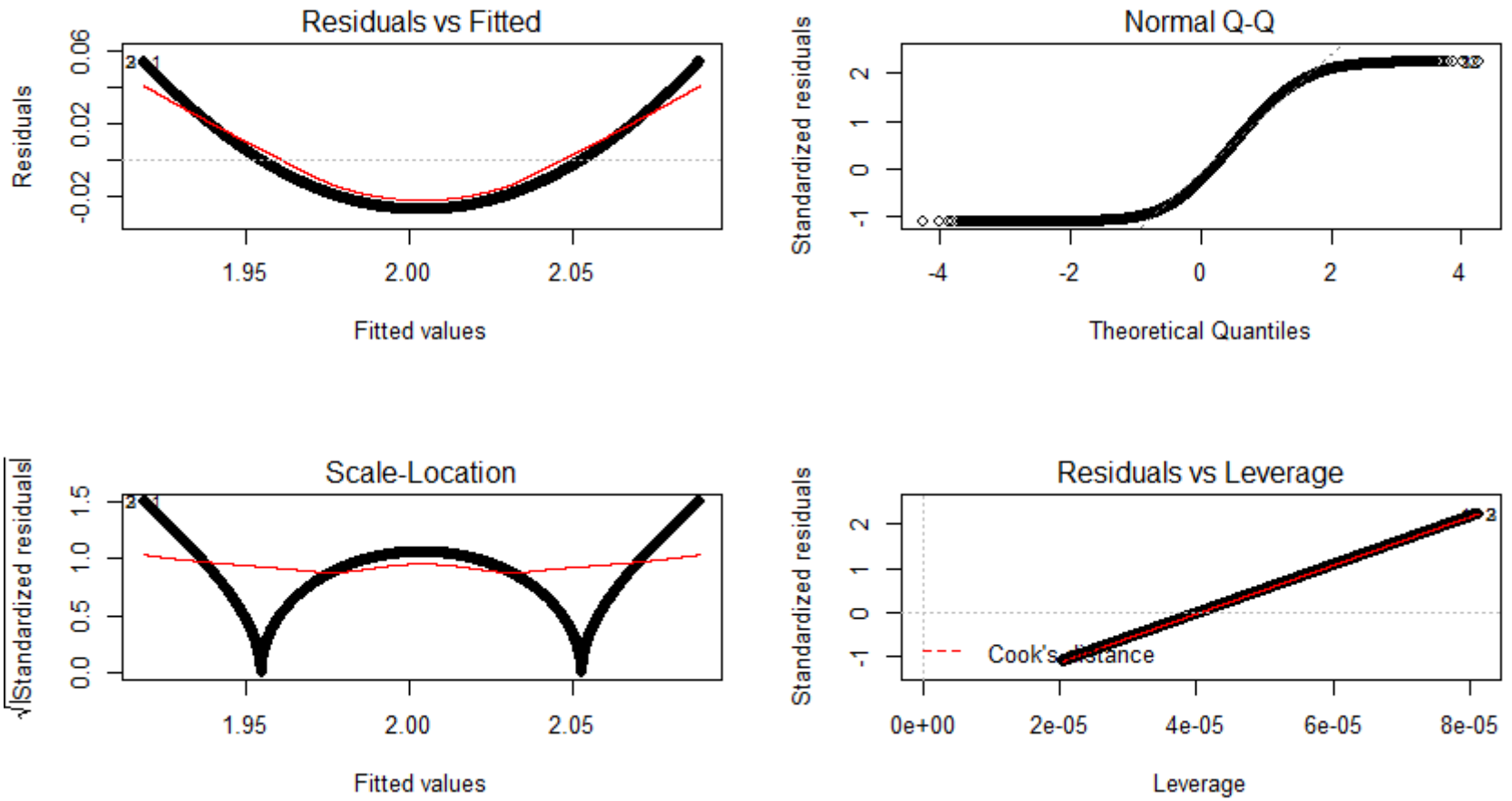
Residuals vs Fitted
Residuals
Fitted values
Normal Q-Q
Standardized residuals
Theoretical Quantiles
Scale-Location
√|Standardized residuals|
Fitted values
Residuals vs Leverage
Standardized residuals
Cook's distance
Leverage

Mossel Bay

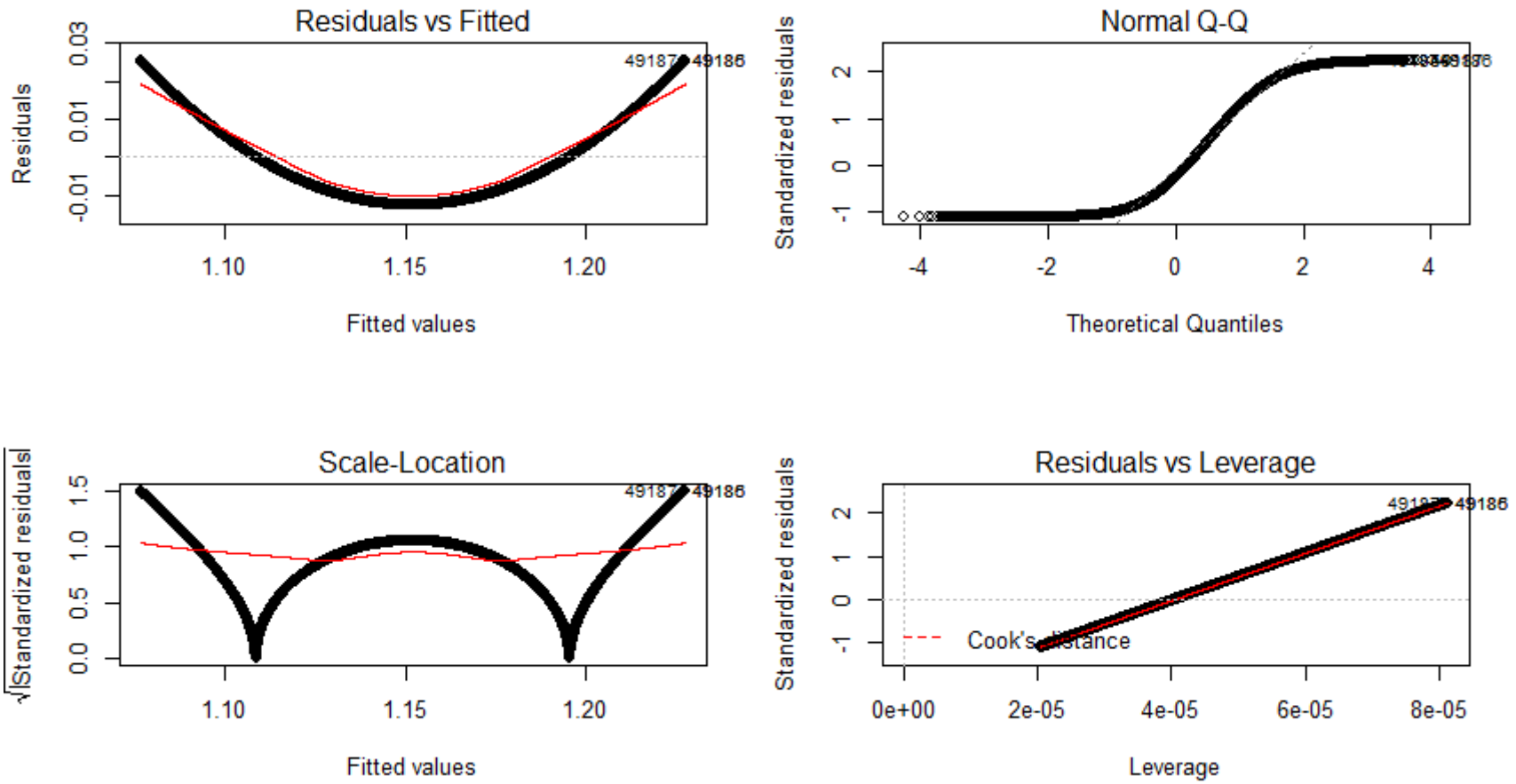
Residuals vs Fitted
Residuals
Fitted values
Normal Q-Q
Standardized residuals
Theoretical Quantiles
Scale-Location
√|Standardized residuals|
Fitted values
Residuals vs Leverage
Standardized residuals
Cook's distance
Leverage

F. Regression analyses – diagnostic plots of the best fit models:

The following plots show the diagnostic plots of the models that best fitted the EMD H_{m0} trend time series for each study site, performed in Rstudio (version 1.1.442). Details of plots explained in section 3.3.3. ii.

Witsand

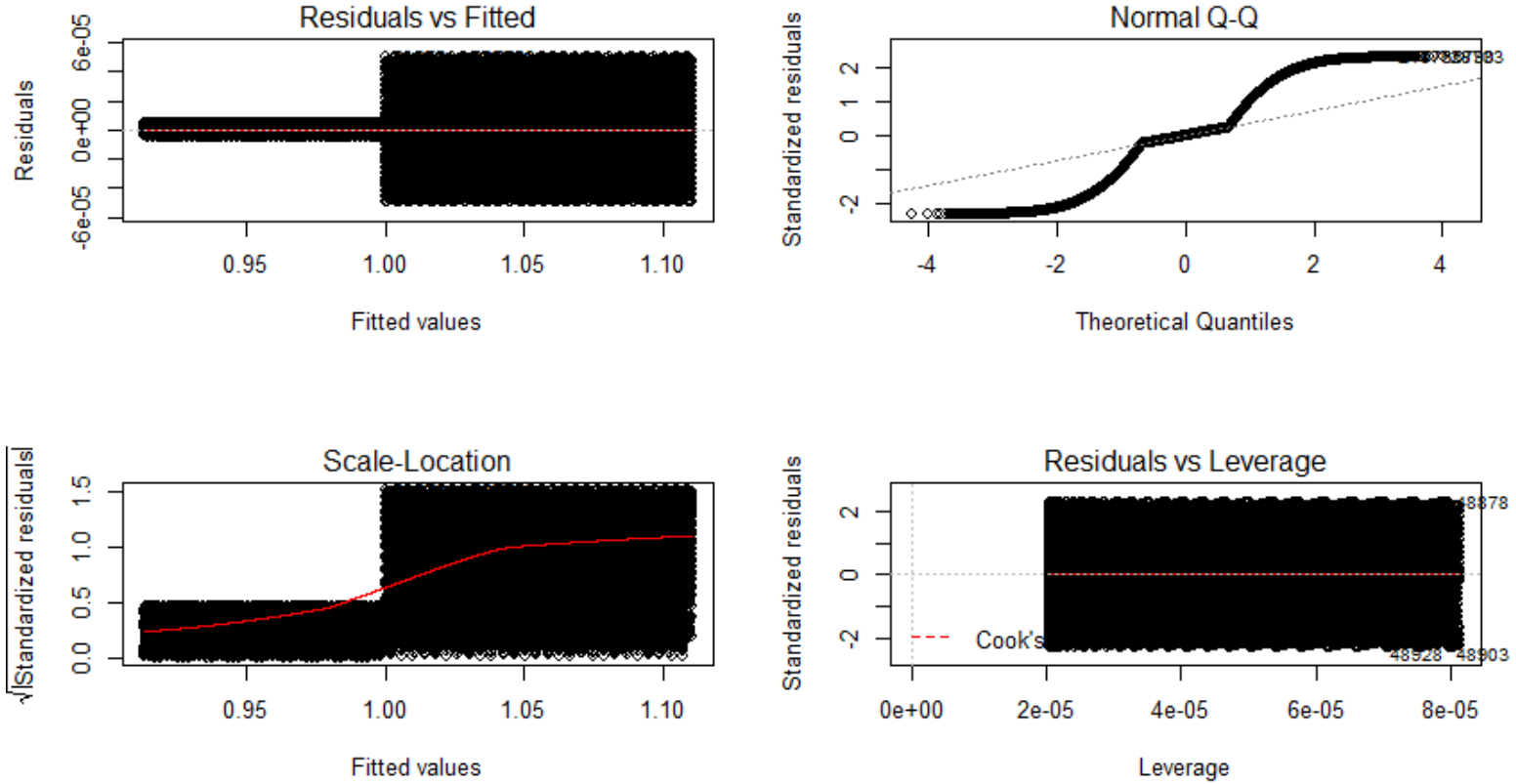

Still Bay

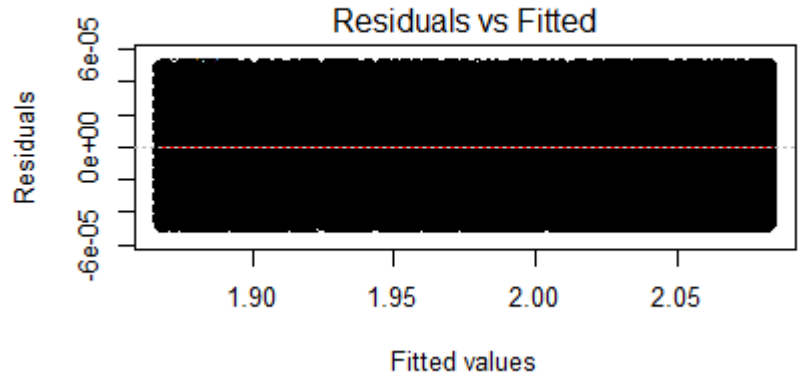
Residuals vs Fitted
Residuals
6e-05
0e+00
-6e-05
1.90
1.95
2.00
2.05
Fitted values

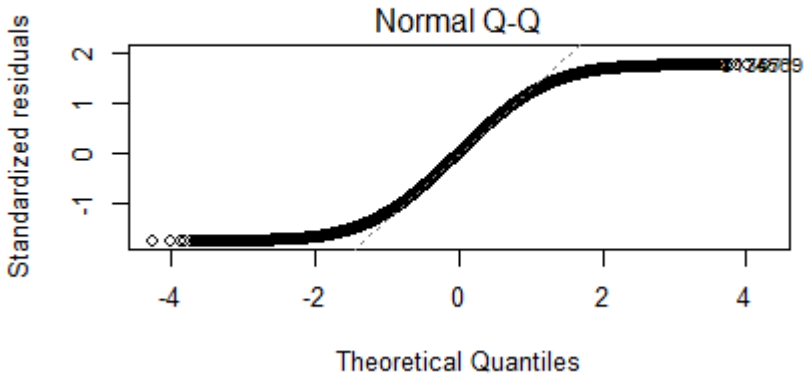
Normal Q-Q
Standardized residuals
2
1
0
-1
-4
-2
0
2
4
Theoretical Quantiles

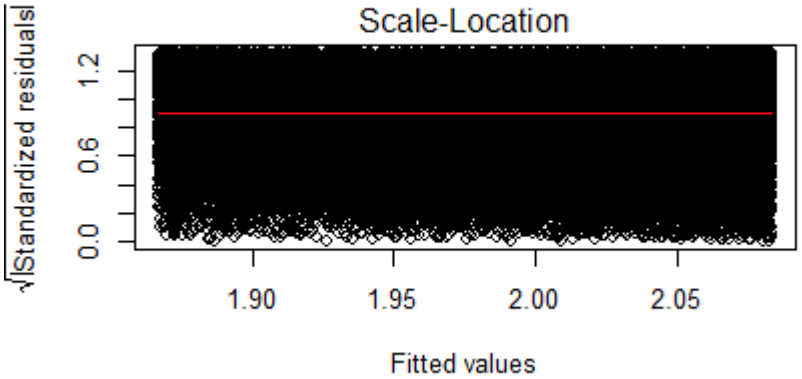
Scale-Location
√|Standardized residuals|
1.2
0.6
0.0
1.90
1.95
2.00
2.05
Fitted values

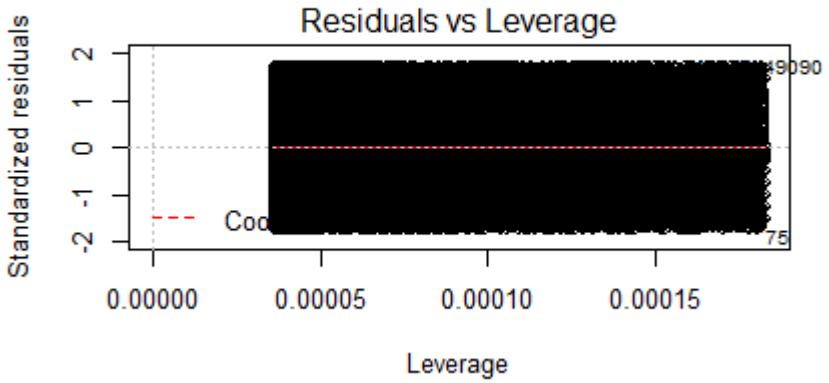
Residuals vs Leverage
Standardized residuals
2
1
0
-1
-2
0.00000
0.00005
0.00010
0.00015
Leverage

Gouritz

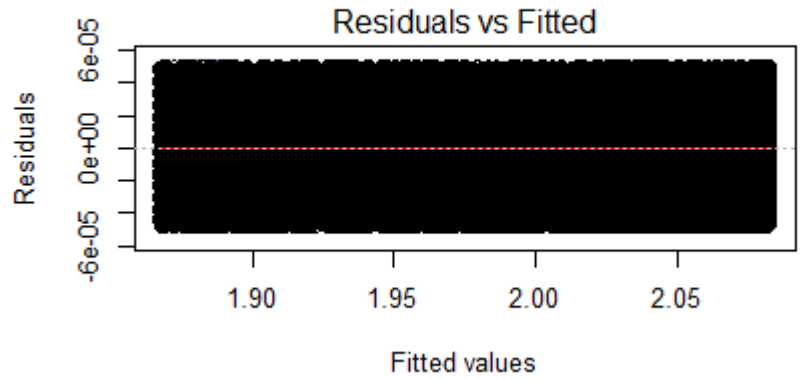
Residuals vs Fitted
Residuals
6e-05
0e+00
-6e-05
1.90
1.95
2.00
2.05
Fitted values

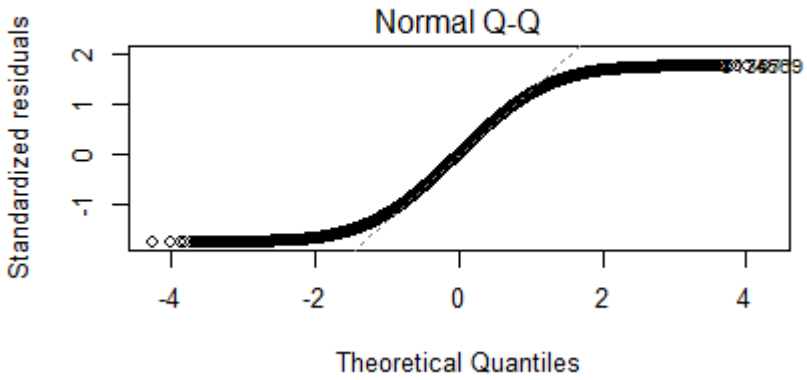
Normal Q-Q
Standardized residuals
2
1
0
-1
-4
-2
0
2
4
Theoretical Quantiles

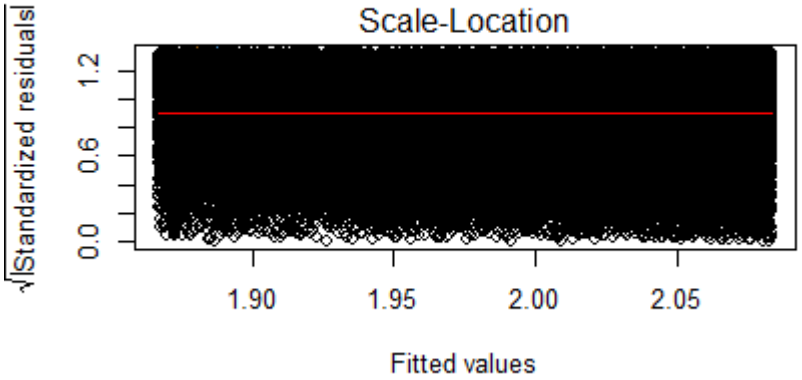
Scale-Location
√|Standardized residuals|
1.2
0.6
0.0
1.90
1.95
2.00
2.05
Fitted values

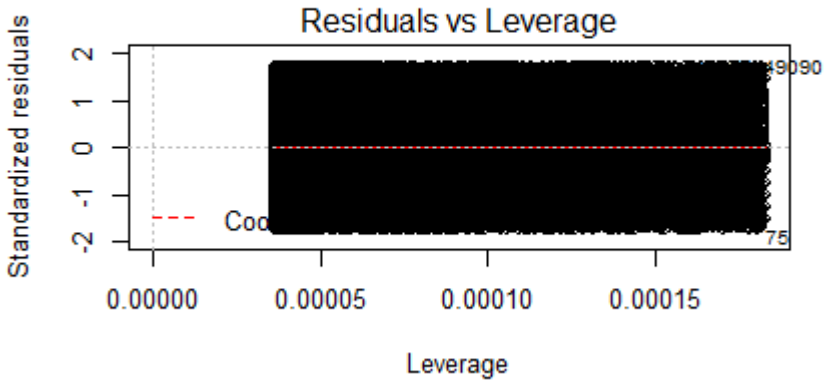
Residuals vs Leverage
Standardized residuals
2
1
0
-1
-2
0.00000
0.00005
0.00010
0.00015
Leverage

Mossel Bay

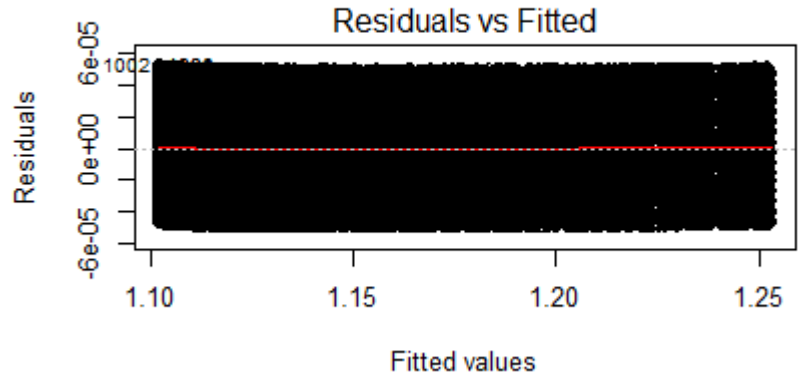
Residuals vs Fitted
Residuals
Fitted values
1.10
1.15
1.20
1.25
-6e-05
0e+00
6e-05

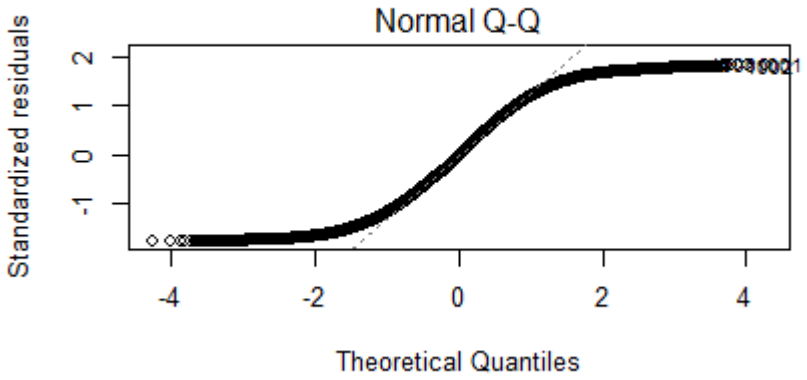
Normal Q-Q
Standardized residuals
Theoretical Quantiles
-4
-2
0
2
4

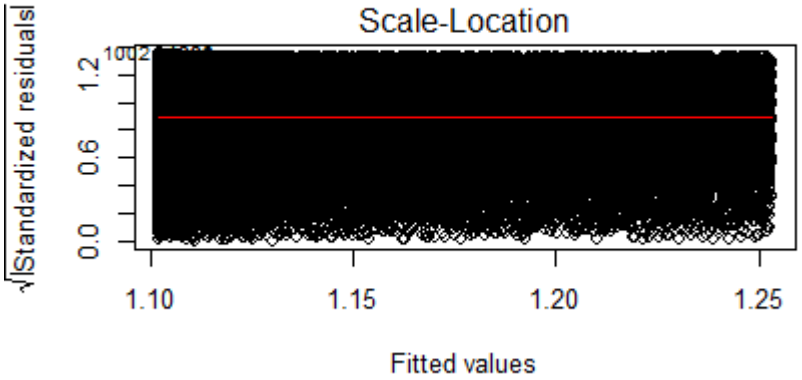
Scale-Location
√|Standardized residuals|
Fitted values
1.10
1.15
1.20
1.25
0.0
0.6
1.2

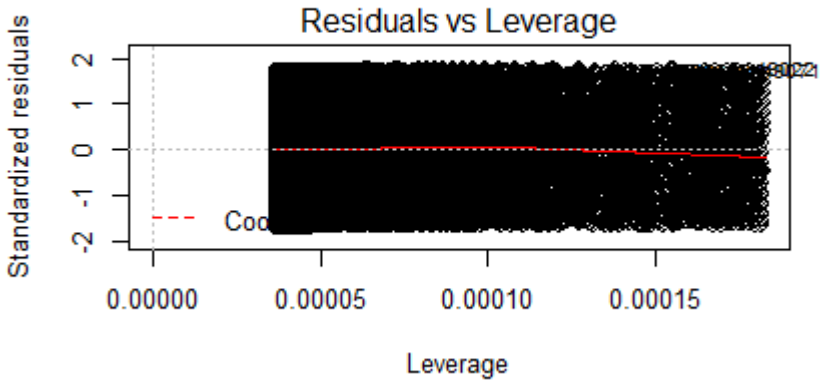
Residuals vs Leverage
Standardized residuals
Leverage
0.00000
0.00005
0.00010
0.00015

G. Sequential Regime Shift Detection (SRSD) sensitivity analyses:

The following table displays the results of the SRSD sensitivity analyses performed on the straight (STR) and pre-whitened (PW) annual averages of the H_{m0} interannual anomaly time series (determined using the Empirical Mode Decomposition (EMD) method) for each study site using seven different parameter inputs (including the default settings). Shifts detected in the same year under 70% or more of the settings during both the straight and pre-whitened analyses were considered 'robust'. Shifts detected between 50-70% of the model settings only during straight analyses were considered 'possible', and only during pre-whitened analyses were considered 'pre-whitened' shifts. l = cut-off length (years); H = Huber parameter; α = significance level.

WITSAND						
	Parameter setting combinations				Robust	Possible
Years of shifts detected	l = 10 α = 0.1 H = 1	l = 10 α = 0.05 H = 1	l = 7 α = 0.1 H = 1	l = 7 α = 0.05 H = 1		
2005			PW		No	No
2006	**STR**		**STR**		No	**Yes (STR)**
2007		**STR**		**STR**	No	**Yes (STR)**
2012	**PW**	**PW**	**PW**	**PW**	**Yes (PW)**	No
STILL BAY						
	Parameter setting combinations				Robust	Possible
Years of shifts detected	l = 10 α = 0.1 H = 1	l = 10 α = 0.05 H = 1	l = 7 α = 0.1 H = 1	l = 7 α = 0.05 H = 1		
2006	**STR**	**STR**	**STR**	**STR**	**YES (STR)**	No

GOURITZ						
	Parameter setting combinations				Robust	Possible
Years of shifts detected	$l = 10$ $\alpha = 0.1$ $H = 1$	$l = 10$ $\alpha = 0.05$ $H = 1$	$l = 7$ $\alpha = 0.1$ $H = 1$	$l = 7$ $\alpha = 0.05$ $H = 1$		
2006	**STR, PW**	**STR, PW**	**STR, PW**	**STR, PW**	**Yes**	No
MOSSEL BAY						
	Parameter setting combinations				Robust	Possible
Years of shifts detected	$l = 10$ $\alpha = 0.1$ $H = 1$	$l = 10$ $\alpha = 0.05$ $H = 1$	$l = 7$ $\alpha = 0.1$ $H = 1$	$l = 7$ $\alpha = 0.05$ $H = 1$		
2005			PW		No	No
2006	**STR**		**STR**	**STR**	**Yes (STR)**	NO
2007		STR			No	No
2012			PW		No	No

H. National Centre of Environmental Prediction (NCEP) wind and wave roses:

Average coarse resolution National Centre of Environmental Prediction (NCEP) annual (a) synoptic-scale wind and (b) offshore synoptic-scale wave roses (full time series from 1997-01-30-03h00 to 2013-11-30-24h00). The wind rose shows direction (degrees, ^{o}) frequency (percentage, %) and magnitude (colour bar) of wind speeds (Ws, m/s). Wave rose shows directional frequency and magnitude of significant wave height (H_{m0}, m).

Wind	Wave
(a) 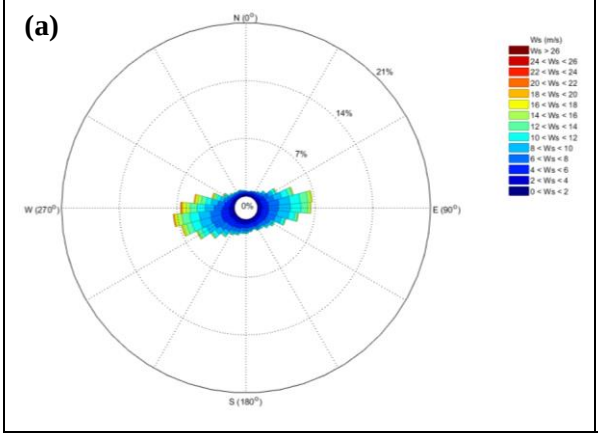	**(b)** 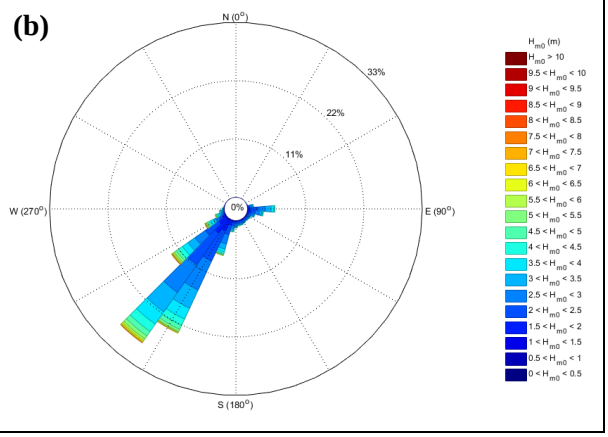

I. Simulating WAves Nearshore (SWAN) wave roses:

Average high resolution Simulating WAves Nearshore (SWAN) annual nearshore wave roses of the full time series (1997-01-30-03h00 to 2013-11-30-24h00) for the study sites at (a) Witsand, (b) Still Bay, (c) Gouritz, and (d) Mossel Bay. Wind roses show direction (degrees, ^{o}) frequency (percentage, %) and magnitude (colour bar) of wind speeds (Ws, m/s). Wave roses show directional frequency and magnitude of significant wave height (H_{m0}, m).

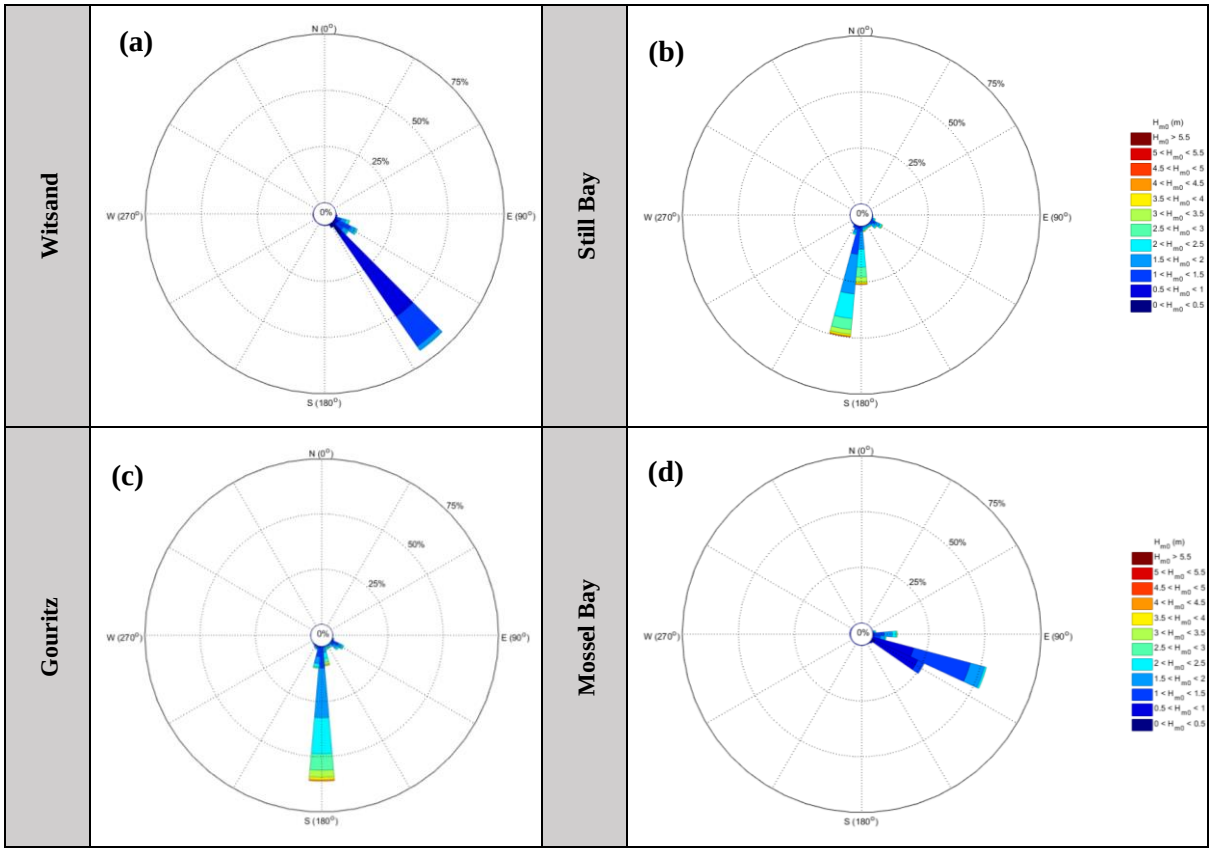

J. Summer sub-daily significant wave height (H_{m0}) difference time series of Witsand, Still Bay and Mossel Bay:

Time series of differences in summer sub-daily significant wave height (H_{m0}) between H_{m0} at 06h00 and 15h00 of each year for (a) Witsand, (b) Gouritz and (c) Mossel Bay. Positive values indicate that the afternoon H_{m0} values are larger than the morning H_{m0} values, while negative values indicate the inverse..

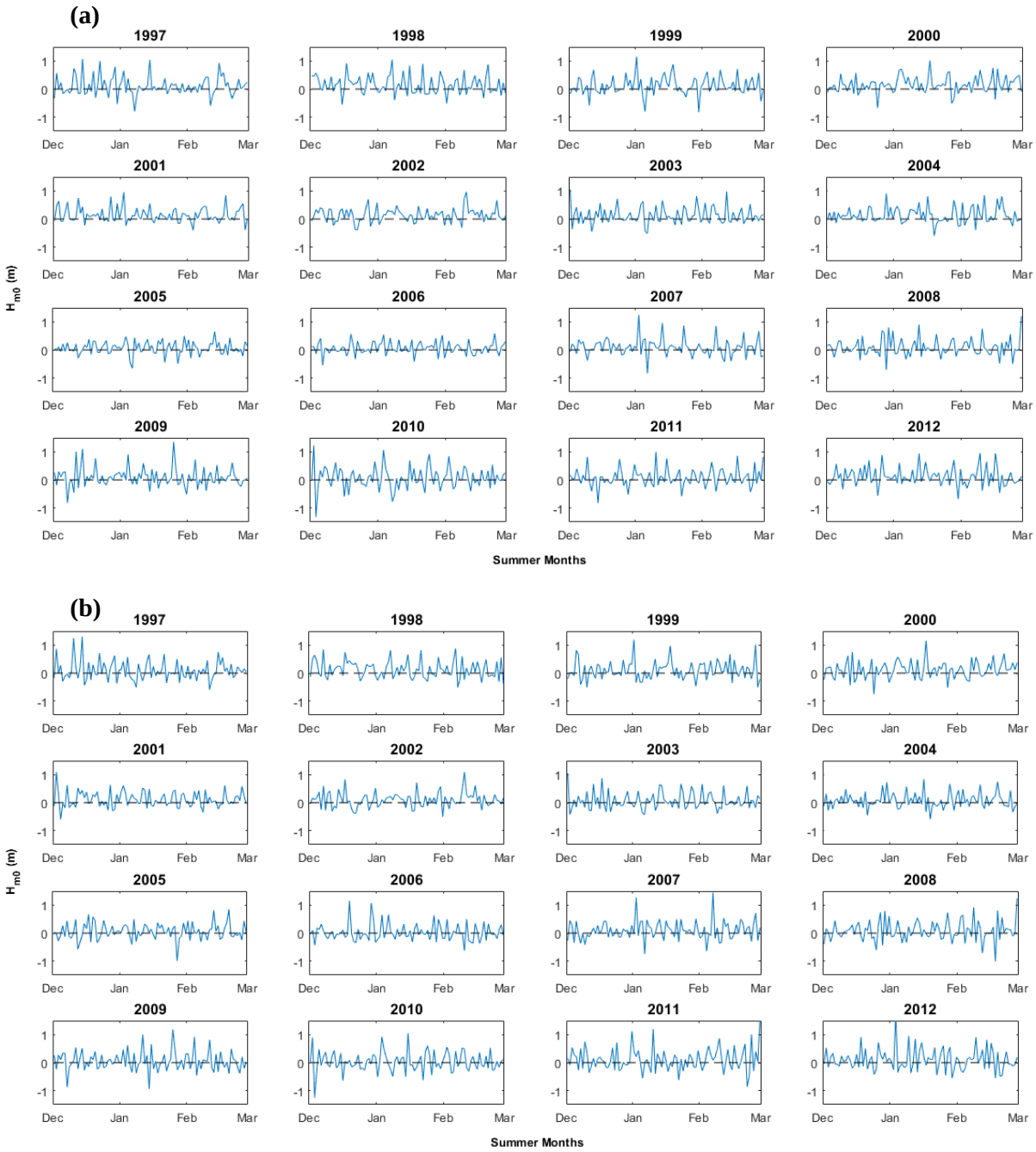

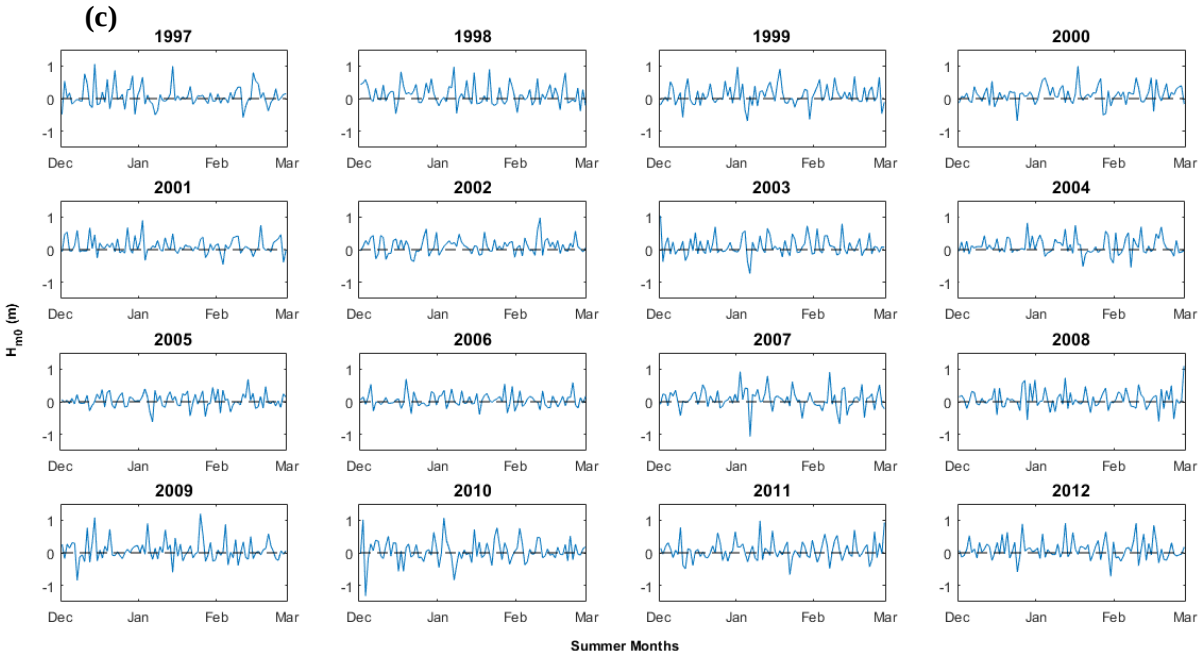
(c)
1997
1998
1999
2000
2001
2002
2003
2004
2005
2006
2007
2008
2009
2010
2011
2012
1
0
-1
Dec
Jan
Feb
Mar
H_{m0} (m)
Summer Months